PULSED LASER GENERATION IN S+/S BAND USING THULIUM FLUORIDE FIBER WITH SATURABLE ABSORBER

SITI AISYAH BINTI REDUAN

INSTITUTE FOR ADVANCED STUDIES
UNIVERSITY OF MALAYA
KUALA LUMPUR

2020

PULSED LASER GENERATION IN S+/S BAND USING THULIUM FLUORIDE FIBER WITH SATURABLE ABSORBER

SITI AISYAH BINTI REDUAN

THESIS SUBMITTED IN FULFILMENT OF THE REQUIREMENTS FOR THE DEGREE OF DOCTOR OF PHILOSOPHY

INSTITUTE FOR ADVANCED STUDIES
UNIVERSITY OF MALAYA
KUALA LUMPUR

2020

UNIVERSITY OF MALAYA
ORIGINAL LITERARY WORK DECLARATION

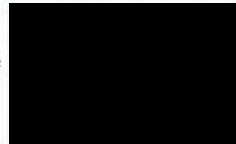Name of Candidate: **Siti Aisyah Binti Reduan**

Matric No: **HHE 150002**

Name of Degree: **Doctor of Philosophy**

Title of Thesis: **Pulsed Laser Generation In S+/S Band Using Thulium Fluoride**

FiberWith Saturable Absorber

Field of Study: **Photonics**

I do solemnly and sincerely declare that:

(1)   I am the sole author/writer of this Work;

(2)   This Work is original;

(3)   Any use of any work in which copyright exists was done by way of fair dealing and for permitted purposes and any excerpt or extract from, or reference to or reproduction of any copyright work has been disclosed expressly and sufficiently and the title of the Work and its authorship have been acknowledged in this Work;

(4)   I do not have any actual knowledge nor do I ought reasonably to know that the making of this work constitutes an infringement of any copyright work;

(5)   I hereby assign all and every rights in the copyright to this Work to the University of Malaya ("UM"), who henceforth shall be owner of the copyright in this Work and that any reproduction or use in any form or by any means whatsoever is prohibited without the written consent of UM having been first had and obtained;

(6)   I am fully aware that if in the course of making this Work I have infringed any copyright whether intentionally or otherwise, I may be subject to legal action or any other action as may be determined by UM.

Candidate's Signature   Date: 27/3/2020

Subscribed and solemnly declared before,

Witness's Signature   Date: 27/3/2020

Name: MUHAMAD ZHARIF SAMION

Designation:

MUHAMAD ZHARIF BIN SAMION
Research Officer
University Of Malaya
50603 Kuala Lumpur

PULSED LASER GENERATION IN S+/S BAND USING THULIUM FLUORIDE FIBER WITH SATURABLE ABSORBER

ABSTRACT

Demands on photonic applications has become highly saturated in C-band and L-band region, forcing the needs to work in S band region for the development of alternative data network and photonics technology tools to fulfill the future needs. There are only a few reports on exploiting S band fiber laser operation which mainly used depressed-cladding erbium-doped fiber (DC-EDF) as gain medium. The region covers only ~1480 nm to 1510 nm as mentioned by previous works. Other than that, there is limitation in the selection of rare-element gain medium to generate the emission in S band region. The use of thulium-fluoride fiber (TFF) as gain medium has been focusing in S band fiber laser since it allows the laser amplification that covers a shorter wavelength in S band region. Besides that, the ability of TFF to generate emission in S band region by a single up-conversion pumping which is a simpler and more cost-effective way, is seen to be the advantages compared to the other pumping scheme. The aim of this study is to investigate the generation of S+/S band fiber laser by using Thulium-Fluoride Fiber as a gain medium purposefully for photonics applications. Besides the investigation on TFF fiber laser in S band region, the gain profile will be calculated to identify the amplification of the proposed fiber laser. The tunability of the TFF laser will be studied by integrating the tunable band-pass filter (TBPF) into the cavity and precisely identifying the wavelength range that can be tuned. The accessibility of the generated laser in S band region for photonics applications will be identified. Saturable absorber (SA) is inserting into the cavity to investigate the generation of pulsed laser which are Q-switching and mode-locking, in S band region. Preparations and characterization of the SA will be done to identify the properties of the SA. The generation of dual-wavelength, Q-switched laser in the proposed experiment will be investigated by inserting an SA and Photonic crystal

fiber (PCF) into the cavity. PCF is the potential optical media that will be used to study the generation of dual-wavelength laser in the proposed experiment. The studies commenced and the results obtained in this study can contribute to expanding telecommunication operation band and availability of photonics applications in shorter wavelength of S+/S band region.

Keywords: Fiber Laser, S+/S band, Thulium-Fluoride Fiber, S band region, Photonic

PENJANAAN LASER BERDENYUT DIDALAM JALUR S+/S DENGAN MENGGUNAKAN GENTIAN THULIUM FLUORIDA BERSAMA PENYERAP BOLEH TEPU

ABSTRAK

Permintaan dalam aplikasi fotonik sudah menjadi sangat tepu dalam rantau jalur-C dan jalur-L, hingga memerlukan kepaksaan untuk melakukan kerja dalam rantau jalur-S bagi pembangunan rangkaian data alternatif dan alat teknologi fotonik demi memenuhi keperluan masa hadapan. Terdapat beberapa laporan sahaja dalam mengeksploitasi operasi laser gentian jalur-S dimana Gentian Optik Berdop Erbium Dengan Rekabentuk Pelapisan Ditekan (DC-EDFA) yang selalunya digunakan sebagai medium gandaan. Rantau yang dapat diliputi hanya ~ 1480 nm himgga 1510 nm seperti yang dilaporkan oleh laporan terdahulu. Selain itu, pemilihan unsur nadir sebagai gandaan medium untuk menjana pancaran dalam rantau jalur-S adalah terhad. Penggunaan gentian thulium fluorida (TFF) sebagai medium gandaan untuk laser gentian jalur-S telah menjadi tumpuan kerana kebolehannya dalam penguatan laser yang meliputi rantau panjang gelombang jalur-S yang lebih pendek. Di samping itu, kebolehan TTF menjana pancaran dalam rantau jalur-S oleh pam penukaran-terhingga tunggal dimana ianya ringkas dan cara yang kosnya lebih efektif, dilihat sebagai kelebihan berbanding skema pam yang lain. Matlamat kajian ini adalah untuk mengkaji penjanaan laser gentian optik jalur S+/S dengan menggunakan Gentian Thulium Fluorida (TFF) sebagai medium gandaan demi penggunaan aplikasi fotonik. Disamping pengkajian laser gentian optik TFF dalam jalur-S, profil gandaan akan dikira untuk mengenal pasti penguatan laser gentian yang dicadangkan. Daya boleh laras laser TFF akan dikaji dengan mengintegrasikan penapis boleh laras (TBPF) ke dalam kaviti dan panjang gelombang yang boleh dilaras dikenal pasti secara tepat. Kebolehcapaian laser yang dijana dalam jalur-S untuk aplikasi fotonik akan dikaji. Penyerap boleh tepu (SA) dimasukkan ke dalam kaviti untuk mengkaji

penjanaan laser berdenyut iaitu Q-suis dan penjanaan mode terkunci, didalam jalur-S. Penyedian dan pencirian penyerap boleh tepu akan dilakukan untuk mengenal pasti sifat-sifat penyerapan tepu. Penjanaan laser berdenyut, dwi-panjang gelombang akan dikaji dengan SA dan Gentian fotonik Kristal (PCF) ke dalam kaviti. PCF adalah media optik berpontensi yang akan digunakan untuk penjanaan laser dwi-panjang gelombang didalam eksperimen yang dicadangkan. Kajian bermula dan keputusan yang diperoleh dalam kajian ini boleh menyumbang kepada perkembangan operasi telekomunikasi dan ketersedian aplikasi fotonik dalam rantau panjang gelombang jalur-S+/S yang lebih pendek.

Kata kunci: Laser Gentian, Jalur S+/S, Thulium Fluorida, Rantau Jalur-S, Fotonik

ACKNOWLEDGEMENTS

TABLE OF CONTENTS

LIST OF FIGURES

LIST OF TABLES

LIST OF SYMBOLS AND ABBREVIATIONS

2D	:	Two- Dimensional
3D	:	Three-Dimensional
ASE	:	Amplified Spontaneous Emission
CNT	:	Carbon Nanotube
CW	:	Continuous Wave
DC-EDF	:	Depressed-Cladding Erbium-Doped Fiber
EDF	:	Erbium-Doped Fiber
ESA	:	Excited State Absorption
FWHM	:	Full-Width at Half Maximum
GaSe	:	Gallium Selenide
GSA	:	Ground State Absorption
GVD	:	Group Velocity Dispersion
In_2Se_3	:	Indium Selenide
IR	:	Infrared
ISO	:	Isolator
LD	:	Laser Diode
MoS_2	:	Molybdenum Disulfide
NF	:	Noise Figure
OFS	:	Optical Fiber Systems
OPM	:	Optical Power Meter
OSA	:	Optical Spectrum Analyzer
OSC	:	Oscilloscope
PCF	:	Photonics Crystal Fiber
RFSA	:	Radio-Frequency Spectrum Analyzer

SA	:	Saturable Absorber
SESAMs	:	Semiconductor Saturable Absorber Mirrors
SiO_2	:	Silica
SMF	:	Single Mode Fiber
SNR	:	Signal-to-Noise Ratio
SPM	:	Self-Phased Modulation
SWCNT	:	Single-Walled Carbon Nanotube
TBP	:	Time Bandwidth Product
TBPF	:	Tunable Bandpass Filter
TDF	:	Thulium-Doped Fiber
TFF	:	Thulium-Doped Fluoride Fiber
TI	:	Topological Insulator
TLS	:	Tunable Laser Source
Tm^{3+} ion	:	Thulium Ion
TMD	:	Transition Metal Dichalcogenide
TMZF	:	Tunable Mach-Zehnder Filter
UV	:	Ultraviolet
VOA	:	Variable Optical Attenuator
WDM	:	Wavelength Division Multiplexer
YDF	:	Ytterbium-Doped Fiber
ZBLAN	:	$ZrFM_4$-BaF_2-LaF_3-AlF_3-NaF

CHAPTER 1: INTRODUCTION

1.1   Introduction

The foundation of laser comes from the concept of stimulated emission, which was introduced by Einstein in 1917 in a theory known as "On the Quantum Theory of Radiation." In this concept, a photon interacts with an excited molecule and causes the emission of a corresponding photon that has a same frequency phase and direction. LASER, on the other hand, stands for "Light Amplification by Stimulated Emission of Radiation." In 1958, Gordon Gould was the first person who coined the word "laser," and he initiated the creation of his own laser in the same year (Taylor, 2002). Theodore Maiman invented the first working laser based on ruby in 1960 (Maiman, 1960). This invention took place at Hughes Research Laboratories. Maiman used a cylindrical ruby crystal in a quartz flash tube with complete reflective mirror and a partially reflective mirror on each of the flash tube's end. Beginning from this invention, he successfully generated a series of fast pulses known as pulse laser.

This chapter begins with a brief history of optical communications, including the relationship between the band names and optical wavelength bands in Section 1.2. Then, the need of S+/S band and the objectives of this study are discussed in Section 1.3 and Section 1.4, respectively. The research methodology of this study as well as the thesis overview are presented in Section 1.5 and Section 1.6, respectively.

1.2   A Brief History of Fiber Lasers

The first fiber laser was invented by Elias Snitzer in 1961 using a flash lamp to pump the Neodymium-doped fiber to generate the laser at 1060 nm (Snitzer, 1961). However, the progress in developing the fiber laser was considerably slow over the following two decades due to the high loss of fibers and low efficient pump sources. In 1973, Stone developed a low absorption loss fiber using silica (SiO_2) as a host glass of the fiber, which

1

was the most critical achievement on enabling the technology of modern communication (Stone et al., 1973). The first demonstration by David Payne in 1987 (Mears et al., 1987) on Erbium fiber laser amplifiers was the impetus to push forward efforts to explore different types of fiber lasers using different rare-earth elements as the gain media. The interest in fiber laser rapidly progressed, and it resulted in a great achievement especially in the field of communication.

Fiber lasers are highly desirable laser sources because of their high efficiencies, smooth beam delivery and alignment-free design (Martinez et al., 2013; Richardson et al., 2010), that can be applied in various areas such as telecommunication, medicine, environmental sensing, imaging and science research (D. Popa et al., 2011; Siniaeva et al., 2009; Xu et al., 2013). There have been reports in previous works on fiber lasers operating in the C-band region (H Ahmad et al., 2016a; H Ahmad et al., 2016b; B. Chen et al., 2015; P. Yan et al., 2015) and L-band region (S.-W. Huang et al., 2015; Tan et al., 2013; Y. Yan et al., 2016; Zhao et al., 2013) using Erbium-doped Fiber (EDF) as a gain medium.

The development of fiber laser vigorously expands since the first fiber laser was demonstrated in 1961 using rare-earth elements which is Nd-doped fiber as a gain medium. Subsequently, numerous new fiber lasers using different rare-earth elements such as erbium, ytterbium, samarium, and thulium as the gain medium (E. Ismail et al., 2016; Zhipei Sun et al., 2010c; Woodward et al., 2014), They can operate over a wide range of wavelength, and these lasers had advantages over a traditional solid-state laser.

The capability of fiber lasers in allowing their source to be easily directed towards the focusing elements while providing a more compact physical size is considered more reliable compared to the solid-state lasers (F. Muhammad et al., 2014). Due to these

advantages, fiber lasers are being considered for applications in many areas such as telecommunications, medicine, scientific applications, and environmental sensing.

Table 1.1: Relationship of band names and optical wavelength band

	O	E	S	C	L	U/XL
Wavelength Range (nm)	1260 - 1360	1360 - 1460	1460 - 1530	1530 - 1585	1565 - 1625	1625 - 1675

Table. 1.1 illustrates the relationship of band names with an optical wavelength band. The operation of fiber laser and amplifier in C- band, and the L- band region using erbium-doped fiber (EDFs) as gain medium (Buxens et al., 2000; Chen et al., 2014; Y. Yan et al., 2016) have been extensively reported. It can be seen from Table. 1.1 that C- and L-band cover a wavelength from 1530 nm to 1625 nm, which is mainly an optical wavelength band that is used for optical communication. Nevertheless, only a few reports found on the generation of fiber laser in S band region, that covers the wavelength from 1460 nm to 1530 nm, forcing the researchers to work on the S band region, even on the shorter wavelength of S band in finding an alternative data network for telecommunications and availability in photonics technology tools. Indeed, the operation of the laser in the S band region has a lower susceptibility to bending loss compared to the C-band and L-band region (Sakamoto, 2001; M. Z. Zulkifli et al., 2011). This is because a longer wavelength will result in a larger mode field diameter and leads to higher bending losses compared to a shorter wavelength loss (Whitaker, 2005). It is reported by John A. Jay that the bending loss starts to increase rapidly above 1550 nm (Jay, 2010). Red highlight on E- and U/Xl- band column represent the bands that have typically been avoided due to their high transmission loss regions.

However, there were also reports about the use of ytterbium-doped fibers (YDFs) and thulium-doped fibers (TDFs) in generating fiber laser and amplifier which covers 1- and

2- micron regions, respectively (J. Liu et al., 2012; Luo et al., 2013), which the wavelength range is not included in Table 1.1.

1.3   The Need for S+/S Band Fiber Lasers

Even though earlier works have covered a vast spectrum covering the C- and L- bands, there is a need to further extend the S band towards a shorter wavelength or S band region. This is to cater to the increasing demands for the bandwidth for data traffic in optical network systems. There is also interest in this wavelength region for other applications such as spectroscopy. Unlike the C- and L-band regions, minimal works revolved around the S band region, and even fewer reports were found. S band is the wavelength band of telecom that covers a region from 1480 nm to 1530 nm, whereas the S+ band covers a shorter wavelength range of S band region which includes 1450 nm to 1480 nm (Caspary et al., 2003; El-Nahal et al., 2013; Yam et al., 2006).

Earlier reports on the S band region fiber lasers are based on depressed-cladding erbium-doped fibers (DC-EDFs) that only cover a wavelength region of between 1480 nm to 1510 nm (Harith Ahmad et al., 2016; M. Z. Zulkifli et al., 2011). Generally, this type of fiber has a secondary cladding that is surrounding the depressed cladding fiber. Figure 1.1 shows that the core, depressed cladding, and secondary cladding have a cross-section in the shape of a circular (Arbore et al., 2005). Depressed cladding fiber is also known as W-profile fiber due to its index profile, which resembles the letter of W. The index profile of single-mode fiber with a depressed cladding is illustrates in Figure 1.2. This shows that the indices between the depressed cladding and secondary cladding average out the n_1 and n_2 (Arbore, 2005b). The core must have a higher average index number than index n_1 of the depressed cladding and index n_2 of secondary cladding to determine the desire fundamental cut-off wavelength.
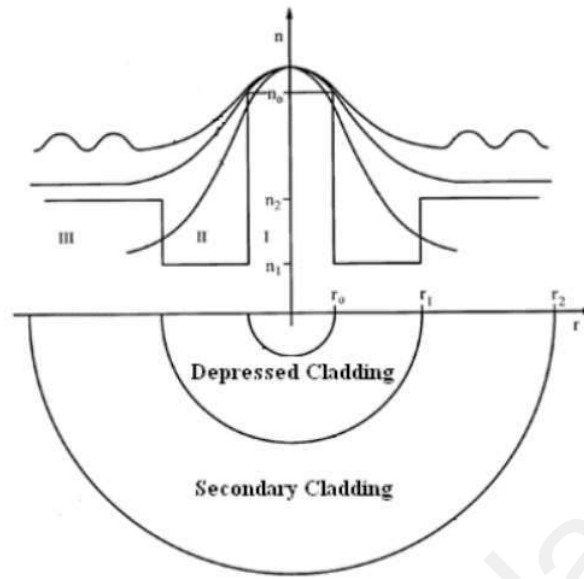
Figure 1.1: Cross sectional view of depressed cladding fiber[1]
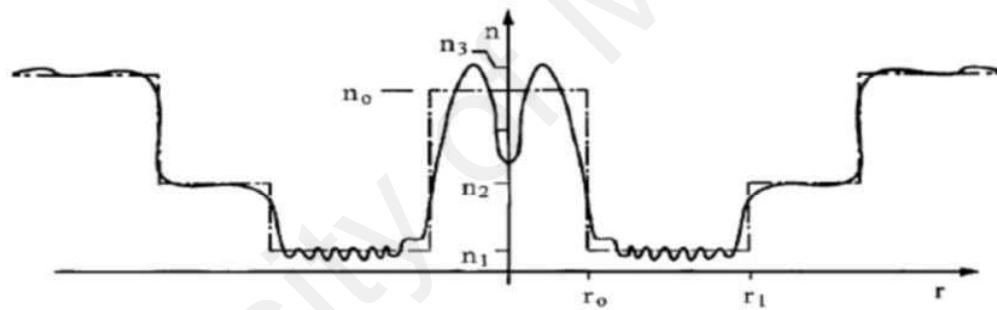
Figure 1.2: Index profile of Single-mode fiber[2]

Apart from the earlier works from this laboratory in the area of DC-EDFs, there are also other reports in this area. These reports, however, used the EDF as a gain medium that only operates in a small region of S band (Cao et al., 2011; Chen et al., 2014). The availability of the DC-EDF is also considerably limited and was only produced in limited quantities in the early 1990s by Optical Fiber Systems (OFS). There were also interests to further expand the S band region to an even shorter wavelength to provide wider

---

[1] (Reproduced with permission from Arbore et al., 2005)

[2] (Reproduced with permission from Arbore, 2005)

bandwidth, stretching from about 1440 nm to beyond 1600 nm. This would provide an extensive bandwidth that will accommodate all data traffic demands for the next 20 years, at least. The development of S band is limited by the choices of rare elements to generate an emission in this region. One of the best approaches is to use fluoride-based materials such as thulium-doped fluoride fibers (TFFs). Thulium-doped fiber based on silica is not preferable for S band emission due to the possible nonradiative decay via intermediate level, especially in a conventional silica fiber host (Peterka et al., 2004). The investigation on a shorter wavelength of S band using TFF will be an approach in exploiting the S band region.

Previously, DC-EDF was used as a gain medium in the generation of fiber laser and laser amplification in the S band region, which only covers wavelength ~1480 nm to 1510 nm (Harith Ahmad et al., 2016; M. Z. Zulkifli et al., 2011). There were also previous works that used EDF as a gain medium that was able to cover a small region of S band (Cao et al., 2011; Chen et al., 2014). Thus, there is still a need to investigate various approaches in fiber laser generation that will cover a shorter wavelength in the S band region, which is a vital band in telecommunication. Other than that, this investigation has the potential to produce the technology tools that will cover a broad spectrum in the S band region.

Previous works had also reported the use of thulium rare-earth element as a gain-medium which was able to produce emission in the S band region, either by single up-conversion pumping or dual wavelength pumping (Floridia et al., 2004; Kasamatsu et al., 1999). However, single up-conversion pumping is straightforward and more cost-effective as it only requires one wavelength pumping compared to dual-wavelength pumping. The two common single up-conversion pumpings for Thulium-doped fiber emission are 1050 nm and 1400 nm (Floridia et al., 2004). The 1400 nm pumping will be

used in this study as a pumping source due to the advantage of the direct ground state absorption (GSA) and the excited state absorption (ESA) (Floridia et al., 2004). The ground state absorption (GSA) is the absorption of a photon from a ground state to an excited state of an atom, molecule, or ion. Whereas, the excited state absorption (ESA) is the absorption of a photon from a lower excited state to a higher excited state of an atom, molecule, or ion. Whereby, 1050 nm pumping is not preferable in this study due to its depopulation, which requires two processes (Floridia et al., 2004).

Apart from the choice of efficient pumping technique, the host fiber of the gain medium also plays a fundamental role in enhancing the efficiency of the proposed fiber laser cavity. Fluoride fiber has low phonon energy (Frerichs et al., 1996) that will eventually strengthen the S band emission in generating the S band fiber laser.

For this reason, TFFs are focused on being used as a gain medium for S band amplification which has already been reported by Tanabe et al. (Tanabe et al., 2003), that covers a region from 1440 nm to 1550 nm corresponding to S band region as well as the shorter wavelength of S band known as S+ band. There was also reported on the development of the TFF amplifier for the S band region that covers the wavelength from 1490 nm to 1500 nm by Caspary et al. (Caspary et al., 2003). Thus, the demonstration of S+/S band fiber laser is achievable using TFF as a gain medium.

In response to this problem, which is the motivation of this thesis, this study will extensively investigate the S+/S band fiber laser. This fiber laser is commonly known as the S+/S band fiber laser. The thesis will employ this approach to investigate the amplification and tunability of the laser operating in this region. The early part of the thesis will consider continuous wave (CW) operation, while the subsequent chapters will investigate pulse generation in this gain medium, especially Q-switching and mode-locking. The thesis will also investigate a dual-wavelength Q-switched laser output. The

primary interest of the dual-wavelength fiber lasers is to look into the possibility of generating Terahertz and radio frequency outputs by mixing the two pulse wavelengths in a non-linear gain medium (Hu et al., 2018; Soltanian et al., 2015; Thambiratnam et al., 2016).

1.4 Research Objectives

The focus of this research is to design and demonstrate a fiber laser cavity using a TFF as a gain medium for the generation of CW and pulsed laser outputs at the S+/S band region. Additionally, this work will also optimize the design of the laser cavity for selected applications.

In this regard, four research objectives will guide this work. These objectives are:

- To design and characterize a laser cavity using a TFF as the linear gain medium and pumped by a 1400 nm source for S band lasing.
- To study the tunability of the TFF laser in the S+/S band region by inserting the Tunable Bandpass Filter (TBPF) into the cavity to tune the central wavelength.
- To investigate the TFF amplifier and its characterization in the S+/S band region in terms of signal gain, gain bandwidth, and noise figure.
- To study the generation of Q-switched, Mode-locked, and Dual-wavelength, Q-switched TFF pulsed lasers in the S+/S band region using an SA from a different type of materials.

1.5   Research Methodology

There are two approaches of saturable absorber used in this study, which included the thin film and exfoliation layers. Single-walled carbon nanotube (SWCNT) and graphene were used as a thin film fabricated and prepared by the Centre for Advanced Photonics and Electronics (CAPE), University of Cambridge, United Kingdom. Whereas, Molybdenum disulfide (MoS_2) and Gallium Selenide (GaSe) were prepared using a simple mechanical exfoliation technique, which will be briefly explained in the next chapter. Both of the SA is then carefully attached to the fiber ferrule. A small portion of index matching gel is used to help stick the SA onto the face of the fiber ferrule. The fiber ferrule is then connected to another fiber ferrule using an FC/PC adaptor, thus creating the complete SA assembly. This assembly is, therefore, the SA that will be incorporated into the laser cavity.

The Raman spectrum of the SA is analyzed using a Renishaw Raman spectroscope at an excitation wavelength of 532 nm and 1800 l/mm grating. Whereas, the linear absorption spectrum of the SA is obtained using white light, and the absorbance of the thin film measures for a region between 900 to 1600 nm. The nonlinear optical absorption measurement of the SA was obtained using the twin detector technique that will be briefly explained in the next chapter.

The experimental setup of the Q-switched and mode-locked TFF laser system in this study consist of 1400 nm FOL1405RTD laser diode (LD), 1400/1500 nm fused wavelength division multiplexer (WDM), Oplink OISSG-1480SO1111 Isolator (ISO), 90:10 optical tap coupler and Agiltron Inc. FOTF-025121332 tunable band-pass filter (TBPF). The gain medium used in this study is Fiberlabs Inc. TFF, with an absorption rate of 0.15 dB/m at the wavelength of 1400 nm, as well as a numerical aperture value of 0.26 and a mode-field diameter of 4.5 μm at 1500 nm.

Anritsu MS9740A Optical Spectrum Analyzer (OSA) is used to examine the spectral characteristics of the generated output, while a Yokogawa DLM2054 Oscilloscope (OSC) and a Newport 818-BB-51F InGaAs, 12.5 GHz photodetector are used to observe the output pulse train. The signal-to-noise ratio (SNR) of the generated laser is obtained using an Anritsu MS2683 Radio-Frequency Spectrum Analyzer (RFSA), while the output power is monitored using a Thorlabs PM100USB optical power meter (OPM) with a powerhead S1444C. In addition, a two-photon absorption Alnair HAC-200 autocorrelator (AC) was used to analyze the pulse width of the mode-locked pulses.

1.6   Thesis Overview

This thesis consists of five chapters, including this chapter, which introduced a background of knowledge on fiber laser development, especially in the S band region. The research objectives of this thesis are also described in the current chapter.

Chapter 2 discusses the properties of TFF, including the elements of rare-earth and host material. Other than that, the brief explanation of population inversion and principle of laser operation, as well as the gain measurement of amplifier, is provided in this chapter. The possible modes of laser operation, including Q-switching, mode-locking, and dual-wavelength Q-switching generates in this study using an SA is presented last.

In Chapter 3, the generation of the TFF laser and amplifier in the S+/S band are presented. The measurement of the ASE, as well as the CW of TFF laser and its tunability, are also discussed in this chapter. The experimental analysis on the gain measurement of the TFF amplifier is discussed in terms of saturation gain, gain bandwidth, and characterization of noise figure. Together with the guidance from my supervisor, I designed, implemented and characterized the generated laser and amplifier in this experiment.

Chapter 4 discusses the generation of pulsed and dual-wavelength of TFF laser in the S+/S band region. First, the passively Q-switched TFF lasers are presented using different SAs, including SWCNT, graphene, MoS_2, and GaSe. Other than that, the generation of dual-wavelength, Q-switched TFF laser, as well as the generation of mode,-locked TFF laser passively using In_2Se_3 as SA, are also presented in this chapter. The above generated pulsed lasers are presented in terms of the experimental setup, characterization of SA, and final results. Chapter 4, in part, is a reprint of the material as it appears in "S-band Q-switched thulium fluoride fiber laser using graphene saturable absorber" in the Journal of Laser Physics authored by H. Ahmad, **S. A. Reduan**, N. A. Hassan, S.I. Ooi and Z. C. Tiu. "Tunable passively Q-switched thulium-fluoride fiber laser in the S+/S band (1450.0 to 1512.0 nm) region using a single-walled carbon-nanotube-based saturable absorber" in Journal of Applied Optics was authored by H. Ahmad, **S. A. Reduan**, A. Z. Zulkifli and Z. C. Tiu, "Molybdenum disulfide (MoS_2)–based, tunable passively Q switched thulium-fluoride fiber (TFF) laser" is published by the Malaysian Journal of Fundamental and Applied Sciences authored by **S. A. Reduan** and H. Ahmad, "S+/S band passively Q-switched thulium-fluoride fiber laser based on using gallium selenide saturable absorber" published in Journal of Optics and Laser Technology was also written by H. Ahmad and S. A. Reduan, "Dual-wavelength Q-switched thulium-fluoride fiber laser for S+/S band using molybdenum disulfide (MoS_2) as a saturable absorber" is published in the Journal of Laser Physics authored by H. Ahmad, **S. A. Reduan** and R. Safaei and "Mechanically exfoliated In_2Se_3 as a saturable absorber for mode-locking a thulium-doped fluoride fiber laser is operating in S-band" in Journal of Applied Optics authored by H. Ahmad, **S. A. Reduan**, S. I. Ooi, and M.A. Ismail. Together with the guidance from my supervisor, I designed, implemented and characterized the generated laser in these reprint materials.

Finally, Chapter 5 summarizes the works in this thesis. The suggestions for future works are also presented in this chapter as an extension of this thesis.

CHAPTER 2: A REVIEW ON THULIUM DOPED FLUORIDE FIBER LASERS

2.1   Introduction

Silica glass has been the leading choice of material for the fabrication of optical fibers due to it being readily available and its abundant quantities. In particular, amorphous silicon dioxide (SiO_2), which is also known as fused silica is the dominating material in fiber fabrication due to its advantageous properties compared to other types of glass. Other than that, silica can withstand a reasonable high temperature for fiber fabrication and can undergo high current arc fusion splicing very well. Silica also has a wide wavelength range with good transparency that allows low absorption and scattering loss, which caters well for communication windows. The most common wavelength range for optical communication windows is between 830 nm to 1550 nm (Wartak, 2013). On top of this, it also has a high degree of chemical resistance as well as being hydrophobic, making it suitable for use in environments that have high humidity levels.

Rare-earth elements can be easily added as dopants in silica optical fibers as well as other host materials such as fluoride and tellurite-based fibers and even ytterbium glass fiber for applications in various fields. These kinds of fibers have successfully generated a high-power laser and amplifier.

In this chapter, TFF is used as a gain medium to generate a laser and amplifier in the S+/S band region. A brief background on the thulium rare-earth element is presented as well as the host materials which is fluoride-based due to its properties of a low phonon energy material that can reduce the non-radiative transition rate of the rare-earth gain element (Peterka et al., 2004). The energy level system and operation of the laser, as well as the gain measurement of the laser amplifier, are given subsequently in the chapter. This chapter also provides some introduction to the different pulse mode operation of a fiber

laser such as Q-switching and mode-locking, and also dual-wavelength, Q-switched operation.

2.1.1 Thulium, Tm^{3+} Ions

Rare-earth elements are the group of seventeen chemical elements in the periodic table as defined by the International Union of Pure and Applied Chemist (IUPAC). These chemical elements are precise elements of 57 (La) to 71 (Li), including Sc and Y (Leigh, 1990). An idea of rare earth element terms refers to a small number of elements that are present in the crust of the earth. The group of elements from 57 (La) to 71 (Lu) is known as lanthanide elements, which have been used in the photonics applications due to their optical behavior.

The rare-earth element plays an essential role in various fields of applications. One of them is known as lanthanides, which is widely used in laser as co-dopant of optical fiber for amplifier and lasers (Bünzli et al., 2005). The favorable optical feature of the lanthanide elements is that they exhibit an incomplete sub-shell of *4f* (Becker et al., 1999). The electrons of the sub-shell of *4f* are not involved in the bonding of the nearby atoms and are located near to the core compared to the valence layer. The electrons can move freely between different energy levels in the sub-shell of *4f* with the well-bounded energy transition. As the Lanthanide ions dissolve in a glass, their transition spectra are nearly similar to the spectra of free ions, as well as become a trivalent rare earth ionization state of elements (Digonnet, 2001). All known trivalent rare elements exhibit a 4-level lasers system. Other than that, the lanthanide ions can break the symmetry encouraged by the perturbations, which results in a possible electronics transition.

One of the well-known lanthanides is Thulium ion (Tm^{3+} ion) that have become a favorable element due to their capability of generating laser in a wide-band region. Figure 2.1 shows the common energy level diagram of Tm^{3+} ion for all the transitions.
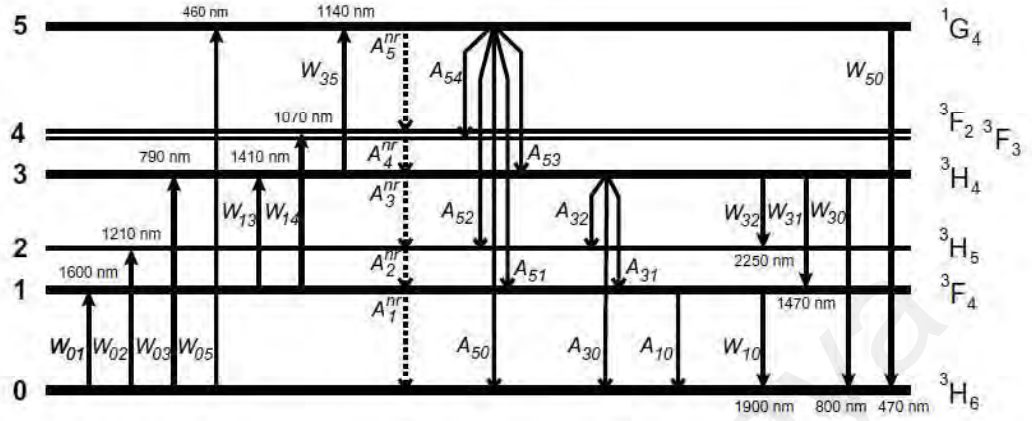
Figure 2.1: Energy level diagram of Tm^{3+} ions with all transition[3]

It can be observed in Figure 2.1 that the emission of S band when the transition takes place from $^3H_4$ to $^3F_4$ with a lasing wavelength of around 1470 nm (Peterka et al., 2004). As reported by Florida et al. (Floridia et al., 2004) and Aosaza et al. (Aozasa et al., 2000a), the emission in S band for Tm^{3+} ion can be achieved by single up-conversion pumping and dual-wavelength pumping. In the dual-wavelength pumping, two pump lasers of different wavelengths are used to accomplish the two-level energy hopping. For instance, a co-pumping mechanism utilizing 800 nm and 1050 nm wavelength lasers into Thulium-doped fiber for S band emission (Gomes et al., 2003). In the co-pumping process, the 800 nm pump induces Thulium GSA from $^3H_6$ to $^3H_4$, while the 1050 nm pump depopulates the lower level $^3F_4$ using a strong ESA to level $^3F_2$; which simultaneously populates the level $^3H_4$, through $^3F_2$. Both the pumping effects are advantageous to create the population inversion. Ultimately, the emission in S band is achieved through the energy relaxation from $^3F_4$ to $^3H_4$.

---

[3] (Reproduced with permission from Peterka, P., Faure, B., Blanc, W., Karasek, M., & Dussardier, B., 2004)

Compared to dual-wavelength pumping, the single up-conversion pumping technique is much less complicated to implement, as it requires only a single pump laser. Two common wavelengths are widely used for single up-conversion pumping; 1050 nm and 1400 nm (Aozasa et al., 2000a; Floridia et al., 2004). Generally, both 1050 nm and 1400 nm wavelength pumps perform GSA from $^3H_6$ to $^3F_4$ and ESA from $^3F_4$ to $^3H_4$.

Nevertheless, in the details of energy hopping, 1050 nm requires two depopulation processes from $^3H_5$ to $^3F_4$ energy level, and $^3F_2$ to $^3H_4$ energy level. Therefore, 1400 nm wavelength pumping technique has the advantage of direct GSA and ESA compared to the 1050 wavelength pumping technique. Previous work by Aozasa et al. (Aozasa et al., 2000a) had used a 1400 nm pumping source for S band amplification in the Tm-doped fiber amplifier, which resulted in gain covering a wavelength range from 1480 nm to 1510 nm. Thus, it proves that 1400 nm is an efficient pumping source for generating laser in the S+/S band region.

The absorption and emission cross-section spectra of thulium are given in Figure 2.2. It can be seen that the possible transition of absorption and emission in the S band region falls on the same energy level of transition, which is in between $^3F_4$ and $^3H_4$. This is supported by a previous reported work by Aozasa et al. (Aozasa et al., 2000a).
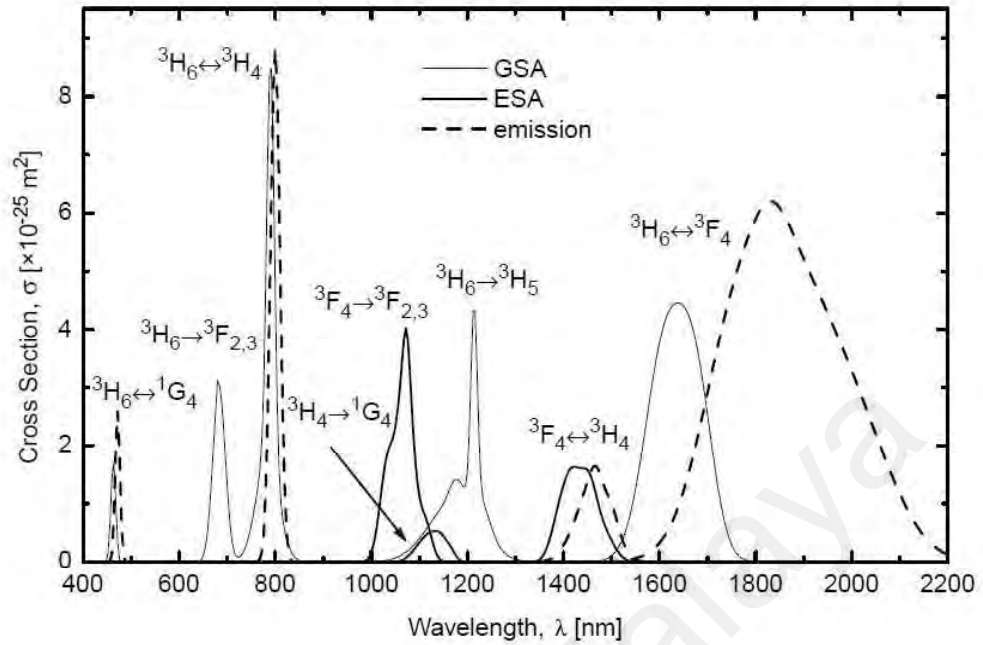
Figure 2.2: The absorption and emission cross-section spectra of Tm^{3+} ions[4]

2.1.2   Fluoride as Host Materials

In this work, fluoride fiber is used as the host material for the Tm^{3+} rare-earth dopant. Although thulium can be doped into silica fibers, which is available in the market, these would only be able to operate in the 2-micron region. For the shorter wavelength region of S+/S as one, the emissions in this region is inhibited. This is due to the substantial probability of possible nonradiative decay via the intermediate level $^3H_5$ that occur in between the transition of $^3H_4$ to $^3F_4$, especially for silica fiber host (Peterka et al., 2004). Therefore, the host fiber of a gain medium plays a vital role in enhancing the efficiency in generating the fiber laser. In this regard, fluoride fiber is used as a host material in this study.

The fluoride fiber used in this work as a host material is known as a ZrFM$_4$-BaF$_2$-LaF$_3$-AlF$_3$-NaF (ZBLAN). Fluorizirconate glass was discovered by Poulain and Lucas in

---

[4] (Reproduced with permission from Peterka, P., Faure, B., Blanc, W., Karasek, M., & Dussardier, B., 2004)

1975 at the University of Rennes in France (Poulain et al., 1975). Other than being the most stable fluoride glass for fiber fabrications, ZBLAN has a broad transmission window that covers a UV to mid-IR region. Figure. 2.3 shows the attenuation loss of ZBLAN over a different wavelength (Jia, 2017).
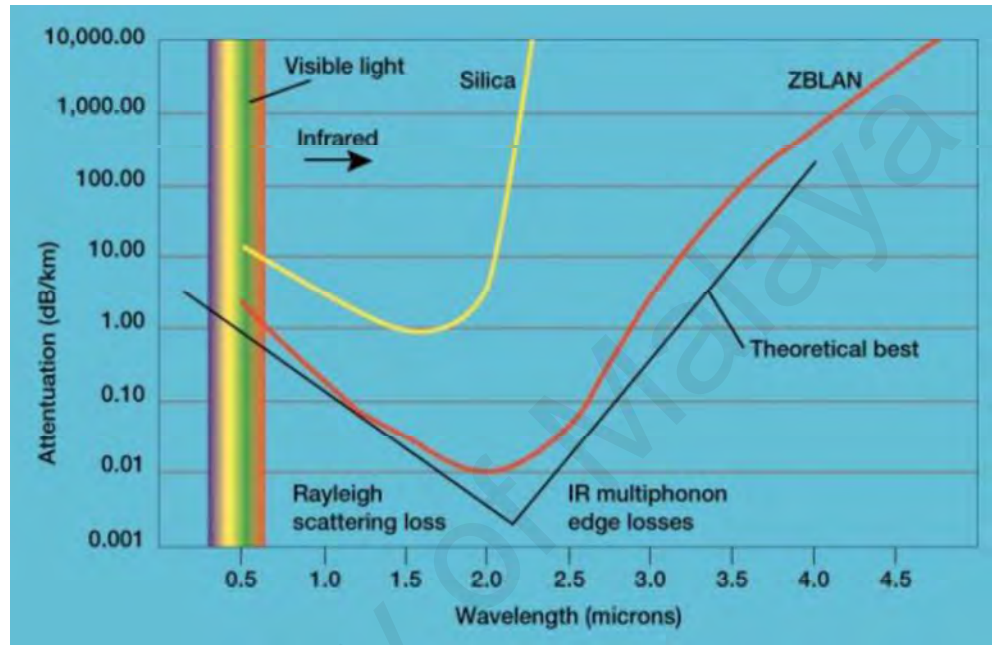
Figure 2.3: The attenuation loss of ZBLAN over a different wavelength[5]

In Figure 2.3, the attenuation trends of ZBLAN show that it is nearest to the theoretical curve compared to the silica glass, which proves that the capability of ZBLAN glass as a good host for generating a fiber-based laser. Other than that, ZBLAN has small phonon energy of 600 cm[-1,] which makes it a suitable candidate as a host material. Other than that, ZBLAN exhibits a low glass transition temperature, low-temperature dependence of refractive index, and low refractive index. Table 2.1 shows the characteristics of ZBLAN.

---

[5] (Reproduced with permission from Jia, C., 2017)

Table 2.1: Characteristics of ZBLAN (fluorizirconate glass composition, ZrFM4-BaF2-LaF3-AlF3-NaF)

Properties	Value
Transmission Window	~ 250 nm to 7 µm
Refractive Index	~ 1.5
Glass Transition Temperature	260 °C
Phonon Energy	600 cm^{-1}

2.1.3 Population Inversion: Four- Energy Level System Thulium-Fluoride Fiber

The lasing action is based on a 4 level system (Kozak et al., 2004) whereby the population inversion must be achieved in the laser cavity. In this circumstance, population inversion plays a crucial role in generating a laser, and it only occurs when the number of electrons in the excited state is higher than the number of electrons in the lower state. The statistics of the distribution of the particles in thermal equilibrium followed the Boltzman distribution law shown in Eq. 2.1. This is known as the basic statistics on the distribution of particles at thermal equilibrium.

$$N_2 = N_1 \exp\left(-\frac{E_2 - E_1}{k_B T}\right) = N_1 \exp\left(-\frac{h v_0}{k_b T}\right) \qquad (2.1)$$

where $E_2 > E_1$ ($E_2 - E_1 = h v_0$). v_0 is the resonant frequency between to two energy level, T is the temperature in Kelvin, k_B is the Boltzman's constant, E_2 is the energy at level 2 and E_1 is the energy at level 1.

To achieve population inversion, the higher energy state has a greater population than the lower energy state, then the light in the system undergoes a net increase in intensity. This can be written as

$$N_2 > N_1$$

The process of attaining a population inversion is called a pumping process. Figure 2.4 illustrates the simple energy level in achieving the population inversion. A four energy

level system is one of the basic pumping schemes of laser operation to create a population inversion. The system is pumped with radiation of energy E_{41} then atoms in State 4 relax to State 3 non radiatively. The electrons from E_3 will now jump to E_2 to give out radiation. Then they will return to ground state Level 1 through non-radiative relaxation.
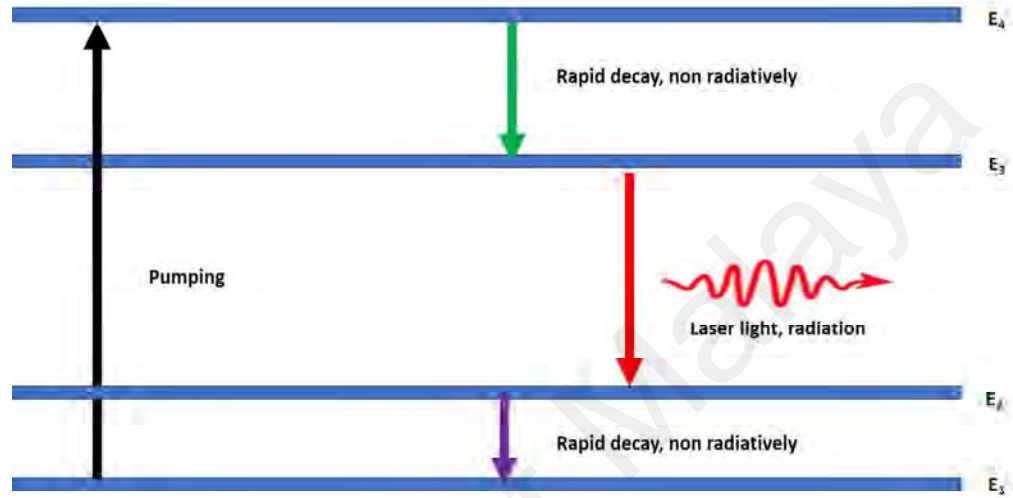
Figure 2.4: The energy level on achieving the population inversion

2.1.3.1 Transition energy of Tm^{3+} ions

One of the rare earth elements which exhibit emission in a wide spectral range, as shown in Figure 2.1, is important in many fields of application. It can be seen from the figure that the S band emission takes place from $^3H_4$ to $^3F_4$. Whereas the absorption used in this study is at the wavelength of 1400 nm. Figure 2.5 shows the pumping scheme of Tm doped fiber amplifier for emission in the S band region using a 1400 nm source as a pumping source (Aozasa et al., 2000a).
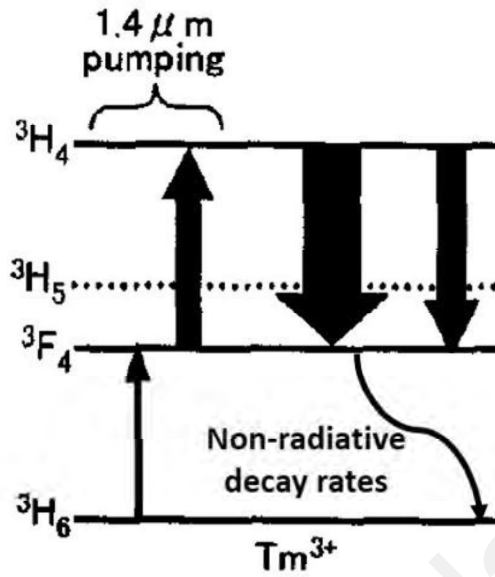
Figure 2.5: Pumping scheme of Tm-doped fiber using 1400 nm pumping source[6]

Atomic rate equations are used to model the gain of the Tm^{3+} ions depending on their corresponding energy level of transition. This work used a 1400 nm pumping mechanism that only involves a four-level system, as shown in Figure 2.5. For simplicity, only the rate equations for the populations of ion, N at the ground, first and third level are presented as follows (Peterka et al., 2004)

$$\frac{dN_0}{dt} = -N_0(W_{01} + W_{03}) + N_{1(}A_{10} + A_1^{nr}) + N_3 A_{30} \tag{2.2}$$

$$\frac{dN_1}{dt} = N_0 W_{01} - N_1(W_{13} + A_1^{nr} + A_{10}) + N_3(W_{31} + A_3^{nr} + A_{32} + A_{31}) \tag{2.3}$$

$$\frac{dN_3}{dt} = N_1 W_{13} - N_3(W_{31} + A_3^{nr} + A_{31} + A_{30}) \tag{2.4}$$

$$N_t = N_0 + N_1 + N_3 \tag{2.5}$$

---

[6] (Reproduced with permission from Aozasa, S., Sakamoto, T., Kanamori, T., Hoshino, K., Kobayashi, K., & Shimizu, M., 2000)

where W_{ij} is the stimulated absorption and emission rate for the amplified spontaneous emission (ASE), whereas A_{ij} and A_3^{nr} are the spontaneous decay rate for the radiative and non-radiative decay rates from Level i to j, respectively. N_t is the total thulium dopant concentration.

2.1.4 Principle of TFF Laser Operation

The fiber laser operates on the same basic principle as a conventional laser, comprising of a gain medium and an optical cavity with a feedback loop. In this work, a ring cavity is normally used instead of a linear version. Figure 2.6 shows the setup of a simple fiber laser cavity that includes a wavelength division multiplexer (WDM), gain medium, isolator (ISO), output coupler, and pumping source.
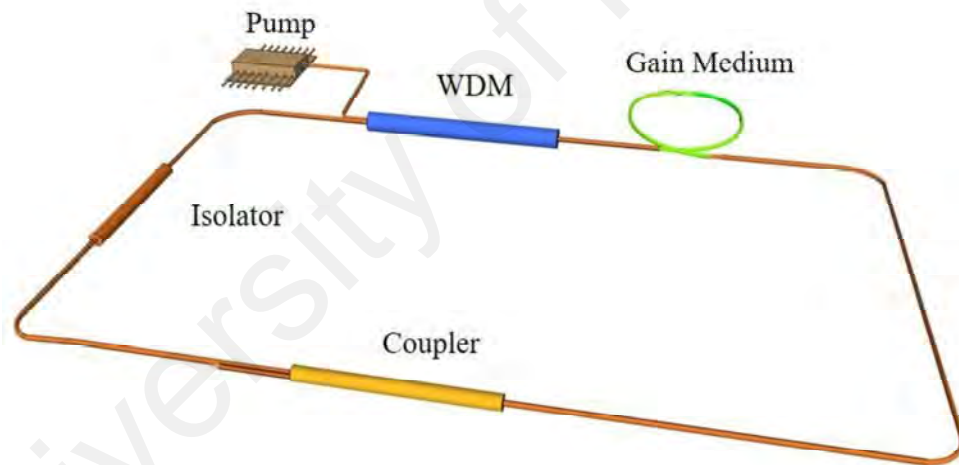
Figure 2.6: Simple fiber laser cavity setup

Figure 2.6 shows the typical ring fiber laser cavity laser consists of a pumping source, WDM, gain medium, coupler, and isolator. WDM is used to pump the light into the ring cavity system whereby the gain medium is served to amplify the light. ISO is needed in the cavity to ensure the unidirectional of the light propagating in the cavity. Whereas, a coupler is employed to ensure a certain amount of light propagates back into the cavity, and another ratio is extracted out from the system for analyzing purpose.

The energy level diagram of the TFF laser and the flow of stimulated emission in the system using a single wavelength pump power source at 1400 nm is illustrated in Figure 2.7. These figures show the transitions between energy levels of $^3H_6$, $^3F_4$, $^3H_5$, and $^3H_4$. One of the reasons for choosing 1400 nm as a single-wavelength pump source in this study was due to its preferable wavelength in the optical pumping process that has a variety of available optical components.
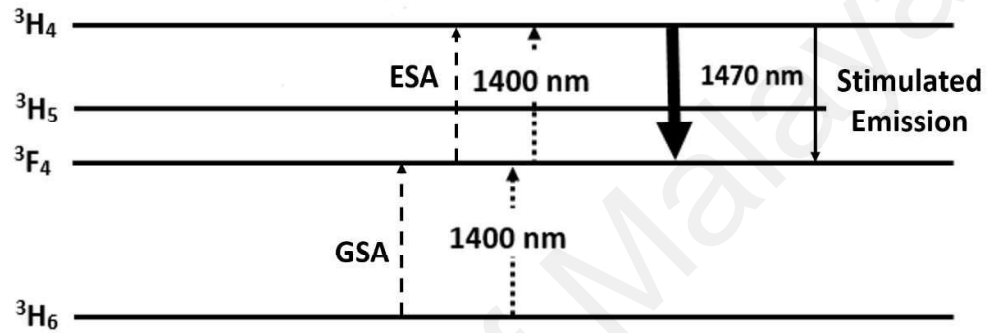
(a)
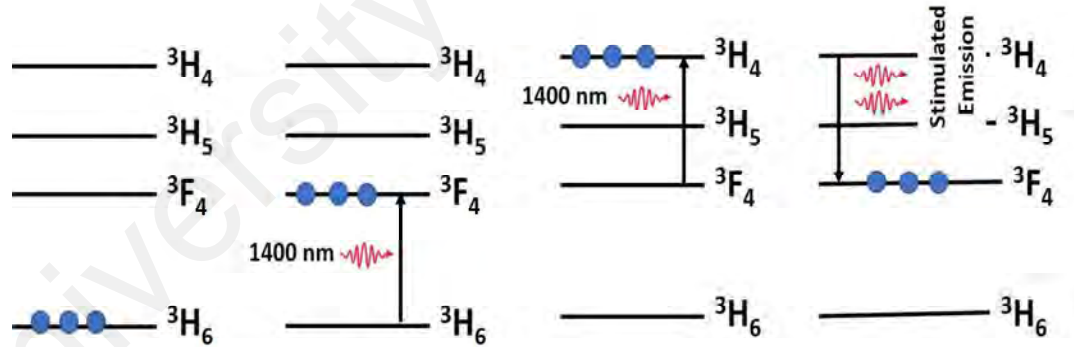
(b)

Figure 2.7: (a) Energy level diagram of Thulium-Fluoride fiber laser for 1400 nm pumping scheme. (b) The flow of stimulated emission of Thulium-Fluoride system

From Figure 2.7, it can be seen that a single up-conversion pumping technique is utilized in this pumping scheme. The single up-conversion pumping technique is preferable compared to the dual-wavelength pumping technique due to its effectiveness in implementation. Single up-conversion pumping involves two or more pump sources to

excite the laser ion to the excited state (Simpson et al., 2008). As the gain medium is pumped by the 1400 nm pump source, the Tm^{3+} ions excite from the $^3H_6$ ground state to the $^3F_4$ state by GSA and then undergoes ESA from $^3F_4$ to $^3H_4$ as shown in Figure 2.7 (a). Then, the transition will drop from $^3H_4$ to $^3F_4$ as the population inversion is achieved and emits a stimulated photon as shown in Figure 2.7 (b). Even though the lifetime of $^3H_4$ is shorter than the lifetime of $^3F_4$, it makes the system a self-terminating laser system (Kozak et al., 2004). However, this problem can be overcome using a thulium-doped fiber with higher Tm^{3+} ions (Aozasa et al., 2000b). In this study, a TDF with around 3,200 ppm mol is used as a gain medium. In this regard, a low population inversion can be achieved between the energy level of $^3H_4$ and $^3F_4$. Thus, this is normally considered as a four-level system. In detail, 1400 nm pumping scheme involves a direct GSA and ESA compared to the 1500 nm pumping scheme that seems to be an advantage using a 1400 nm pump source to generate laser for the TFF laser system.

The host fiber is a critical element in determining the efficiency of amplification in the S band region. In silica fibers, the up-conversion technique is unsuitable due to the high phonon energies of silica, which leads to strong multi-phonon transitions that result in the difficulty to achieve a population inversion. In this regard, fluoride fibers are a good alternative host fiber as they have relatively low phonon energy. Therefore, the S band amplification can be easily achieved by doping thulium into fluoride fibers.

2.1.5   Characteristics of Fiber Amplifier

The amplification of the proposed amplifier setup is determined by calculating the gain profile, G using a simple equation

$$G = \frac{P_{out}}{P_{in}} \tag{2.7}$$

where P_{in} is the input signal power and P_{out} is the output signal power.

Another essential characteristic of the fiber amplifier is the small signal gain that can be defined as the gain that corresponds to the input power levels and independent of the input signal when the signal amplification is not reduced (Derickson, 1998). The input signal power is low for investigating the small signal gain. The expression of the small signal gain of the amplifier is as shown below

$$G(\infty) = \exp\left\{\left[\frac{1-\frac{\eta_p}{\eta_s}}{1} + \eta_p\right]\rho_0\sigma_e L'\right\}b \qquad (2.8)$$

where η_p and η_s, are the ratio of emission to absorption cross-section at the pump and signal wavelength, whereas ρ_o and σ_e are peak dopant density and total emission cross-section, respectively. $L' = \Gamma_s L$ is known as the reduce effective length that accounts for the reduced mode overlap effect.

For an input signal at high power, the gain observed is recognized as a saturated gain. At this stage, the gain curve departs from the linear gain relations. The saturated increase corresponds to the input saturation power for which it can be defined as the input signal power needed to reduce the net amplifier gain by 3-dB, this equivalent to

$$G = G_{max} - 3\,dB \qquad (2.9)$$

where G_{max} indicates a small-signal gain. The measurement of saturated gain is important to characterize the performance of the power amplifier of the system.

2.2   Modes of Operation in TFF laser with SA

There are different modes of laser operation observed in this study; CW, Q-switching, mode-locking, and dual-wavelength, Q-switching. SA is used as a nonlinear optical material to generate the Q-switched and mode-locked pulses in the TFF laser system. The SA used in this thesis is based on two-dimensional (2D) materials, and this will be discussed in detail later in this chapter in Section 2.2.4. Whereas, the combination of SA

and photonics crystal fiber (PCF) are used in the laser system to generate dual-wavelength, Q-switched pulses. The following subsection describes the possible modes of laser operation in the TFF laser system with SA as well as a brief discussion on SAs.

2.2.1 Q-switching

The generation of Q-switched pulses that began in 1961 by Hellwarth, predicted that the laser could emit a short pulse when the loss of optical resonator switches rapidly from high to low. This phenomenon was then experimentally proven by Collins and Kisliuk in 1962 as well as McClung and Hellwarth in 1962. The Q-switching operation can be generated by controlling the quality factor (Q-factor) of the laser resonator, which results in the creation of laser pulses with short duration (microsecond to nanosecond) and high peak power. Q-factor describes the strength of the damping of the system's oscillations. The Q-factor is presented by

$$Q = \frac{2\pi f_0 \varepsilon}{P} \tag{2.10}$$

where f_o represents the resonant frequency, ε is the stored energy in the cavity, and $P = -dE/dt$ as power dissipates. Generally, Q-switching occurs when there is a rapid change of Q-factor from low to high value, which generates an intense lasing compared to CW lasing output. The Q-switching operation is applicable in various fields such as material processing, spectroscopy, sensing, and medicine.

Q-switching operation results in short and intense laser pulses, which are also known as "giant pulses." In this operation, the cavity loss is initially high with a low Q-factor, and eventually, the pump energy is accumulated in the gain medium. Ideally, the Q-factor is controlled using a shutter in the laser system. As the lasing is prevented by the high loss, the population inversion is built up by the pumping process to a more significant value than normal over a period. Eventually, high Q-factor allows the lasing

to generate and then accumulate energy, which will be stored in the gain medium release in an intense pulse laser with a typical duration range from μs tons.

Q-switched pulses can be generated actively or passively. An external device is needed for active Q-switching to modulate the laser in the system, which eventually has a control over the characteristics of the output, including the repetition rate and pulse width. Nevertheless, bulky components, complexity, and high costing are the limitations of this system, which eventually reduces the suitability of the applications (B. Chen et al., 2015). Therefore, the development and enhancement of generating Q-switched passive have become a great interest among the researchers. Passive Q-switching exhibits the advantage of being a compact and cost-effective system even though it provides less control over the parameter of the output pulses.

2.2.1.1 Passive Q-switching

The concept of passive Q-switching operation is generally the same for which the shutter in the laser system is replaced by the intracavity SA. As the SA integrated inside the laser cavity, the laser starts to circulate, and the SA begins to bleach due to the increasing intensity of the laser as the spontaneous emissions occur. Thus, the SA is strongly bleached by the intense lasing, and the process repeatedly occurs. After the SA is being bleached, the laser will gain well in excess of the losses and leads to the generation of Q-switched pulses. Figure 2.8 shows the temporal evolution of gain and losses in a passively Q-switched laser (F. D. Muhammad, 2014).
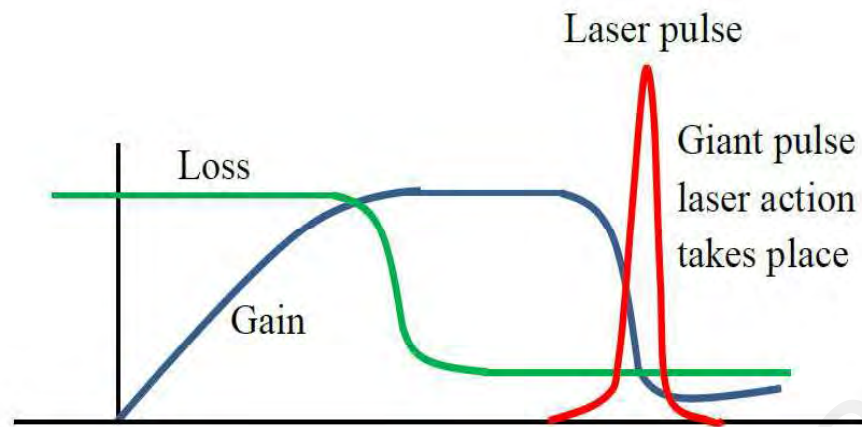
Figure 2.8: Temporal evolution of gain and losses in Passive Q-switched pulsed laser[7]

It can be seen from Figure 2.8 that after the gain of laser exceeds the resonator losses; a short pulse is generated. At the time of laser pulse generation, the gain plummets drastically. The peak intensity of the laser coincides with the point when the gain equals to the loss of the resonator. The characteristics of the Q-switched output pulses are investigated in terms of several parameters, including repetition rate, pulse width, average output power, pulse energy, and peak power.

2.2.2   Mode-locking

Mode-locking is a technique for generating a pulse with femtoseconds to picoseconds durations. These generated pulses, also known as ultra-short pulses. In a conventional laser system, longitudinal modes have a random phase relative to each other. Using this technique, the phases of these modes can be locked together, hence the term mode-locking. The longitudinal modes are being induced to oscillate with each other in a fixed phase to achieve the mode-locking phase. Then, the induced longitudinal modes interfere with each other by oscillating inside the cavity results in the ultra-short pulse train.

---

[7] (Reproduced with permission from Muhammad, F. D., 2014).

Typically, an intracavity loss modulator is used to fix the phase of all the laser modes to generate mode-locked pulses.

The fundamental repetition rate of the generated mode-locked laser is determined by the total length of the laser system as shown

$$Repetition\ rate = \frac{c}{Ln} \qquad (2.11)$$

where L, c and n represent the length of the cavity, speed of light, and refractive index, respectively. The inverse of repetition rate is known as the round-trip time or period, T_R, thus

$$Round - trip\ time\ or\ period, T_R = \frac{Ln}{c} \qquad (2.12)$$

The equation of the repetition rate of the mode-locked pulses shows the repetition rate corresponds to the cavity length of the laser system. Therefore, it can predict that the longer cavity length results in a lower repetition rate and vice-versa.

Similar to Q-switching, the mode-locking operation can be generated actively or passively. In active mode-locking, the periodic modulation of the resonator loss in the system is done using either an acousto-optic or electro-optic modulator. On the other hand, passive mode-locking is commonly used an SA to modulate the resonator loss. The SA is able to modulate the loss faster than and electronic modulator. In this regard, extensive research on the passive generation of the mode-locked pulses is undertaken, which will have applications in various fields such as medicine, sensing, and communications.

2.2.2.1 Passive Mode-locking

As mentioned earlier, SA is used to generate a mode-locking passively. In this operation, the loss inside the intracavity of the laser system is due to the SA, which is relatively small for high intensity and vice-versa, in generating a short pulse. Therefore, loss modulation in the system is produced by a short pulse. This is because the high intensity of the pulse strongly saturates the absorber compared to the low intensity at the wing of the pulse. This modulation loss is due to the fast-initial loss saturation by the pulse duration. Then, a recovery by the SA takes place, which is typically known as "slow recovery" that depends on the absorption's mechanism of the SA.

Other than that, the mode-locking operations start as the circulating pulses saturate the gain until the losses are compensated by the pulse itself. Whereas, the remaining circulating light with a low intensity that had more loss than gain will eventually perish out during the next cavity round trips. As mentioned by Keller et al. (Keller, 2004), the operations start from normal fluctuations of noise in the system for which a single noise spike is strong enough to reduce its loss in the SA. Therefore, the strong enough noise will continuously spike in lowering the loss until it reached a steady state where the stable pulses successfully formed. Figure 2.9 shows the temporal evolution of optical power and losses in a passively mode-locked laser with a saturable absorber. In Figure 2.9, the loss modulation becomes fast due to the loss modulation of the SA, which results in the wing of the pulse, whereby the recovery of the SA takes some time to stabilize.
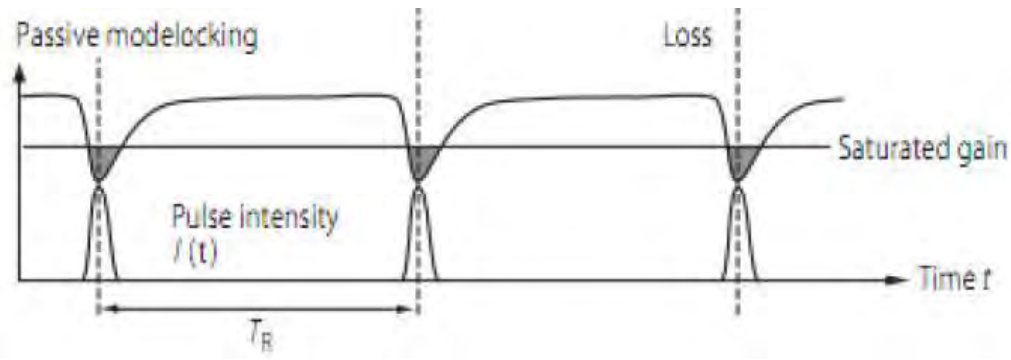
Figure 2.9: The temporal evolution of optical power and losses in a passively mode-locked laser with a saturable absorber[8]

2.2.3 Dual-wavelength Q-switching

In this thesis, PCF is used to generate the dual-wavelength lasing, whereby SA is used to generate the Q-switched pulses. The usage of PCF into the laser cavity is to produce the Mach-Zehnder interferometry effect on the laser operation that leads to the generation of dual-wavelength laser output. The procedure involves the mechanism of tunable Mach-Zehnder filter (TMZF), based on the interference of two coherent monochromatic sources affected by the length of difference and, eventually, the phase difference between two sources. As in this case, the core and cladding of the PCF act a role as arms of Mach-Zehnder filter, whereby the splicing points between PCF and single-mode fiber (SMF) play a role as couplers splitting or combining light powers in the arms of the filter. As the refractive index of the cladding is smaller than the core, the different optical paths which correspond to the arms of the Mach-Zehnder filter could be achieved and leads to the accumulation of phase difference along the PCF to generate a dual-wavelength operation. Figure 2.10 illustrates a brief explanation of the TMZF mechanism.

---

[8] (Reproduced with permission from Keller, U., 2004)
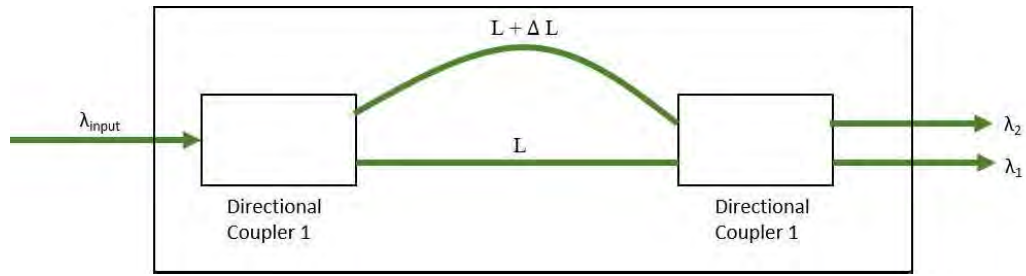
Figure 2.10: Principle of Tunable Mach Zehnder Filter (TMZF)

The TMZF is based on the interference of two coherent monochromatic sources that are affected by the length difference and eventually, the phase difference of two paths, as shown in Figure 2.10 (Agrawal, 2001; Djordjevic et al., 2010). As shown in Figure 2.10, the optical power input is equally split (directional coupler 1) when entering into a waveguide, in which the two arms of the Mach-Zehnder filter have a length difference of ΔL. These lights combine (directional coupler 2) at different phases, for which each wavelength interferes constructively with one of the two output port and destructive on the other, based on the phase variation and the position of the output fiber (Agrawal, 2001; Djordjevic et al., 2010). Thus, by adjusting the quantity of ΔL, the Mach-Zhender filter can be tuned to obtain the desired phase shift at the output port. Therefore, controlling the propagation delay of the path $L + \Delta L$ with respect to path L will allow it to control the phase shift.

There are various applications based on dual-wavelength lasers such as Raman scattering spectroscopy (Ganikhanov et al., 2006), multi-color pump-probe process (Manzoni et al., 2006) and conversion of nonlinear frequency (Zhu et al., 2013). Other than that, this phenomenon is believed able to enhance functionality in microwave generation and LIDAR (Jia, 2017). Sierra-hernandes et al. (Sierra-Hernandez et al., 2013) had successfully demonstrate a dual-wavelength laser using PCF at the wavelength region of 1530 nm to 1556 nm. However, there are no reports on generating a dual-wavelength in the S+/S band region.

2.2.4 Saturable Absorber

An SA is defined as an optical device that exhibits a lower loss for an intense light. SA is capable of absorbing light in different degrees, which depends on the intensity of the incident light. A high degree of absorbance corresponds to the low intensity that will eventually cause a low degree of absorbance by a saturated absorption for an intense light.

SAs, including semiconductor saturable absorber mirrors (SESAMs) and more recently 2D and three-dimensional (3D) nanomaterials such as carbon nanotubes (CNTs) and graphene (D Popa et al., 2011; Zhipei Sun et al., 2010b) are typically integrated into the fiber laser cavities to generate Q-switched outputs, with the latter seeing increasing application due to their low fabrication cost and complexity. Such is the potential for SAs in developing compact, and high-performance Q-switched fiber lasers that research efforts into developing new SA materials have intensified. These include the exploration of topological insulators (Lee et al., 2015; Lee et al., 2014) as well as transition metal dichalcogenides (TMDs), such as molybdenum disulfide (MoS_2) (Lin et al., 2015). These materials are able to generate a consistent and high-performance Q-switched pulse.

Four types of material are used in this experiment from different groups of material, including graphene, carbon nanotube (CNTs), TMD, which is molydenum disulfide (MoS_2), and the topological insulators are gallium selenide (GaSe) and Indium Selenide (In_2Se_3). Graphene, a flat 2D carbon monolayer, has attracted attention due to its applicability in various applications in photonics because of its remarkable optical. Graphene exhibits an ultrafast recovery time that results in an excellent saturable absorption property (Bao et al., 2009; Z. Sun et al., 2010) as well as having a zero bandgap energy. Another well-known and amongst the earliest SAs is the single-walled carbon nanotubes (SWCNTs) (Harun et al., 2012; Martinez et al., 2013; Zhou et al., 2010). SWCNT has a direct bandgap, which is efficient in absorbing and emitting the light that

becomes one of the reasons SWCNT has become a great discovery of 2D materials as SAs (M. A. Ismail, 2015).

Another promising 2D material in generating pulses is Transition Metal Dichalcogenides (TMDs). Molybdenum disulfide (MoS_2) is one of the high potential TMD materials that act as an SA (Luo et al., 2014; M. Zhang et al., 2015). This is because of their characteristics of exhibiting a thickness-dependent band-gap and electronic band structure (Q. H. Wang et al., 2012) as well as having a strong optical saturable absorption and light-matter interaction (Du et al., 2014).

As mentioned earlier, topological insulator (TI) is another suitable SA to generate a pulsed laser. In this thesis, two types of TI are used, including GaSe and In_2Se_3. GaSe is usually used for the applications of optoelectronics (Leontie et al., 2009), terahertz systems (X. Li et al., 2014), and nonlinear optics (Lei et al., 2013). Other than that, GaSe exhibits a significant nonlinear coefficient, broad transparency range, and extremely low optical losses (Kübler et al., 2004) as well as having up-conversion luminescence (Ni et al., 2013). Whereas, In_2Se_3 has a broadband absorption and excellent saturable absorption property (Yüksek et al., 2010), which makes it the right candidate to be chosen as SA. These materials have been used in this study to generate a pulsed TFF laser presented in Chapter 4.

2.2.4.1 Nonlinear Measurement of SA

The nonlinear absorption property of the material is one of the critical features of SA. In this study, the twin-detector technique (Chen et al., 2014) is used to measure this property of SA. The experimental configuration of the twin-detector technique, as shown in Figure 2.11, is reproduced from my earlier work (H. Ahmad et al., 2018). Mode-locked fiber laser is used as a seed laser for which the output from the seed laser is amplified by a low-dispersion amplifier. Then, the output port of the amplifier is connected to the

variable optical attenuator (VOA) and next, linked to the 3-dB output coupler. One of the outputs is integrated with the SA, whereas the other port acts as a reference port. Each port is connected to an optical power meter (OPM) for measuring purposes. The measured data is then fitted into the saturation model equation (Bao et al., 2009; Woodward et al., 2015a)

$$\alpha(I) = \frac{\alpha_s}{1 + I/I_{sat}} + \alpha_{ns} \qquad (2.13)$$

where α_s is saturable absorption, α_{ns} is the non-saturable absorption, I is intensity and I_{sat} is the saturation intensity.
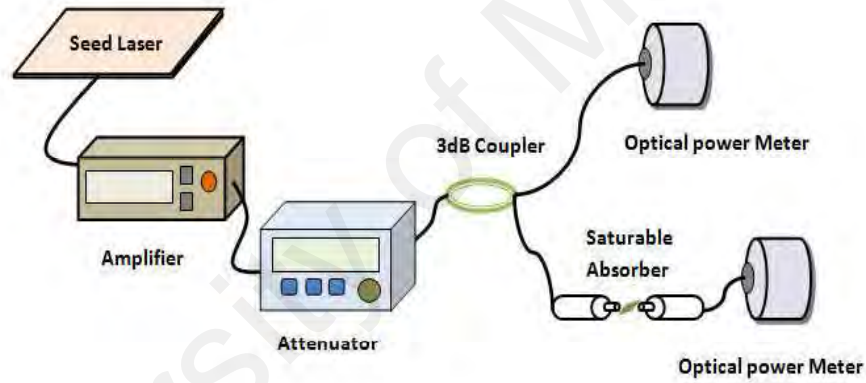
Figure 2.11: Experimental setup of the nonlinear saturable absorption measurement experiment using twin-detection technique[9]

---

[9] (Reproduced with permission from Ahmad, H., Reduan, S. A., Ooi, S. I., & Ismail, M. A., 2018)

2.3   Summary

The properties of thulium-fluoride are described in this chapter, including a brief explanation of rare-earth element as well as fluoride as a host material. The population inversion, principle of lasers, and characteristics of fiber amplifiers are also shown. The modes of laser operation with SA are also presented in this chapter, including Q-switching, Mode-locking, and Dual-wavelength, Q-switching. At last, a brief discussion on SA, as well as the nonlinear measurement of SA, is described.

CHAPTER 3: THULIUM-FLUORIDE FIBER AMPLIFIER AND LASER IN THE S+/S BAND

3.1 Introduction

As mentioned earlier, the S band covers a region from 1480 nm to 1530 nm, whereas the S+ band covers a shorter wavelength range of S band region which is 1450 nm to 1480 nm (Caspary et al., 2003; El-Nahal et al., 2013; Yam et al., 2006). These bands are vital for the development and expansion of current telecommunication systems in the C- and L- bands, which have become saturated. Furthermore, laser operation in the S band region has a lower susceptibility to bending loss compared to the C- and L- band regions (Sakamoto, 2001; M. Z. Zulkifli et al., 2011). Still, there have been only a few reports on fiber lasers in the S band region from 1460 nm to 1540 nm.

As discussed in the previous chapter, thulium is a rare-earth element that can be used to induce emissions in the S band region by a single up-conversion pump wavelength (Floridia et al., 2004; Kasamatsu et al., 1999). In this study, pumping at 1400 nm is used due to its advantages of being able to induce direct GSA and ESA (Floridia et al., 2004). Other than that, fluoride fiber is used as a host fiber of a gain medium, which plays a vital role in enhancing the performance of the lasing output. Therefore, the existence of thulium elements in the fluoride fiber will significantly enhance the S band emission in generation S+/S band fiber laser.

This chapter will discuss the application of the TFF first as an amplifier, and then as a fiber laser. The typical characteristics of the TFF as an amplifier will be studied, including its ASE, gain, and noise figure. This will then be followed by a discussion on the application of the TFF as a CW laser, and will also explore the tuning capabilities of the laser. This chapter will serve as the basis for the next chapter, which will discuss the development of a pulsed TFF laser that is capable of operating in the S+/S region.

3.2 Experimental analysis of the thulium-fluoride fiber amplifier gain and noise figure measurement

The TFF is set up as an amplifier, as shown in Figure. 3.1. In this mode, the saturation gain, gain bandwidth, and noise figure of the TFF based amplifier will be determined. The experimental setup consists of a 1400 nm laser diode (LD), ISO, a 1400/1500 nm WDM and a 14.5 m long TFF. The TFF is manufactured by Fiberlabs Inc and has a thulium dopant concentration of about 3,200 ppm mol with an absorption rate of 0.15 dB/m at the 1400nm, a 0.26 numerical aperture value and a mode-field diameter of 4.5 μm at 1500 nm. A tunable laser source (TLS) from Santec TSL-550 is used to produce an input signal at 1470 nm at varying input power. The measurements are then carried out and analyzed using the optical spectrum analyzer (OSA) from Anritsu MS9740A. These measurements are investigated using the interpolating technique.
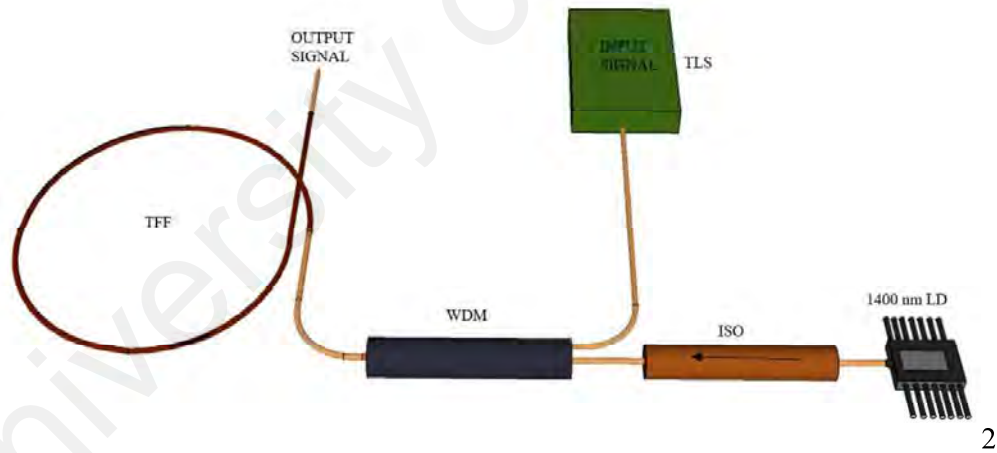
Figure 3.1: TFF amplifier using 1400 nm LD, ISO, 1400/1500 nm WDM, 14.5 m TFF and Santec TSL-550 TLS

3.2.1 ASE Measurement

The first characteristic of the TFF based amplifier to be studied is the ASE. For this measurement, 1400 nm LD is used as a pump source, creating a setup as illustrated in Figure 3.2.
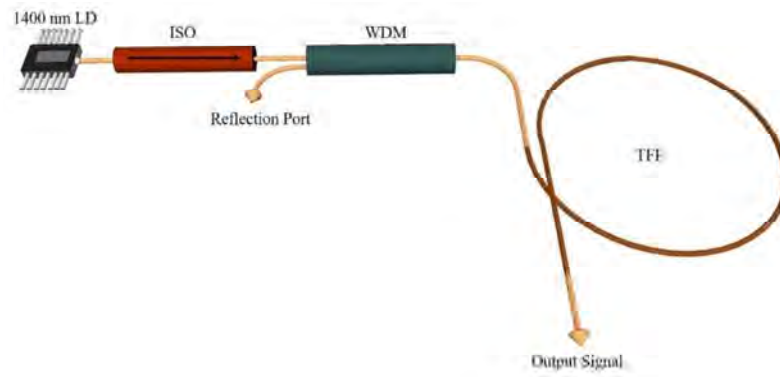
Figure 3.2: Schematic diagram of the ASE measurement of TFF

Figure. 3.3 shows a measured ASE spectrum at OSA at the pump powers of 65.1 mW, 88.7 mW, 112.2 mW, 135.8 mW, 159.3 mW, 182.9 mW, 206.0 mW and 230 mW, respectively. It is observed that the ASE amplification regions increases as the pump powers increases, but the ASE peaks region remains unchanged at around 1468 mn. As the pump power increases to 230 mW, the ASE spectrum spanning around 77 nm from ~ 1435 nm to 1512 nm with a full width at half maximum (FWHM) bandwidth of around ~ 29 nm is observed.
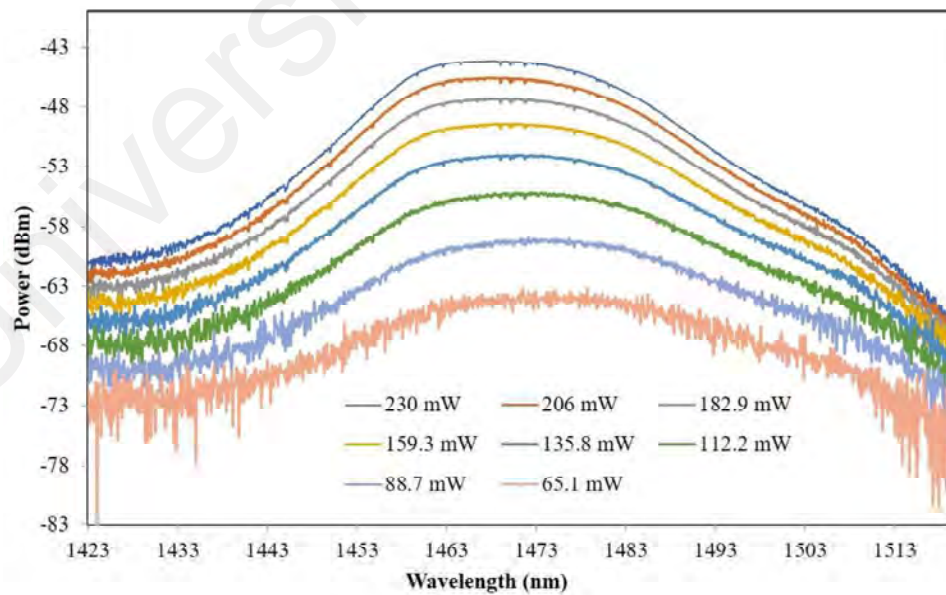
Figure 3.3: Measured ASE spectra of 14.5 m TFF under a different pump power

3.2.2   Saturation gain and gain bandwidth

The saturation gain of the TFF is measured to identify the input signal power that is required to reduce the net amplifier gain by 3-dB (Mohd Zamani, 2012). A large input signal needs to be injected into the amplifier cavity to investigate the saturation gain, and to observe the amplification trends as the TFF amplifier departs from its linear behavior (Arbore, 2005a). This measurement is important to characterize the power amplifier performance of the TFF, which will generate a very high saturation gain. In addition to this, the small signal gain is also measured to determine the performance of the TFF amplifier to boost a very weak signal. A small signal gain, also known as unsaturated gain, is typically defined as the region of operation in which the gain curves are linear. The gain performances of the 14.5 m TFF with a 1470 nm signal and different signal power at a pump power of 76.0 mW is shown in Figure 3.4. The threshold laser of the TFF cavity is at the pump power of 76 mW. The measurements show that a lower gain is obtained as a higher signal power is being amplified, which agrees with the theoretical assumptions (Emmanuel et al., 1994). Moreover, it is expected that the depletion in the active gain region will increase when the signal power is higher than the saturation power (Siegman, 1986).
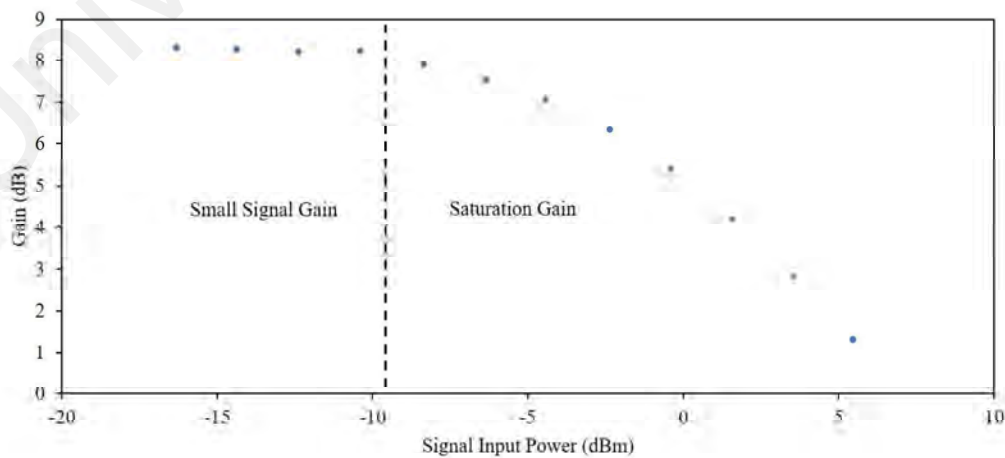
Figure 3.4: Gain performance for different signal input power at the pump power of 76.0 mW

Another important parameter in the optical amplifier is the gain bandwidth, which is the ratio of the optical amplifier's gain over the bandwidth at 3-dB from the peak value. The gain bandwidth is also known as 3-dB gain bandwidth, which is defined as the bandwidth of the gain when the maximum gain of the signal wavelength drops by 3 dB. In this study, low input signal power (-17 dBm) and high input signal power (0 dBm) with the constant pumping power of about 76.0 mW was set as a parameter on the equipment to identify the gain bandwidth of TFF amplifier.

Figure 3.5 exhibits the gain performance at the low input signal power of -17 dBm with the different input signal wavelength from 1455 nm to 1500 nm. As shown in Figure 3.10, the gain from 1455 nm increases to 1480 nm with a maximum gain of 9.32 dB. This trend begins decreasing from 1480 nm to 1500 nm where the gain drops from the maximum to 5.97 dB. This pattern is observed to follow the ASE curve due to the lower signal power, which is unable to suppress the generated ASE. It can be seen in the inset of Figure 3.5 that the curvature of the ASE spectrum is nearly similar to the gain performance curve, thus indicating that the ASE curves and the trend of gain bandwidth are related. The shaded region in the inset of Figure 3.5 indicates the corresponding input signal wavelength. The gain performance against a high input signal power (0 dBm) at different wavelengths is shown in Figure 3.6. It can be observed from Figure 3.6 that the gain trend increases almost linear from 1455 nm to 1490 nm with a maximum gain of 6.4 dB but dropping to 5.53 dB at a wavelength of 1500 nm.
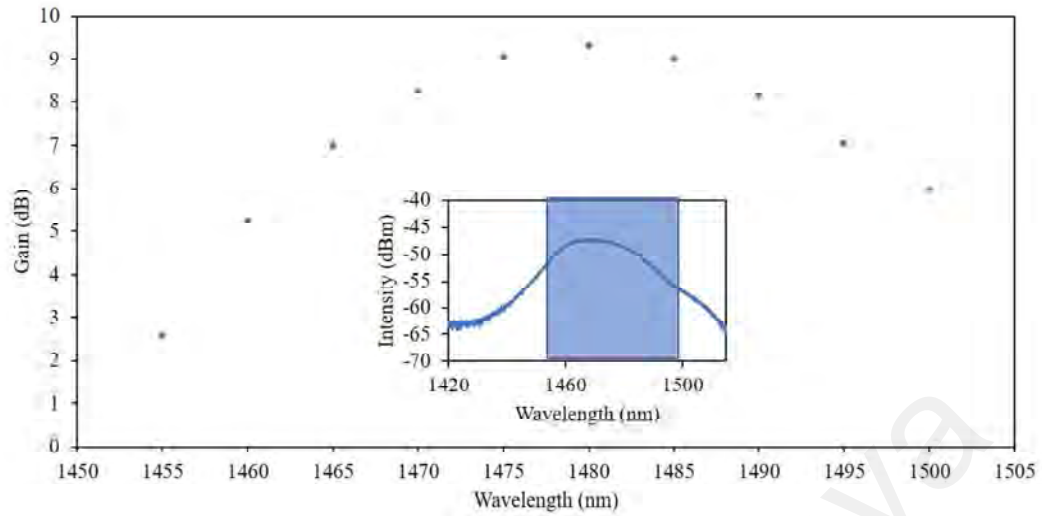
Figure 3.5: The gain performance at the low input signal power of -17 dBm with the different input signal wavelength
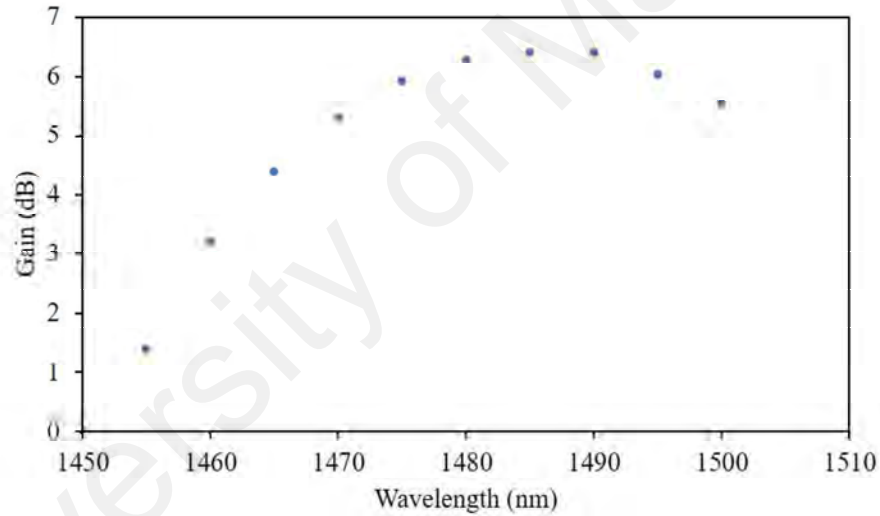
Figure 3.6: The gain performance at different input signal wavelength with a 0 dBm signal input power

3.2.3   Noise Figure Characteristics

The noise figure (NF) is another important parameter of the optical amplifier. A low NF indicates excellent performance alongside other parameters such as high gain and wide bandwidth. The NF is defined as the ratio of the input signal to noise (SNR_i) against the output signal to noise ratio (SNR_o). The interpolation technique is used to determine the NF in this work with the assistance of the OSA. In this technique, the ASE level, just above and just below the signal wavelength, is measured to determine the ASE of the

amplifier at the signal wavelength. These measurements are then interpolated to identify the level of the ASE level at the signal wavelength (Mohd Zamani, 2012). The NF has different input signal powers, but at a constant pump power of 76.0 mW is shown in Figure 3.7.
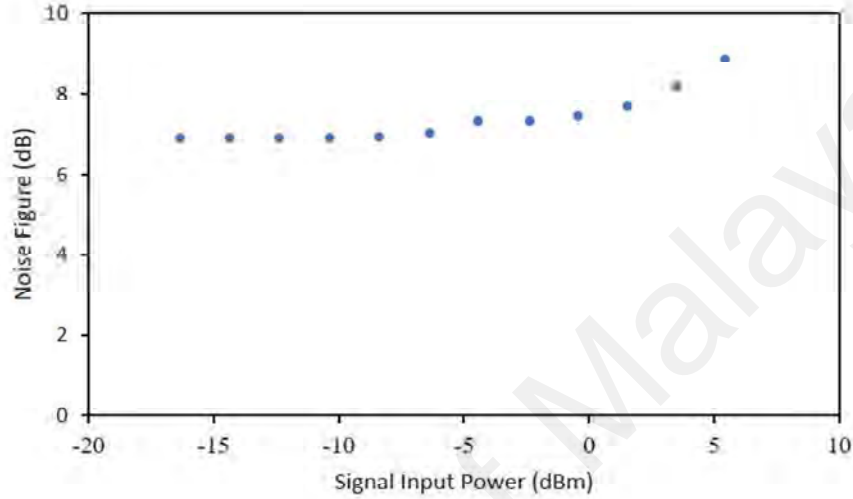
Figure 3.7: The performance of NF with the different input signal power but constant pump power at 76.0 mW

The recorded NF trend is determined to be almost constant at around 7.0 dB from an input signal -17.0 dBm to -0.43 dBm, which can be considered as a low input signal. However, the NF is observed to increase as the input signal rises to a maximum value of 5.5 dBm, giving the highest NF of 8.9 dB. These trends could be the result of a mixture of the self-induced saturation effect by the signal-induced saturation and the backward ASE, which eventually changes the distribution of the ASE along with the fiber (Emmanuel et al., 1994). The backward ASE near the fiber input end is reduced by the power of signal-induced saturation that makes the medium inversion higher in this region. In this regard, the TFF amplifier has a higher NF as the input signal becomes higher.

Figure 3.8 shows the performance of the NF against different input signal wavelengths at an input power of -17.0 dBm. Based on Figure 3.8, the trends of NF linearly decrease from 9.6 dB to 5.7 dB over a wavelength range of 1455 nm to 1485 nm. The NF remains

nearly at the same value of 5.7 dB, which starts from 1485 nm to 1500 nm. The minimum NF observed is around 5.7 dB at the wavelength of 1500 nm.
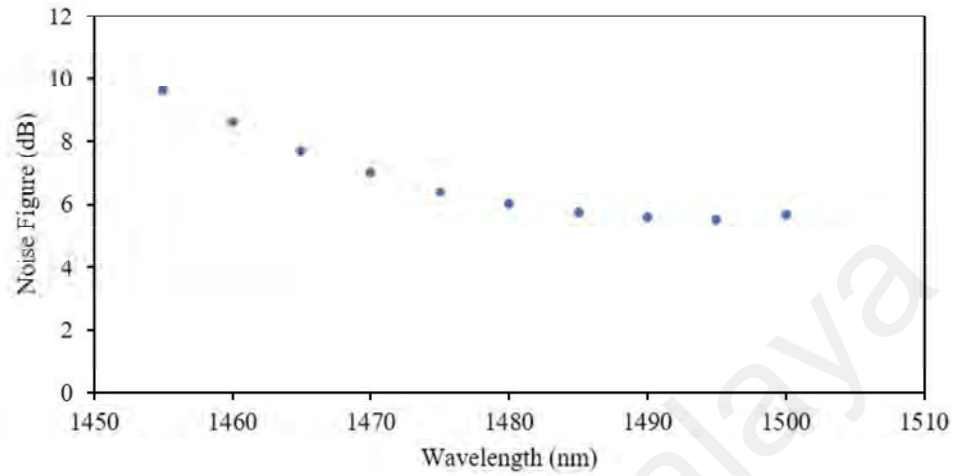
Figure 3.8: The performance of NF with different input signal wavelength at an signal input power of -17 dBm

3.3 Thulium-fluoride fiber

The transition of electrons from the $^3F_4$ to $^3H_4$ energy levels of thulium ions results in an emission at ~1480 nm is located in the S band region. This emission is applicable as a pump source of EDFAs as well as Raman amplifiers. Furthermore, this is also a suitable wavelength for the detection of water as this lasing wavelength coincides with the liquid water absorption peak (Jia, 2017).

As mentioned above, there are two possible pumping sources to obtain emissions at this lasing wavelength, which is either by single up-conversion or dual-wavelength conversion (Floridia et al., 2004; Kasamatsu et al., 1999). However, single up-conversion pumping is more straightforward and more cost-effective as it requires only one pumping wavelength compared to the dual-wavelength pumping scheme. Figure 3.1 shows the different energy level diagrams between the single-up conversion pumping and dual-wavelength pumping. The two standard single up-conversion pumping wavelengths for TFF emissions are 1050 nm and 1400 nm (Floridia et al., 2004). In this study, 1400 nm pumping will be used due to its advantage of direct GSA and ESA. Furthermore, 1050 nm

pumping is not preferable in this study due to the depopulation when it is being pumped at this wavelength. It will require two processes, thus adding complexity to the cavity's operation (Floridia et al., 2004).
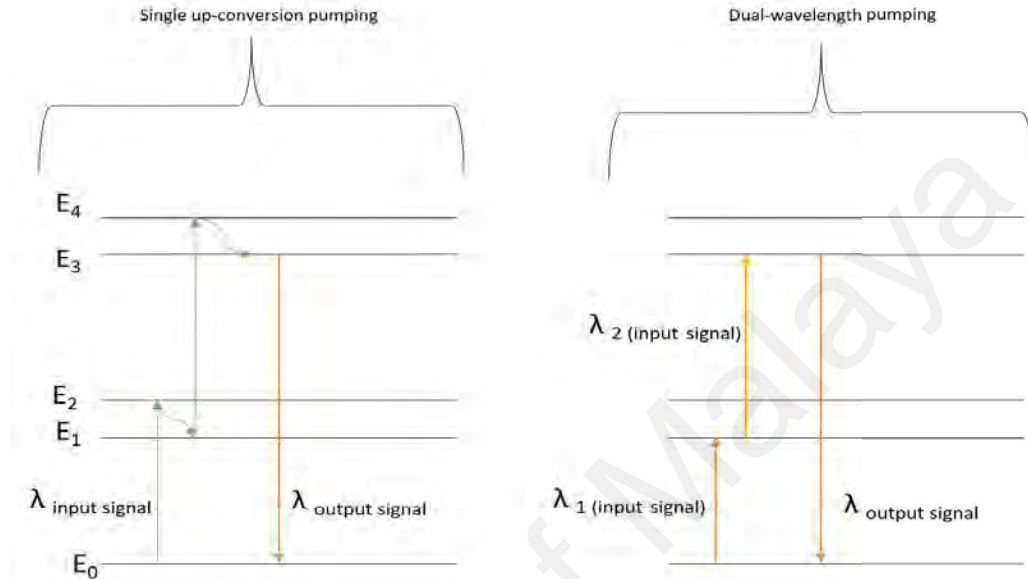
Figure 3.9: Energy level diagram between single up-conversion pumping and dual-wavelength pumping

In addition to the choice of efficient pumping technique, the choice of the gain medium's host fiber also plays a critical role in optimizing the efficiency of the proposed fiber laser cavity. Among the different available host materials such as silica, tellurite, and fluoride fibers, fluoride fibers enabling the non-radiative transition rate to reduce significantly (Frerichs et al., 1996). Therefore, the existence of thulium ions as the dopants in the fluoride fiber will greatly enhance S band's emissions for the development of the laser cavity in this work.

TFFs have already been the choice of fiber for use as a gain media for S band amplification as reported by Tanabe et. al. (Tanabe et al., 2003). Earlier TFFs have been demonstrated covering a region from 1440 nm to 1550 nm corresponding to S+/S band region. There have also been reports on the development of TFF amplifier in the S+/S

band region that covers a wavelength range from 1490 nm to 1500 nm by Caspary et. al (Caspary et al., 2003). This has shown that S+/S band fiber lasers are achievable using TFF as a gain medium.

This section will focus on the development of a 1400 nm fiber laser as a pumping source for a CW TFF laser. The performance of the laser will be characterized and the tunability of the laser will also be studied. The proposed fiber laser will find important applications in instrumentations, spectroscopy, communications and sensing.

3.3.1   CW Thulium-fluoride fiber laser

The transition from the $^3H_4$ to $^3F_4$ levels will result in lasing at ~ 1480 nm which is located in the S band region. The generation of lasing wavelengths in the S band region is crucial as it provides an alternative data network to the C- and L- band for use as optical wavelengths for communication.

Fiber lasers operating at different wavelength regions are highly desirable due to their advantages of being high efficiency and alignment-free sources (Martinez et al., 2013). The operation of fiber laser in C- and L-band region have been mostly reported using EDFs as a gain medium (Chen et al., 2014; Digonnet, 1989; Y. Yan et al., 2016). The C- and L-band regions start from 1530 nm to 1625 nm, which is the typical optical wavelength region used for optical communications. There have also been reports on the use of ytterbium-doped fibers (YDFs) and thulium-doped fibers (TDFs) for generating lasing outputs in the 1- and 2- micron regions respectively (Kasamatsu et al., 1999; Luo et al., 2013). Nevertheless, only a few reports have been found on fiber lasers in the S band region, even though the S band is quickly proving to be necessary as an alternative network for telecommunication systems to be able to address issues of limited bandwidths.

Figure 3.10 shows the schematic diagram of the CW TFF in the S band region. A 1400 nm LD is used as a pump source, while the output of the LD is connected to an ISO to prevent back reflections to the LD. The isolator's output is connected to the 1400 nm port of a 1400/1500 nm fused WDM. The common output of the WDM is channeled to the 14.5 m long TFF, which is the same fiber used in the cavity of Figure 3.1. The TFF's output is now connected to another ISO to ensure unidirectional propagation before reaching a 90:10 optical coupler, with the 90 % of optical coupler being connected to the 1500 nm port of the WDM to complete the optical circuit. The 10 % port is used to extract a portion of the signal for further analysis.
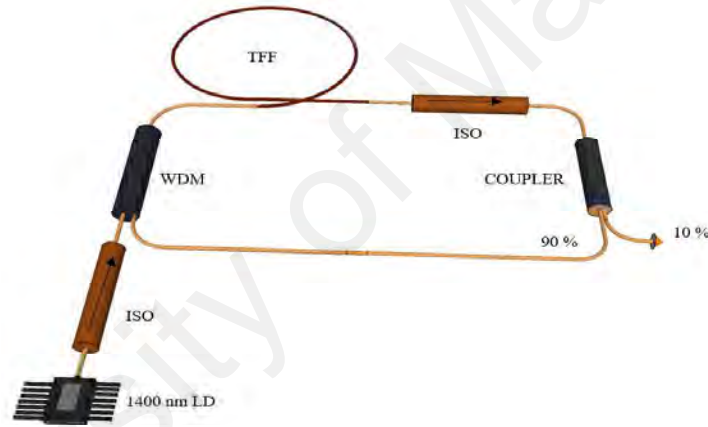
Figure 3.10: Schematic diagram of TFF laser: 1400 nm LD, ISO, WDM, TFF and coupler

The Anritsu MS9740A OSA is used to examine the spectral characteristics of the output laser, while the output pulse train is observed using the Yokogawa DLM2054 oscilloscope (OSC) with a 1.2 GHz photodetector. An Anritsu MS2683 radio-frequency spectrum analyzer (RFSA) is used to obtain the SNR of the generated output while a Thorlabs SC144C OPM is used to monitor the output power.
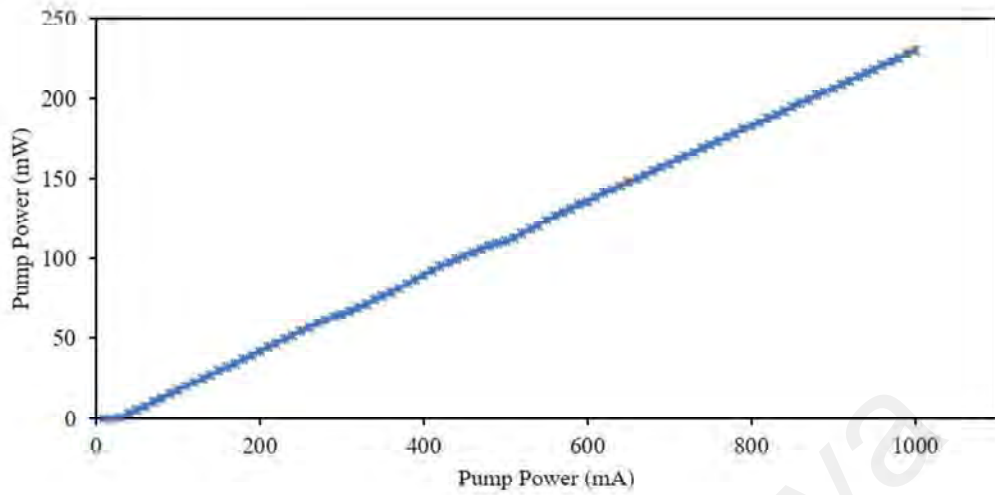
Figure 3.11: Characterization of pump power

The characterization of the pump power is shown in Figure 3.11 for an LD power from 10 mA to 1000 mA at the steps of 10 mA, equivalent to the pump power increments of 0.002 mW. In this study, the pump power is varied from 0.002 mW to 230.0 mW. Lasing operation is observed at a wavelength of 1505.0 nm. Figure. 3.12 shows the optical output spectrum at the threshold pump power, which starts at 76.0 mW for lasing at 1505.0 nm. The maximum pump power used is set to 230 mW due to the limitations in the current driver, as well as to prevent the damage to the laser diode.
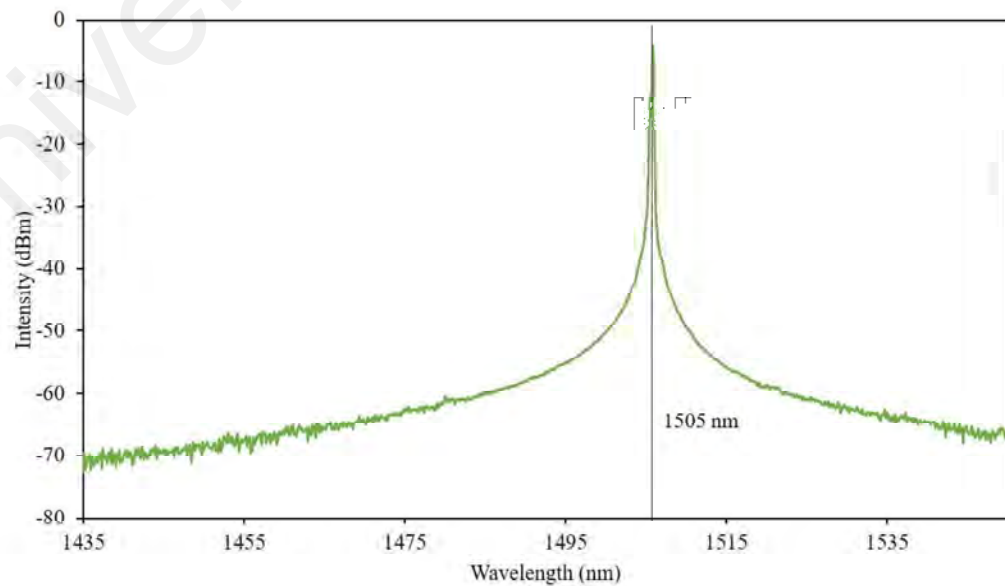
Figure 3.12: Optical spectrum of CW laser

3.3.2 Tunability of CW Thulium-fluoride fiber laser in S+/S band region

The tunability of the CW TFF laser is investigated using a tunable bandpass filter (TBPF). Figure. 3.13 shows the experimental setup for generating a tunable CW output using the TFF laser. An Agiltron Inc. FOTF-02512133 tunable bandpass filter (TBPF) is used in this experiment. As shown in Figure 3.13, the output port of the coupler is connected to the TBPF, which is then linked to the 1500 nm port of WDM. The purpose of TBPF is to tune the lasing wavelength of the cavity. The output spectra of the tunable CW TFF laser are shown in Figure 3.7 which covers a wavelength from 1450.0 nm to 1512.0 nm, with a tuning range of 62.0 nm.

Figure 3.13: Schematic diagram of fiber laser with TBPF: 1400 nm LD, ISO, WDM, TFF, TBPF and coupler
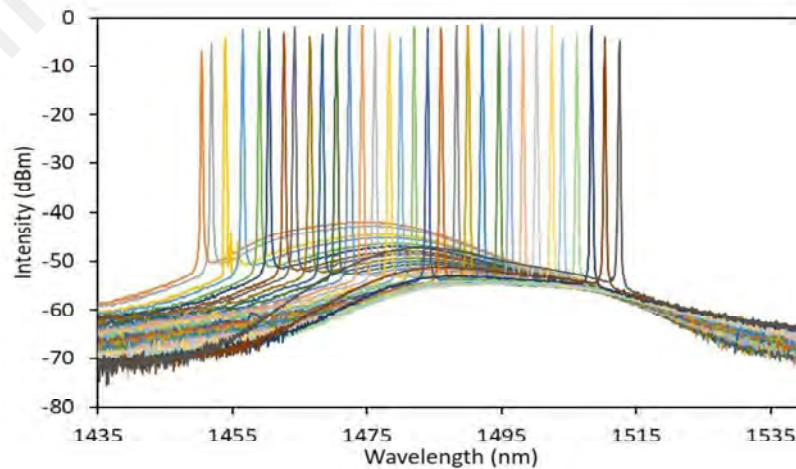
Figure 3.14: The output spectra of the tunable CW TFF laser

From Figure 3.14, it can be seen that the generated tunable CW TFF laser is able to operate in a broadband region, especially at the shorter wavelength of the S band region of the S+ band region. All other parameters are kept constant, including the pump power, which is set at 182.9 mW, while the lasing wavelength is tuned by the TBPF. Thus, by tuning the TBPF results in a CW lasing from 1450.0 nm to 1512.0 nm, covering the S+/S band region over a wavelength range of 62 nm. It is expected to have a high loss from the TBPF as it is optimized for C-band operation. Therefore, a better tunability range can be obtained using TBPF that optimized in the S band region.

3.4 Conclusion

Using a ring cavity configuration, a single wavelength CW laser can be generated at the wavelength of 1505.0 nm The integration of the TBPF shows the tunability of the lasing operation to covers a wide-band region including S and S+ band region which covers a wavelength region from 1450 nm to 1512 nm as observed in this study. The gain of the TFF is investigated to observe the performance of TFF as an amplifier under a weak signal. In this regard, trends of the TFF's gain follows the trends of ASE curves due to failing to suppress the ASE by the lower signal power. Other than that, the NF of TFF is investigated using an interpolating technique. These observed results seem to support the theory of the quantum limit (Caves, 1982). From this experiment, the generated output of the TFF laser in the S+/S band region may find significant application in communications, spectroscopy, and sensing.

CHAPTER 4: GENERATION OF Q-SWITCHED, DUAL-WAVELENGTH Q-SWITCHED AND MODE-LOCKED THULIUM-FLUORIDE FIBER LASER IN S+/S BAND

4.1   Introduction

High-energy pulsed lasers have become desirable sources for use in various applications including sensing, medicine, and scientific analysis (Paschotta et al., 1999; Sharma et al., 2004; Siniaeva et al., 2009; Xiang et al., 2014). Pulsed lasers are compact systems that are cost-effective and robust (Orazio, 2010). Q-switched and mode-locked pulses are the well-known pulsed laser.

The generation of dual-wavelength lasers also finds numerous applications in areas such as laser processing, metrology, telecommunications and biomedical diagnostics (Harith Ahmad et al., 2014; D. Liu et al., 2006; Q. Lou et al., 2008; Urquhart, 1988; Yao et al., 2006). Dual-wavelength lasers also accomplish the application of new capabilities as well as enhancing the functionality in the generation of microwave, LIDAR, and dual-band OCT imaging spectroscopy (Jia, 2017).

Currently, most pulsed fiber lasers operate in the C- and L- band region (H Ahmad et al., 2016a; Y. Chen et al., 2015; Chen et al., 2014), as well as in 1.0- and 2.0-micron region (J. Liu et al., 2011; J. Liu et al., 2012; Woodward et al., 2015b). However, there were only limited reports in the S band region. There had been demonstrations on generating pulsed outputs in the S band region by utilizing depressed-cladding erbium-doped fibers (DC-EDFs) (H. Ahmad et al., 2017a; M. Zulkifli et al., 2011). However, DC-EDFs exhibits a short bandwidth, which is from 1490 nm to about 1515 nm, which limits their usefulness.

A potential solution to this problem is using the TFF as a gain medium to generate a wide-band pulsed laser. Previous works have reported the use of the TFF for S band

amplification and laser applications due to its sizeable operational bandwidth, which is capable of stretching from 1440 nm to 1500 nm to cover an S+/S band region (Caspary et al., 2003; Tanabe et al., 2003).

This chapter discusses a passively Q-switched TFF laser using a different type of SAs such as SWCNT, graphene, MoS_2, and GaSe. A dual-wavelength, Q-switched TFF laser is also presented using MoS_2 and PCF. Finally, passive mode-locking is also discussed using recent 2D materials such as In_2Se_3 as the SA. Each subsection will describe the experimental setup, results, and discussion.

4.2   Passively Q-Switched Thulium-Fluoride Fiber Laser

The generation of Q-switched fiber laser has attracted interest among the researchers due to their ability to have a pulse with longer pulse duration and higher pulse energies (Svelto, 2010). This pulsed laser is applicable in many applications such as sensing, material processing, medicine, and scientific research (D Popa et al., 2011; Xiang et al., 2014). Passive Q-switching operation has attracted the attention of researchers on developing and enhancing this operation due to their advantages of being a compact and cost-effective system to generate a pulsed laser (Tsai et al., 2009).

4.2.1   Experimental Setup of Passively Q-Switched TFF Laser

The experimental setup for the passively Q-switched TFF laser with and without a TBPF is given in Figure 4.1. The laser is configured as a conventional ring cavity, where TFF acts as a gain medium, and the SAs serves as a Q-switcher. A 1400 nm FOLI405RTD LD is used to drive the TFF laser via 1400 nm port of 1400/1500 nm WDM. An isolator (ISO) is located between the LD and WDM to avoid any back-reflections that may be reflected in the LD and damage it. The universal port of the WDM is then connected to the 14.5 m long TFF from Fiberlabs Inc. The TFF exhibits an absorption rate of 0.15 dB/m at 1400 nm and a numerical aperture value of 0.26 as well as a mode-field diameter

of 4.5 µm at 1500 nm. The NA of the commercial TFF is higher than the NA of the conventional SMF-28 fiber to increase the light collected for the propagation in the TFF. The end port of TFF is connected to another ISO to ensure the unidirectional of the propagating light inside the laser cavity. Next, the output port of the ISO is linked to a 90:10 output coupler, which extracts 10 % of the signal from the laser system to be analyzed. The 90 % port of the output coupler connected to the SA assembly and then connected to the 1500 nm port of WDM. Thus, completing the laser cavity. TBPF is inserted in between the output coupler, and the SA assembly for the experimental setup involves the tuning of the central wavelength of the Q-switched TFF laser. The total cavity with and without the TBPF is estimated around 24.5 m and 26.5 m, respectively.

The Anritsu MS9740A OSA and Yokogawa DLM2054 OSC with a 1.2 GHz photodetector were used to measure the observed spectrum and the pulse trains of the output pulsed laser, respectively. On the other hand, the signal-to-noise ratio of the pulsed laser is obtained using Anritsu MS2683 RFSA. Whereas, Thorlabs SC144C is used to measure the output power of the pulses.
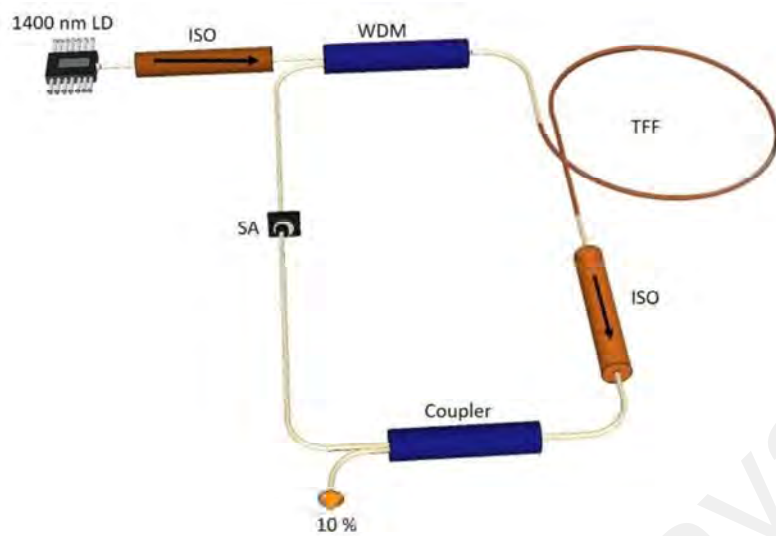
(a)

(b)

Figure 4.1: Experimental Setup of Passively Q-switched TFF laser, (a) without TBPF and (b) with TBPF

4.2.2 Passively Q-Switched TFF Laser Using SWCNT SA

4.2.2.1 SA Characterization

The SWCNT SA used in this work is a thin film fabricated and prepared by the Centre for Advanced Photonics and Electronics (CAPE), University of Cambridge, United Kingdom. The Raman spectrum of the SWCNT is obtained using a Renishaw Raman Spectroscope at the excitation wavelength of 532 nm, as shown in Figure 4.2. A single peak at 1549 cm^{-1} is distinctly observed in the Raman spectrum, which also corresponds

to the G peak. Thus, it confirms the presence of carbon nanotubes in the sample, as demonstrated by Gaufrès et al. (Gaufrès et al., 2014) and Kim et al. (Kim et al., 2014). This also proves the absence of any impurities in the sample, which would affect the output of the experiment.
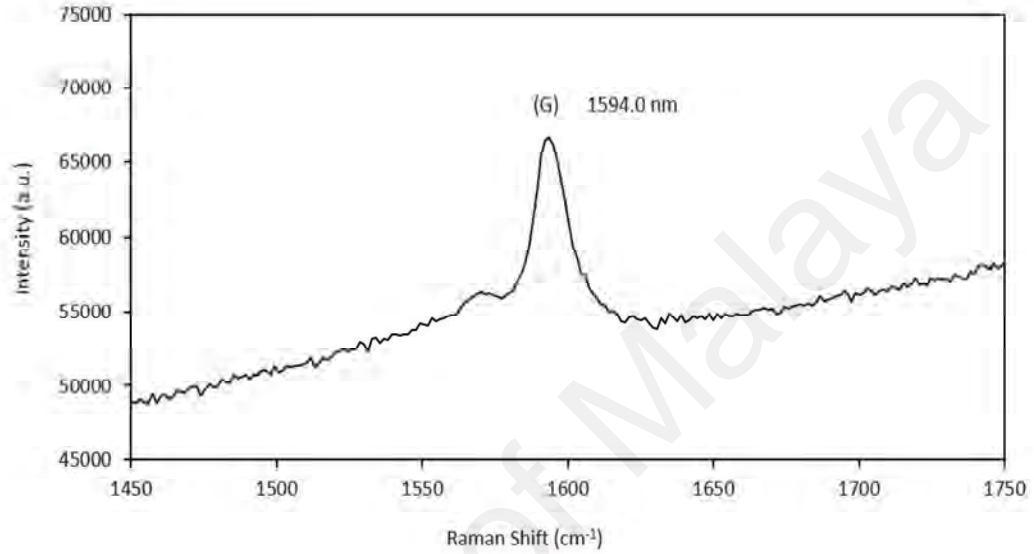
Figure 4.2: Raman spectrum of SWCNT SA

The linear and nonlinear absorption spectrum of the SWCNT thin film is shown in Figure 4.3. A white light source is used to measure the linear absorbance of the thin film from 900 nm to 1600 nm, as shown in Figure 4.3 (a). From the figure, two shaded regions exhibit good absorbance at the wavelength region of 900 nm to 1100 nm, and 1350 nm to 1500 nm indicates as Region 1 and Region 2, respectively. Region 2 indicates that the thin film well operated in the S+/S band region.

The twin detector technique is used to identify the nonlinear optical absorption spectrum of the SWCNT thin film. A mode-locked laser, with a central wavelength of 1560 nm, a repetition rate of 27.8 MHz, and a pulse width of 0.68 ps, was used as a source. The measurement data obtained were fitted into the saturation model, which result in a modulation depth and saturation intensity of ~ 18.6 % and 35.8 MW/cm^2, respectively, as

given in Figure 4.3 (b). These measurements were compared to the previous work by Chiu et al. (Chiu et al., 2010) and Sun et al. (Sun et al., 2012).
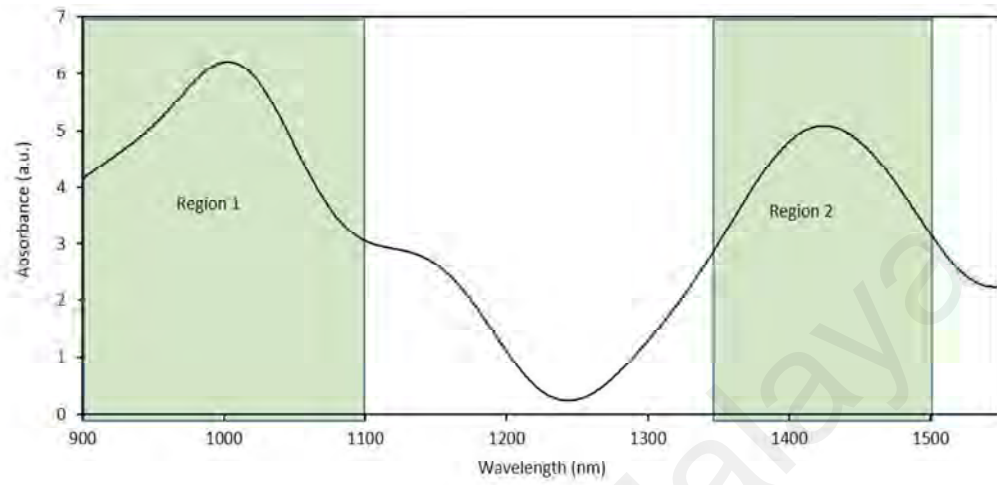
(a)
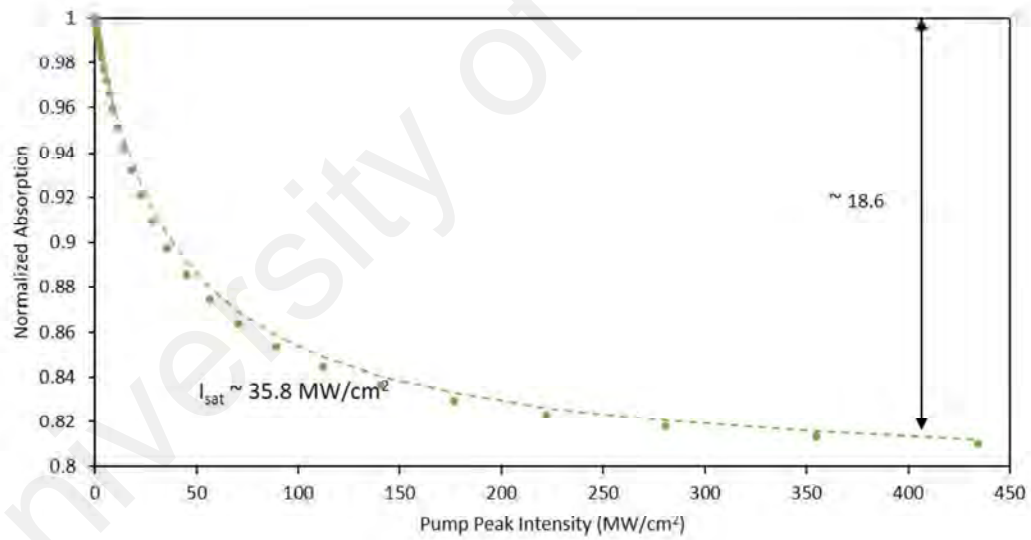
(b)

Figure 4.3: (a) Linear absorption and (b) Nonlinear absorption spectrum of SWCNT SA

4.2.2.2 Results

TBPF was used in this experiment by inserted it between the output coupler and 1500 nm port of WDM. The purpose of the TBPF was to tune the central wavelength of the generated pulsed laser. The center wavelength of the output laser was initially fixed at 1492 nm using TBPF, for which the cavity losses are found to be at the lowest at this central wavelength. The Q-switching operation starts at the pump power of 115.7 mW, and the CW operation starts at 89.7 mW. The characteristics of the Q-switched output are shown in Figure 4.4, including the pulse train in Figure 4.4 (a), pulse profile in Figure 4.4 (b), and RF spectrum in Figure 4.4 (c). The characteristics are obtained at a pump power of 182.9 mW with the central wavelength fixed at 1492.0 nm.
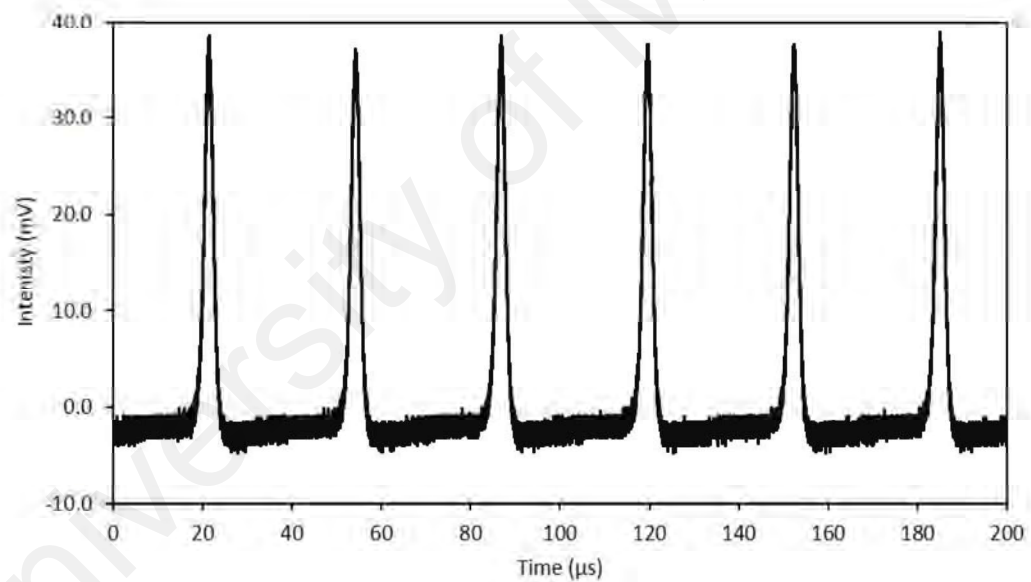
(a)
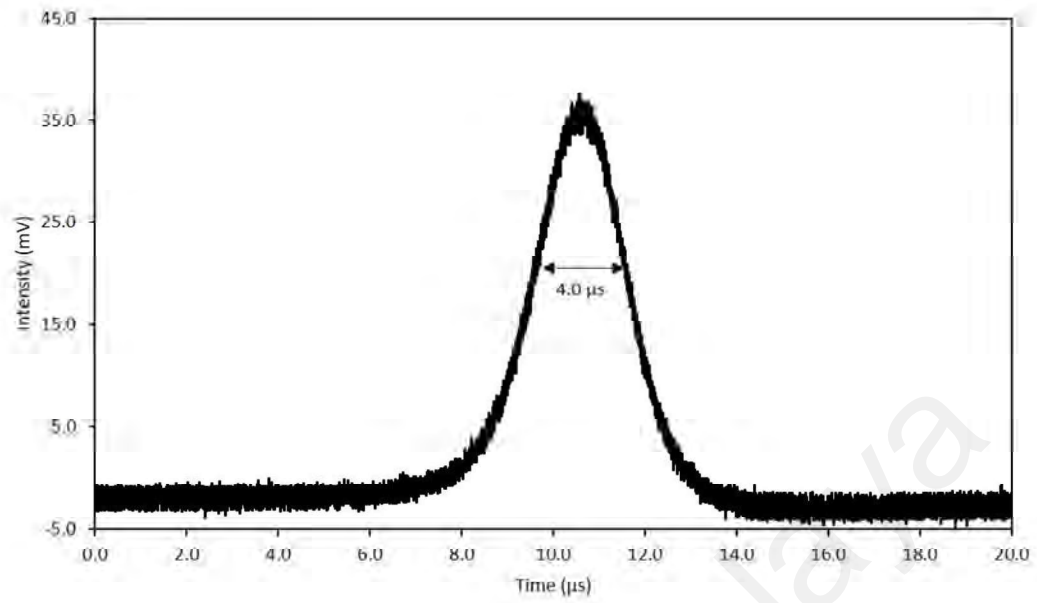
(b)
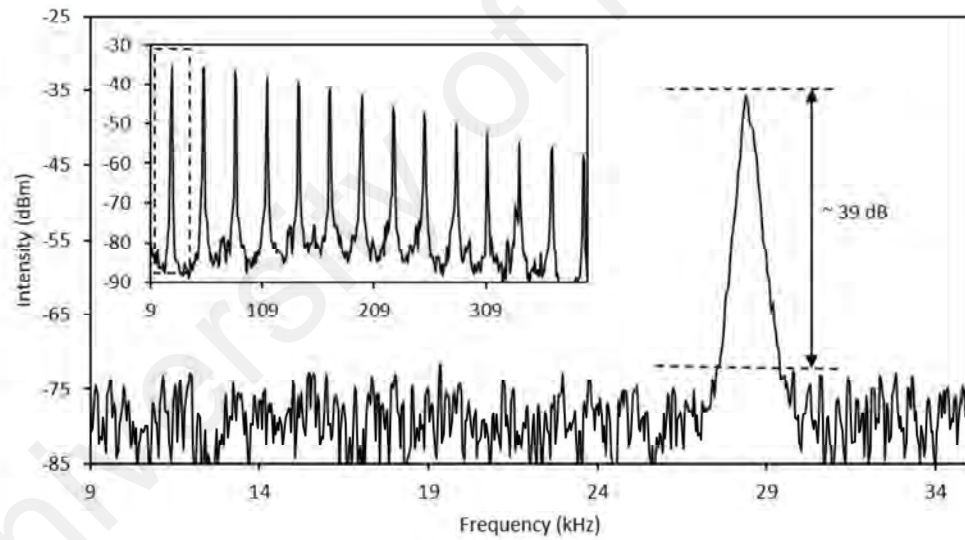
(c)

Figure 4.4: Characteristics of Q-switched operation, showing (a) the pulse train, (b) the pulse profile and (c) the RF optical spectrum at a pump power 89.7 mW. The inset of Figure 4.4 (c) shows the wideband RF spectrum

As shown in Figure 4.4 (a), the resulting pulse train shows a Q-switched pulses with a repetition rate of 28.6 kHz, which corresponds to a period of 35. 0 μs. The pulse profile indicates the full width at half maximum (FWHM) of each pulse trains of around 4.0 μs as given in Figure. 4.4 (b). The RF spectrum of the generated Q-switched pulses is shown in Figure 4.4 (c) and shows that the SNR of the output pulses is measured to be around 39.0 dB. Other than that, the inset of Figure. 4.4 (c) shows that only fundamental and harmonic frequencies are present in the wide-band spectrum.

In order to confirm whether the generated Q-switched pulses are due to the presence of the SA, the experiment without the SA is also performed. No pulses are generated when the SA is removed from the cavity, thus confirming that the SA is responsible for generating the pulsed output.

Figure 4.5 shows the characteristics of the Q-switched output pulsed attained in this experiment with a different pump power from 115.7 mW to 229.9 mW. The trends of repetition rate and pulse width of the output pulses over the pump power are given in Figure 4.5 (a). It is observed that the repetition rate linearly increases from 14.0 kHz to 36.4 kHz at the pump power of 115.7 mW to 229.9 mW, respectively. Nevertheless, the repetition rate begins to fluctuate as the pump power reaches 220.0 mW. This is due to the complete saturation of the SA, which itself causes the unstable generated Q-switched pulses. The trend of the pulse width exponentially decreasing from 6.2 μs to 3.6 μs over the pump power, which is a typical characteristic of Q-switching operation (B. Chen et al., 2015; Chen et al., 2014). This shows that the pulse width starts to fluctuate as the pump power increases, and this is attributed to the full saturation of SA. It is also believed that as the Q-switched pulses begin to become unstable until they reach a fully saturated SA, the SA would become transparent. Other than that, the SA might also start to sustain thermal damage at this state. Nevertheless, the repetition rate and pulse width of the

Q-switched pulses results in the same values as the pump power reduces, proving that the

SA has not encountered any thermal damage.
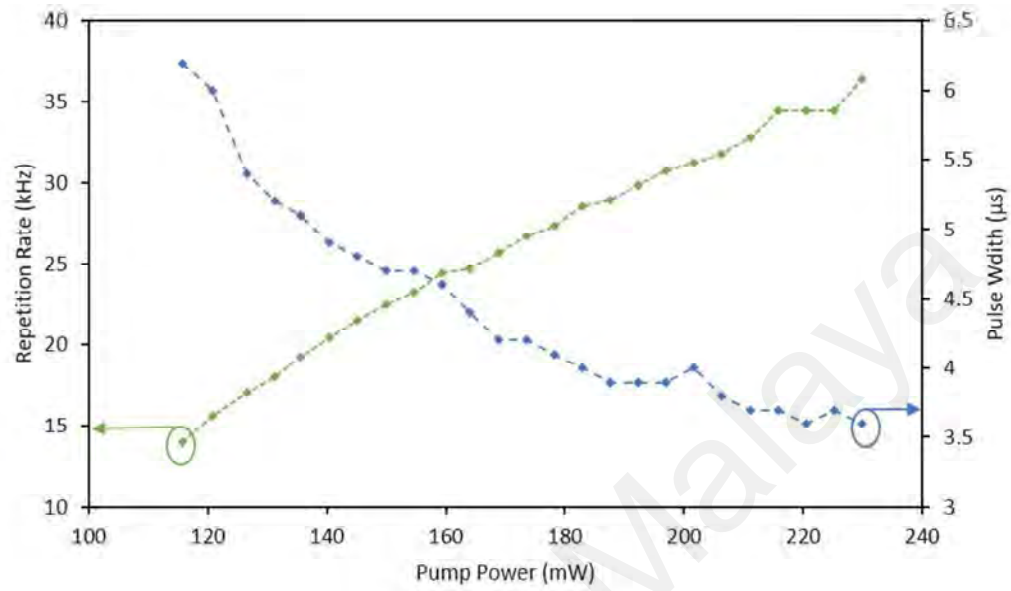
(a)
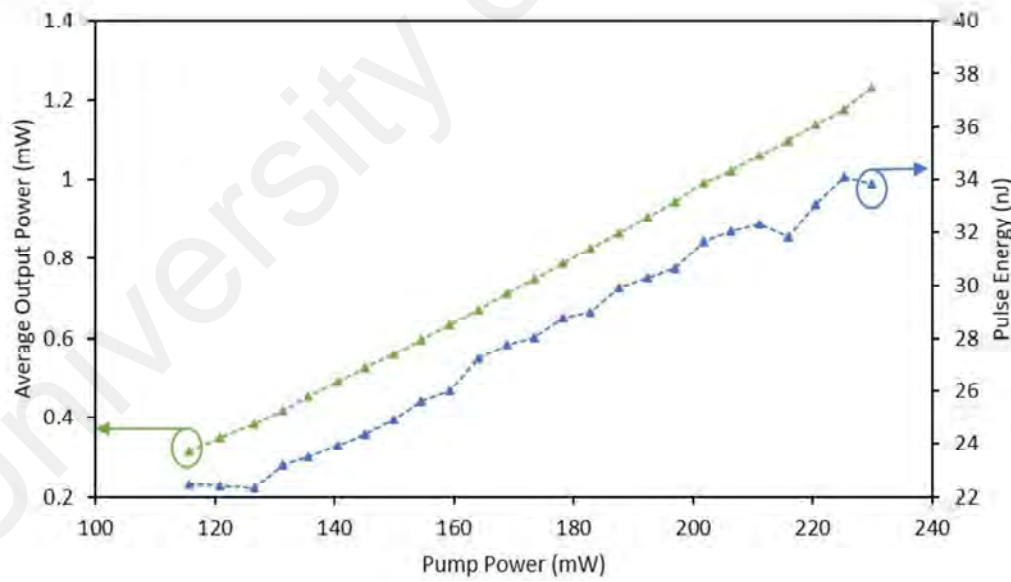
(b)

Figure 4.5: The trends of (a) repetition rate and pulse width and (b) average output power and pulse energy of the TFFL as a function of pump power

The trends of average output power and pulse energy over the pump power are shown in Figure 4.5 (b). The average output power and pulse energy are observed to increase linearly as the pump power rises with the maximum pulse energy and maximum average output power of 34.1 nJ and 1.2 mW, respectively. In addition, the pulse energy starts to fluctuate at the high pump power due to the fluctuation of the repetition rate.
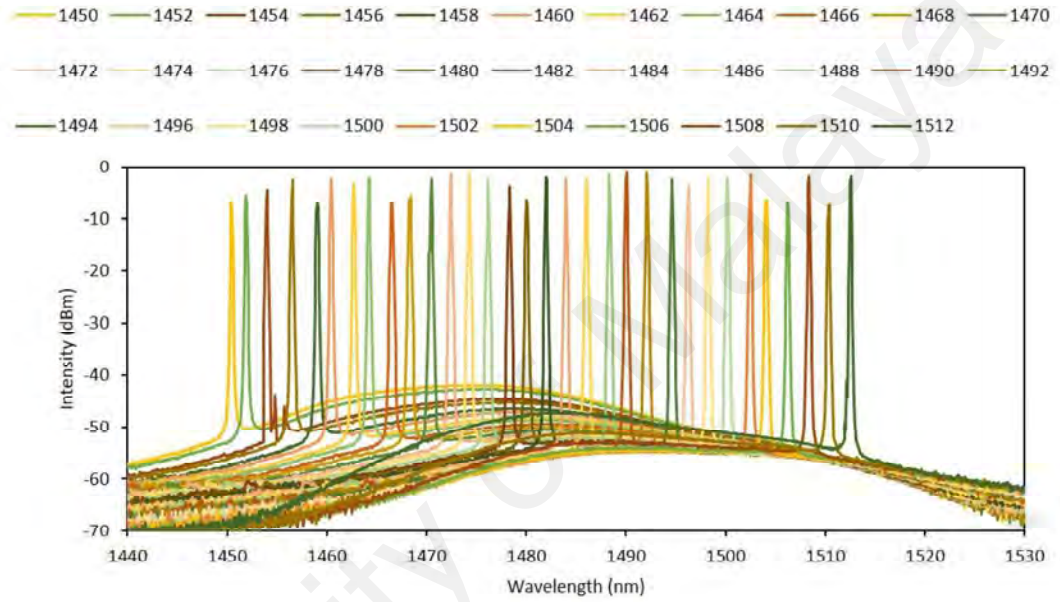
(a)
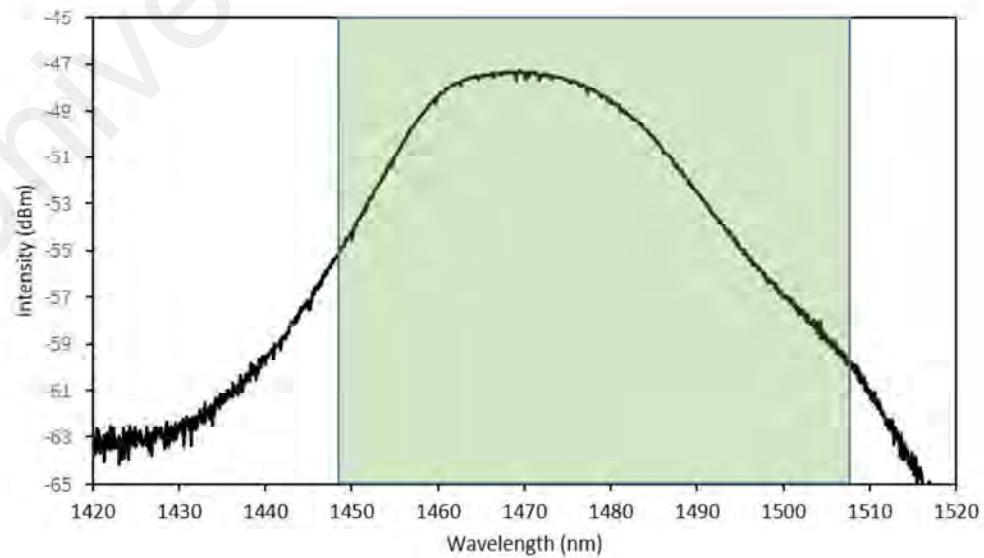
(b)
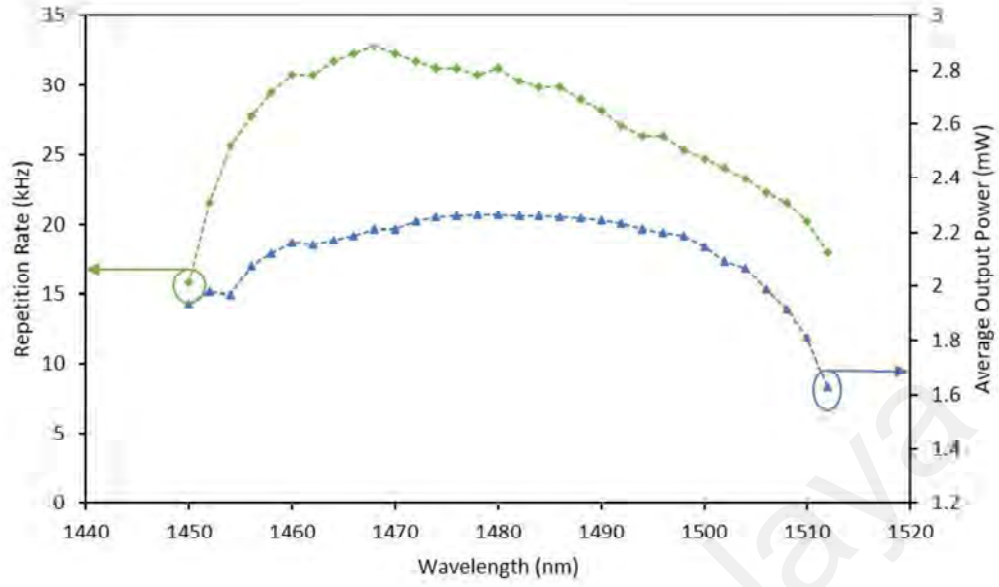
(c)

Figure 4.6: The (a) Output spectra for 32 central tuning wavelengths and, (b) ASE spectrum of the TFF laser (c) Trends of repetition rate and average output power as a function of central wavelength at pump power of 182.9 mW

The Q-switched pulses are tuned to different wavelengths using TBPF. Stable Q-switching operation is obtained over a range of 1450.0 nm to 1512.0 nm, by maintaining the pump power at 182.9 mW. Figure 4.6 (a) shows the output spectra observed for different central wavelengths from 1450.0 nm to 1512.0 nm with an increment of 2 nm. It can be seen from the figure that the tunability approximately covers 60% of TFF's ASE region, which including an S+/S band region. The tunability of the central wavelength starts to drop in peaks power, which leads to instability of pulsed laser as the tuning falls outside of the peak ASE range. The highlighted area in Figure 4.6 (b) shows the range that the Q-switched pulses can be obtained based on the ASE spectrum.

The repetition rate and average output power against the different central wavelengths are given in Figure 4.6 (c). Both trends show a similar curve as the ASE spectrum due to the ASE gain variation, which leads to a more significant repetition rate and more substantial average output power as the gain becomes larger (H. Ahmad et al., 2015; R.

Li et al., 2019). The trend of the repetition rate steeply increases until the maximum repetition rate of 32.8 kHz from the wavelength of 1450.0 nm to 1468.0 nm; then, it starts to decrease slowly following the curve of the ASE spectrum. Higher gain results in a higher repetition rate due to the stronger intracavity lasing operated at, the broader gain region of the gain medium which causes the SA to bleach faster since the population inversion starts to occur rapidly and leads to a higher repetition rate (Y. Huang et al., 2014). The maximum single pulse energy and minimum pulse width obtained in this experiment are 122.8 nJ and 3.5 µs, respectively.

4.2.3   Passively Q-Switched TFF Laser Using Graphene SA

4.2.3.1   SA Characterization

The Graphene SA used in this experiment is a composite thin film fabricated by the CAPE, University of Cambridge, United Kingdom. The nonlinear absorption spectrum of the SA is measured using the twin detector technique with a mode-locked laser source at the central wavelength of 1560 nm. The obtained modulation depth and saturation intensity of this SA are around 1.5 % and 0.993 MW/cm^2, respectively, as shown in Figure 4.7. These values are comparable with a previous work (Bonaccorso et al., 2014).
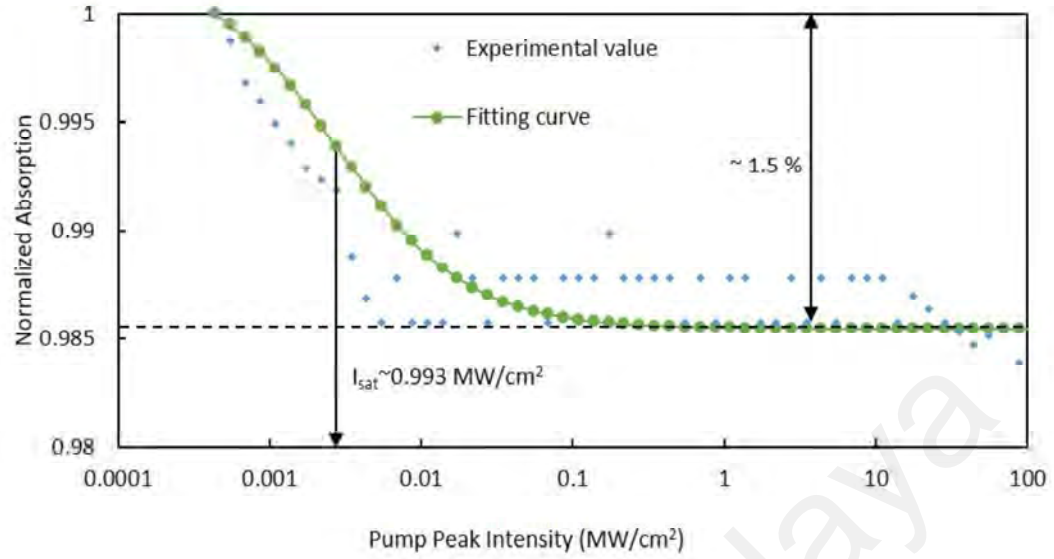
Figure 4.7: Nonlinear measurement of Graphene SA

4.2.3.2 Results

The Q-switching operation is based on graphene as SA has a threshold at 108.1 mW with the central wavelength of 1501 nm as seen in Figure 4.8 (a), as reproduced from my earlier work (H. Ahmad et al., 2017b). As seen in the figure, the spectrum of the Q-switched pulses has a broad 3 dB bandwidth around 4 nm compared to the 3-dB bandwidth of the spectrum without the SA. This phenomenon occurs because of the spectral broadening as the Q-switched pulses generated possibly due to the self-phase modulation occurred in the cavity system (Agrawal, 2001). Figure 4.8 (b) shows a pulse profile and pulse train of the generated Q-switched pulses, which has a pulse width of 3.2 µs and a repetition rate of 36.3 kHz.
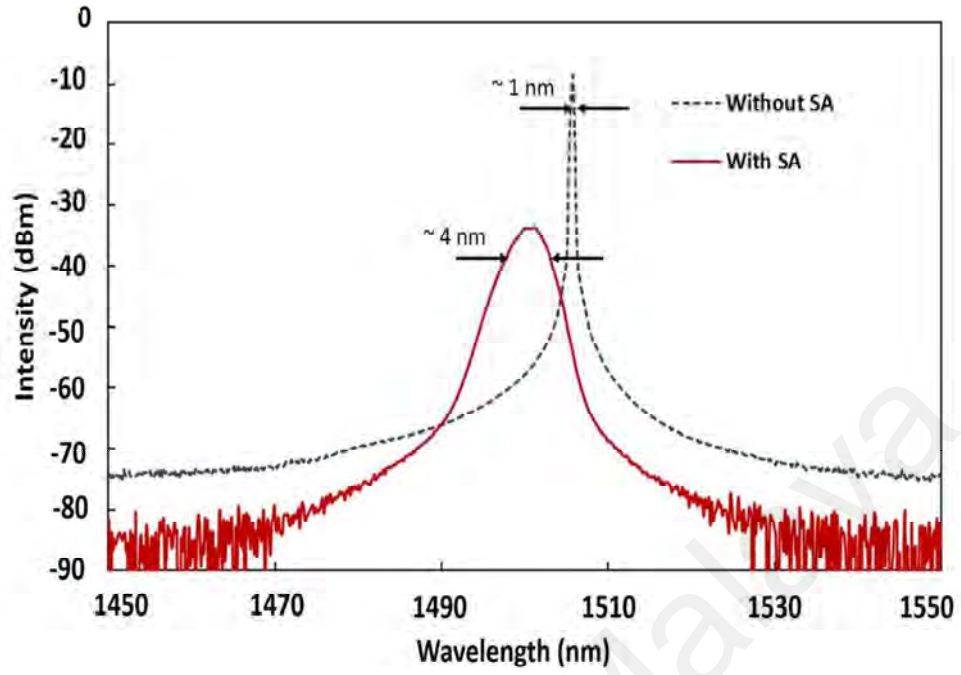
(a)
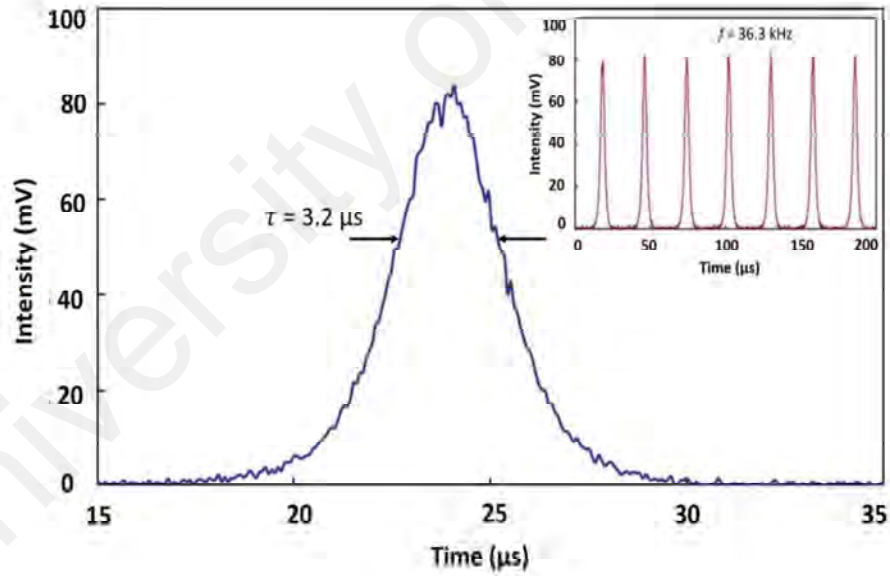
(b)

Figure 4.8: (a) The TFFL optical spectrum with and without the graphene SA and (b) The Q switched pulse profile at the maximum pump power of 230.4 mW. The inset show the corresponding pulse train obtained at the same pulse power[10]

---

[10] (Reproduced with permission from Ahmad, H., **Reduan, S.**, Hassan, N., Ooi, S., & Tiu, Z., 2017b)
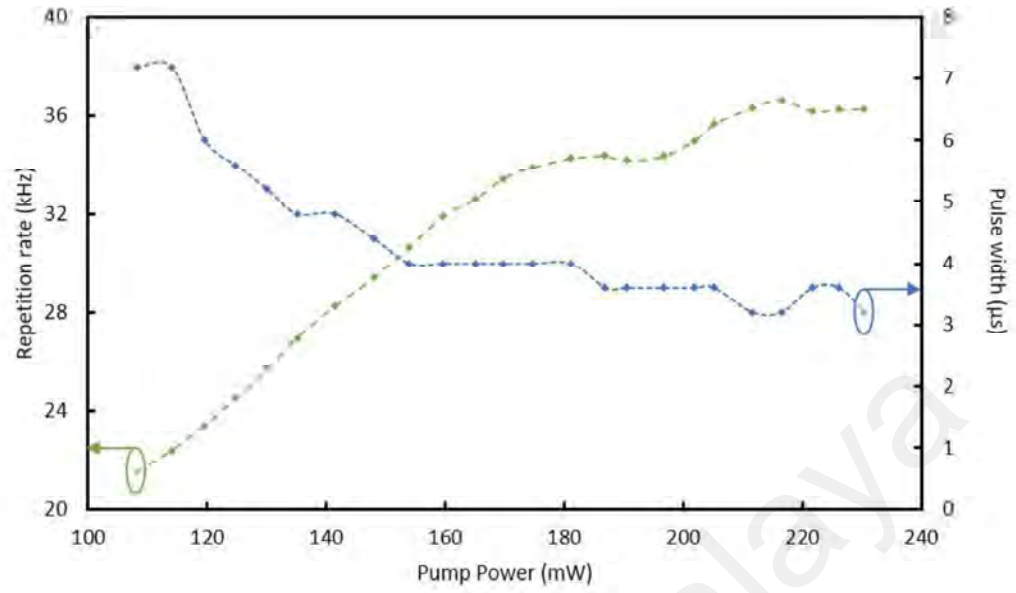
(a)
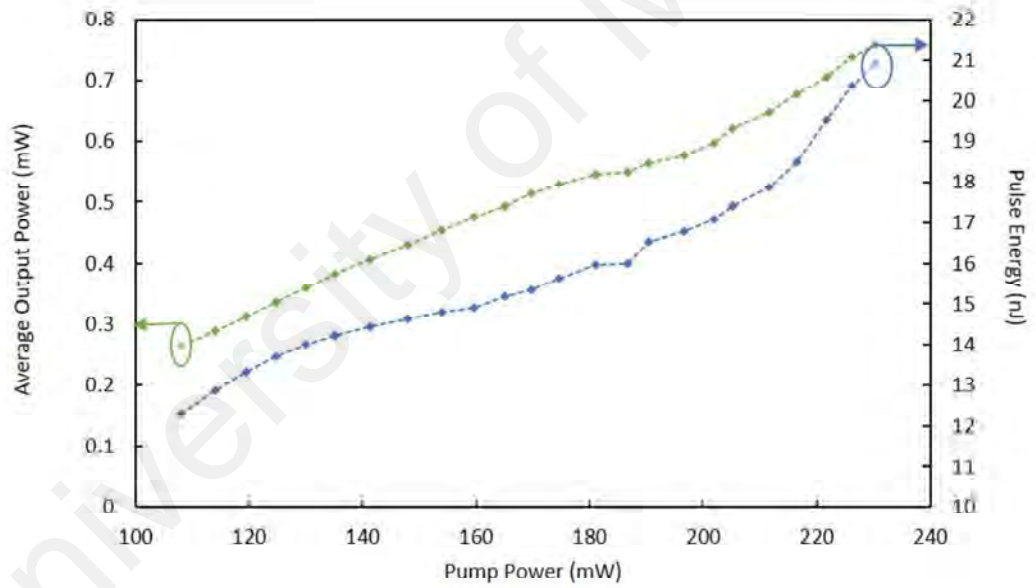
(b)

Figure 4.9: (a) Repetition rate and pulse width and (b) output power and pulse energy of the proposed Q-switched TFF laser against pump power

The repetition rate and the pulse width against the rising pump power are given in Figure. 4.9 (a). As expected, the repetition rate of the pulses increases from 21.5 kHz to 36.3 kHz as the pump power increases from 108.1 mW to 230.4 mW, whereas the pulse width drops from 7.2 μs to 3.2 μs over a similar pump power. Whereas the trends of average output power and pulse energy increase almost linearly as the pump power rises, as shown in Figure 4.9 (b). The maximum average output power and maximum pulse energy obtained in this experiment are 0.76 mW and 20.9 nJ, respectively.

4.2.4   Passively Q-Switched TFF Laser Using MoS$_2$ SA

4.2.4.1 SA Characterization

The MoS$_2$ SA used in the experiment is prepared by a simple mechanical exfoliation method with the flow of preparation shown in Figure 4.10. Initially, a small piece of MoS$_2$ crystal flake is cut out and then placed between two sides of scotch tape, as given in Figure. 4.10 (a) and (b). The MoS$_2$ crystal flake is obtained from Graphene Supermarket. Next, the scotch tape is folded into two and repeatedly pressed to exfoliate the MoS$_2$ crystal on one part of the scotch tape, as shown in Figure. 4.10 (c). The thin layer of MoS$_2$ is formed on the other side of the tape, as given in Figure. 4.10 (d). Finally, the exfoliated MoS$_2$ that acts as the SA is removed carefully and placed onto the fiber ferrule, as shown in Figure. 4.10 (e), reproduced from my earlier work (Reduan et al., 2017).
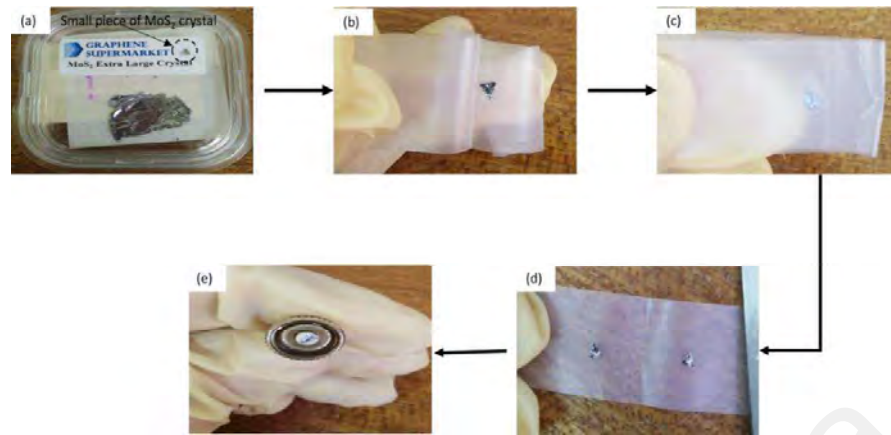
Figure 4.10: Flow of mechanical exfoliation in preparing MoS$_2$ SA[11]
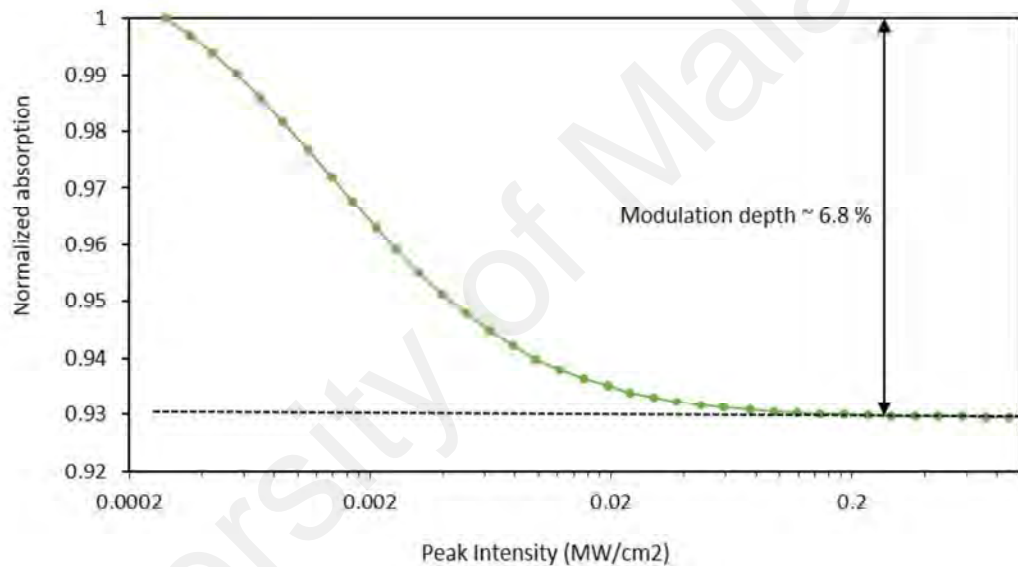
Figure 4.11: Nonlinear measurement of MoS$_2$ SA

The nonlinear absorption measurement of MoS$_2$ SA is shown in Figure. 4.11, which is obtained using the twin-detector technique. The mode-locked laser is used as the source with the central wavelength of 1560 nm exhibiting a repetition rate and pulse width of 28.1 MHz and 0.68 ps, respectively. From the measurements, the SA has a modulation depth of 6.8 % and 0.0018 MW/cm^2, respectively.

---

[11] (Reproduced with permission from **Reduan, S. A.**, & Ahmad, H., 2017)

4.2.4.2 Results

In this study, the Q-switching operation is investigated with the TBPF integrated into the cavity system. The CW threshold starts at 90.0 mW, whereby the Q-switched pulses begin at 93.4 mW, with the central wavelength of 1496.0 nm. No observation of Q-switching operation is observed as the SA is removed from the cavity which shows that the SA attributes to the generation of the Q-switched output pulses.

(a)
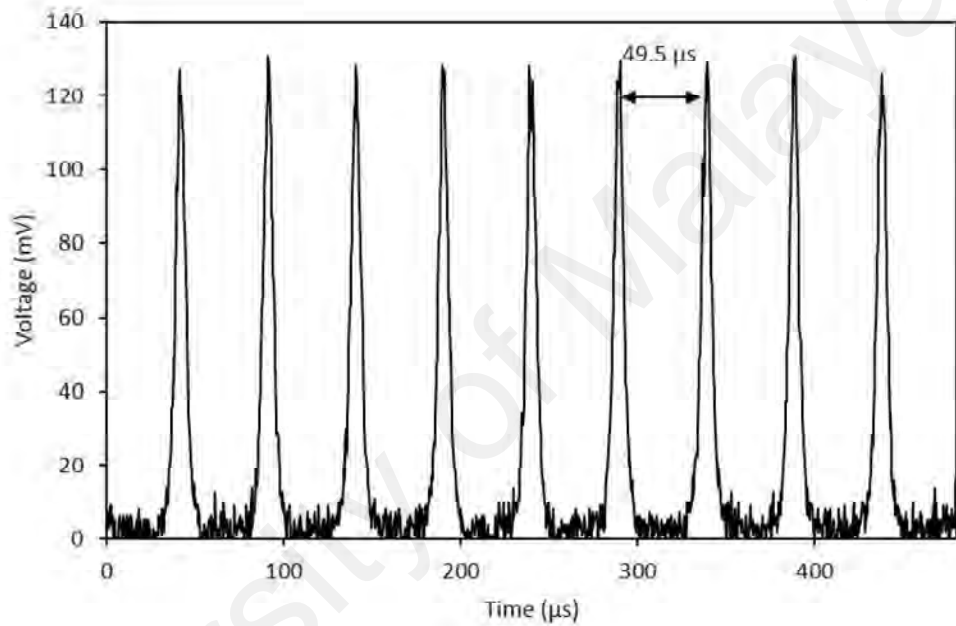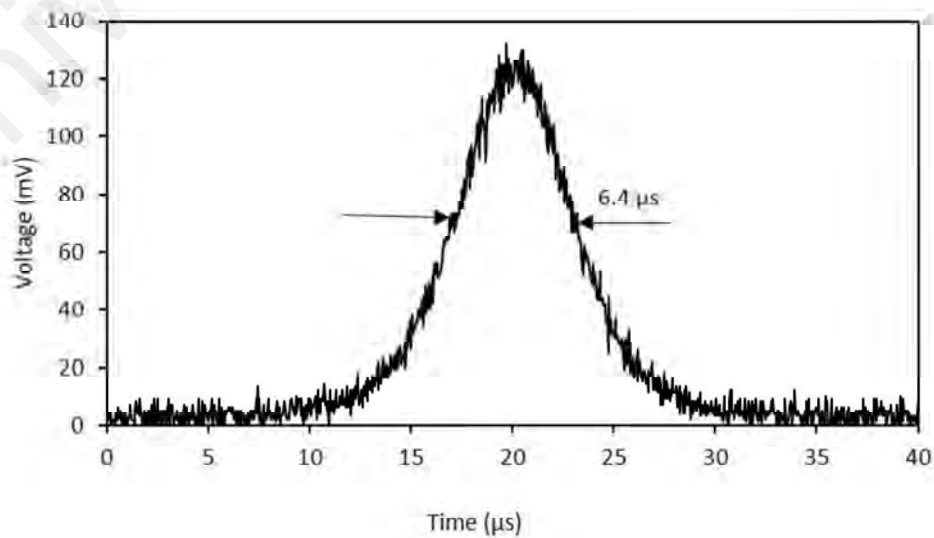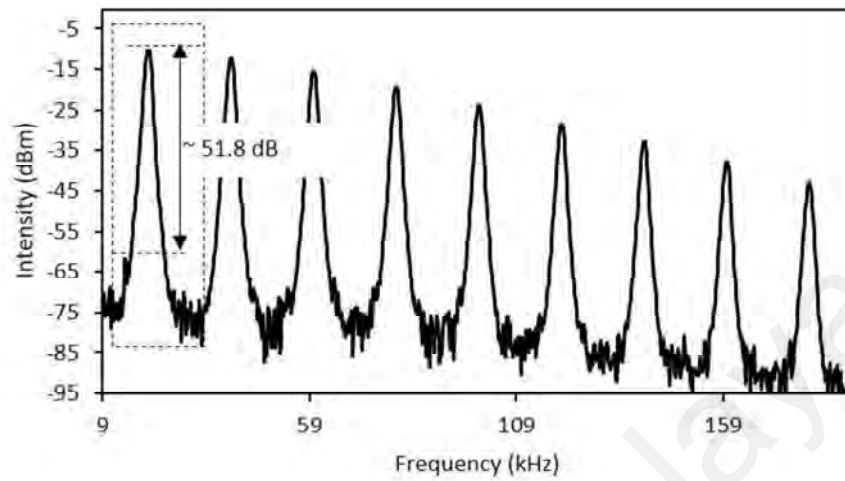
(c)

Figure 4.12: Characteristics of Q-switched pulses at a pump power of 98.1 mW showing (a) the pulse train, (b) the single pulse profile and (c) the RF spectrum of the operation

The typical characteristics of Q-switched pulses are shown in Figure. 4.12 at a pump power of 98.1 mW. Figure. 4.12 (a) shows a pulse train of output pulses with a repetition rate of 20.2 kHz and a period of 49.5 μs. Each of the individual pulses has an FWHM of around 6.4 μs, as given in Figure 4.12 (b). The output pulses have an SNR of ~ 51.8 dB in the obtained RF spectrum as illustrated in Figure 4.12 (c), this confirms the stability of the Q-switched pulses which is comparable to the previous works (B. Chen et al., 2015; Chen et al., 2013).
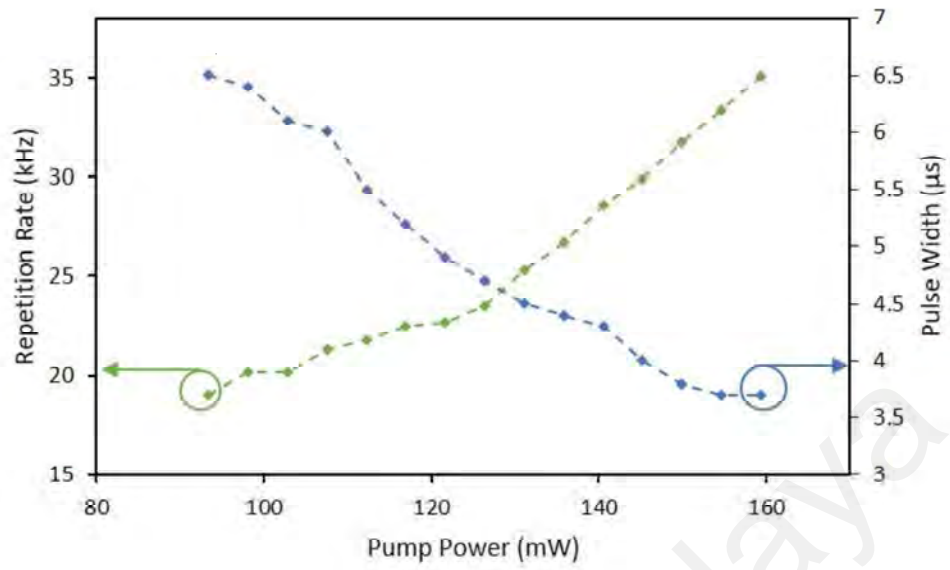
(a)
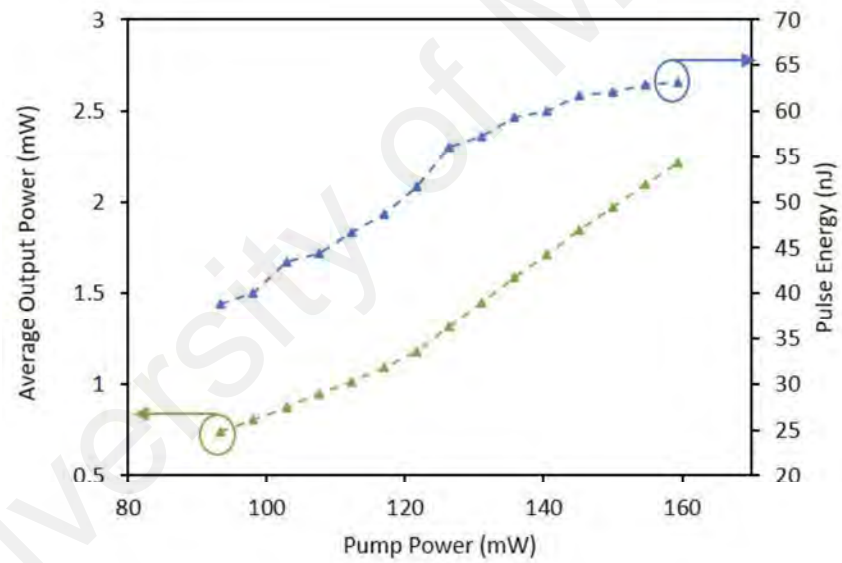
(b)

Figure 4.13: Trends of (a) repetition rate and pulse width and (b) average output power and pulse energy of Q-switched TFF laser as a function of pump power.

Trends of repetition rate against the pump power increase linearly from 19.9 kHz to 35.1 kHz with the rising of the pump power, as shown in Figure 4.13 (a). However, the pulse width decreases from 6.5 µs at the pump power of 93.4 mW to 3.8 µs at the pump power of 149.9 mW, and the pulse width is nearly unchanged at 3.7 µs until the maximum pump power of 159.5 mW. This is due to the 'complete' saturation of the SA. Both the average output power and pulse energy against the pump power are given in Figure 4.13 (b). The trends increase linearly with increasing pump power. From the experiment, the generated output pulses have an average output power of 2.2 mW and maximum pulse energy of 63.2 nJ.
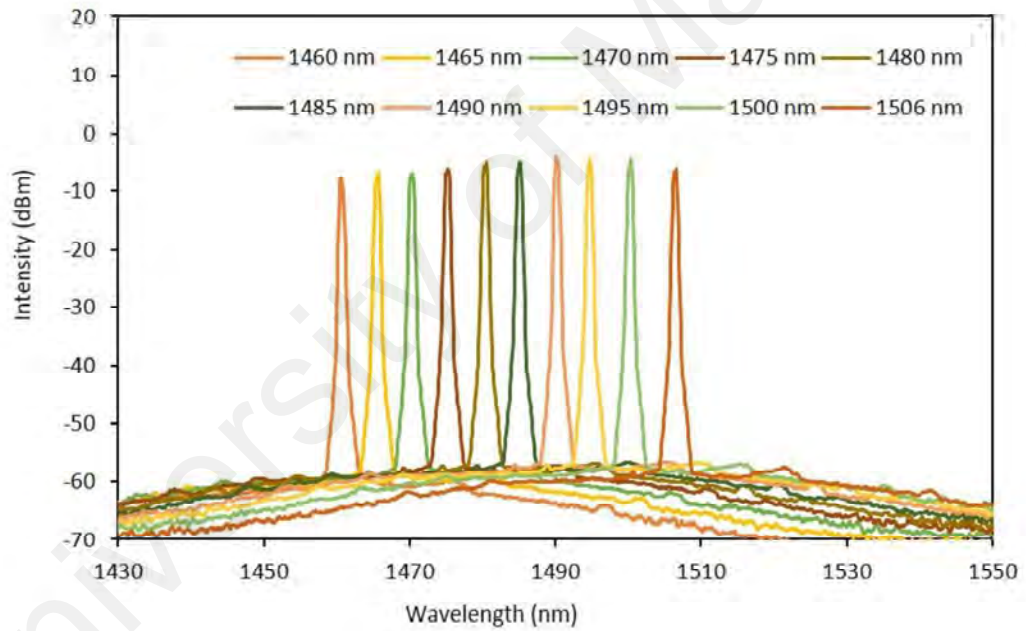
(a)
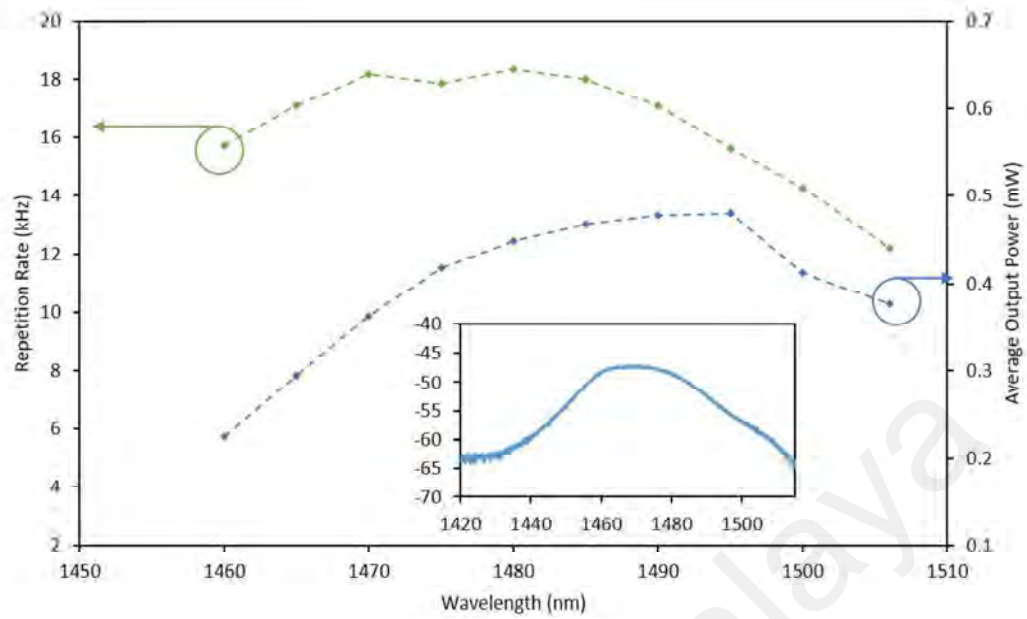
(b)

Figure 4.14: (a) Output spectra for 10 tuning central wavelengths. (b) Trends of repetition rate and average output power as a function of wavelength. Inset illustrates the ASE spectrum of the laser cavity

The central wavelength of the Q-switched pulses can be tuned from 1460 nm to 1506 nm, with a tuning range of 46.0 nm using the TBPF to tune the central wavelength, as illustrated in Figure 4.14 (a), which cover the region of S+/S band. Other than that, the trends of repetition rate and average output power against the wavelength have a similar spectrum of the ASE, as shown in Figure 4.14 (b). This is attributed to the trend of the ASE gain where the larger average output and larger repetition rate results from the larger gain (H. Ahmad et al., 2015; R. Li et al., 2019).

4.2.5 Q-Switched TFF Laser Using GaSe SA

4.2.5.1 SA Characterization

A simple mechanical exfoliation technique is used to prepare the GaSe SA in this experiment. The flow of preparation is similar, as explained in Section 4.2.4.1. However, GaSe crystal flake obtained from 2D semiconductors is exfoliated in this experiment. The Raman spectra of GaSe in bulk and exfoliated form is given in Figure 4.15. The spectra are analyzed using a Renishaw Raman Spectrosccopy at a grating of 1800 l/mm and an excitation wavelength of 532 nm. In this study, the purpose of Raman spectra is to identify the type of material used for the experiment as well as to estimate the number of layers of the exfoliation layer of the GaSe-SA.
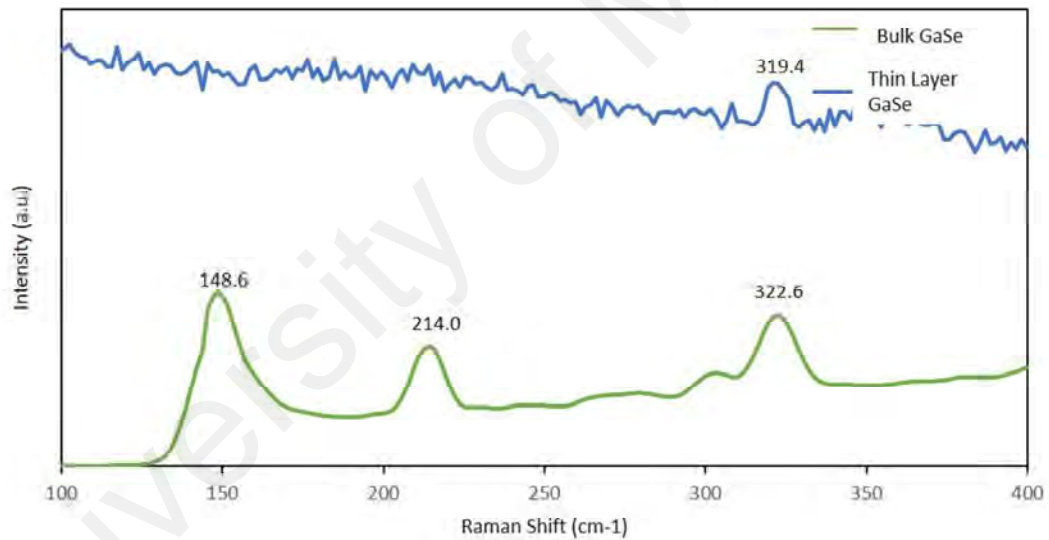
Figure 4.15: Raman Spectrum of GaSe in bulk form and thin layers

The obtained spectrum shows a single peak for a thin layer of GaSe compared to the spectrum of bulk GaSe, in which three peaks can be observed. The single peak obtained at 319.4 cm^{-1} is comparable with previous works by Lei et al. (Lei et al., 2013) and Yuan et al. (Yuan et al., 2015). Three distinct peaks for the Raman spectrum of bulk GaSe are observed at 148.6 cm^{-1}, 214.0 cm^{-1}, and 322.6 cm^{-1}, which are expected and augur well with previous works (Late et al., 2012; Lei et al., 2013). Other than that, the intensity of

the Raman spectrum for a thin layer GaSe SA is higher compared to the intensity of the Raman spectrum for bulk GaSe due to a reduction in the GaSe scattering state which results in less effective Raman scattering (X. Li et al., 2014). The average number of GaSe layers after the exfoliated process is about 1-3 layers, which corresponds to the reduction of Raman peak intensity and redshift between both spectra (Lei et al., 2013; Yuan et al., 2015).
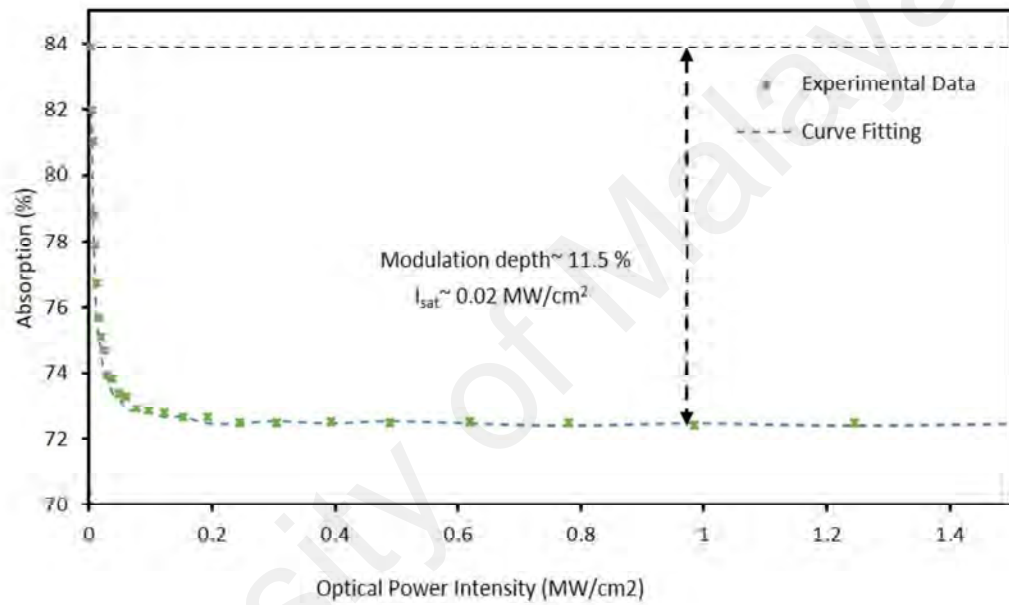
Figure 4.16: Nonlinear absorption measurement of GaSe SA

The twin detector technique is used to measure the nonlinear absorption measurement of the GaSe SA, as shown in Figure 4.16. A passively mode-locked laser is used as a laser seed with a central wavelength of 1560 nm. The modulation depth and the saturation intensity of the GaSe SA are 11.5 % and 0.02 MW/cm^2, respectively. The modulation depth of the SA is comparable to other SAs based on materials such as Bi$_2$Se$_3$ at 11.1 % (H. Ahmad et al., 2015) and MoS$_2$ at 9.7 % (F. Lou et al., 2015).

4.2.5.2 Results

The threshold power of the Q-switching operation in this experiment starts at the pump power of 76.2 mW until a maximum pump power of 133.6 mW. The typical characteristics of the Q-switched pulses are shown in Figure 4.17 taken at the pump power of 109 mW. The generated Q-switched pulses have a central wavelength of 1502 nm, which are located in a shorter wavelength region of S band with a 3-dB spectral width of about 1.0 nm, as given in Figure 4.17 (a). The corresponding pulse trains and pulse profile of the output pulses are shown in Figure 4.17 (b) and Figure 4.17 (c) with a repetition rate, period, and pulse width of 23.3 kHz, 42.4 μs and 3.9 μs, respectively. There is no amplitude modulation on the corresponding pulse profile, as seen in Figure 4.17 (c). The RF spectrum of the output pulses is given in Figure 4.17 (d) with the SNR value of around 52 dB at the fundamental frequency with the resolution bandwidth of 300 Hz. It is also observed that the only fundamental and harmonic frequencies are present in the spectrum, as shown in the inset of Figure. 4.17 (c). This indicates that the generated Q-switched output is a stable pulse (B. Chen et al., 2015). The stability of the Q-switching operation is also investigated by recording the RF spectrum over one hour for every 10 minutes at a pump power of 109 mW as illustrated in Figure 4.17 (e). The SNR value is maintained at around 52 dB over time and proves that the output pulses exhibit a stable Q-switching operation.
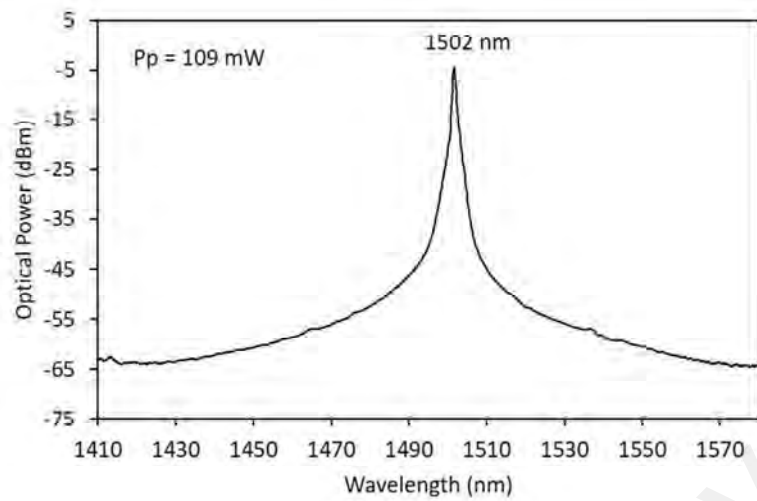
(a)
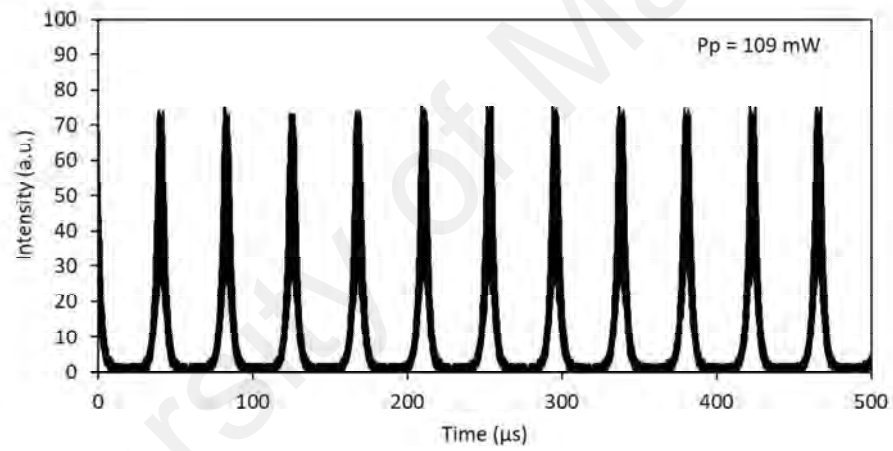
(b)
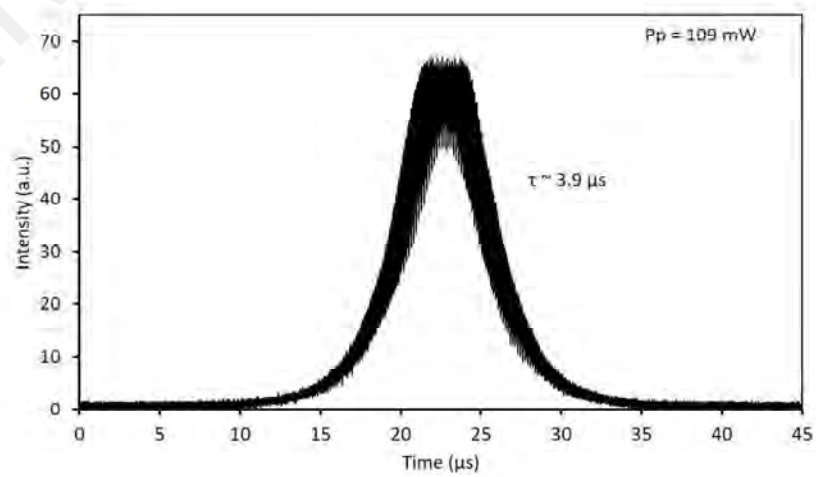
(c)
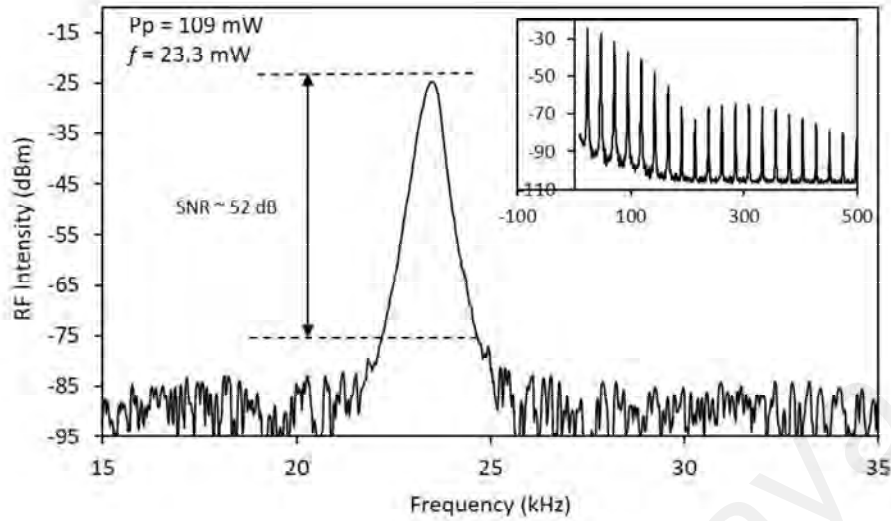
(d)
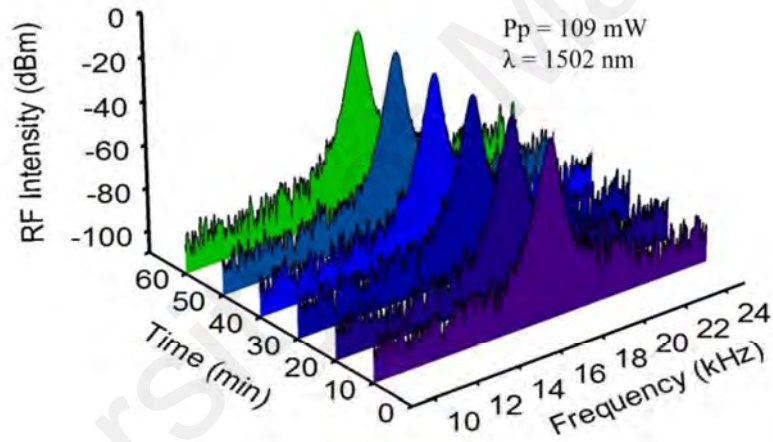
(e)

Figure 4.17: Typical Q-switching operation characteristics at a pump power of 109 mW. (a) Optical spectrum (λ = 1502 nm), (b) pulse train of the Q-switched pulses, (c) single pulse profile of the Q-switching operation, and (d) RF spectrum at the fundamental frequency (f=23.3 kHz). Inset is the wide-band RFSA spectrum (e) Q-switching operation stability, with RF spectra measured at 10 minutes interval for 1 hour[12]

---

[12] (Reproduced with permission from Ahmad, H., & **Reduan, S.,** 2018).
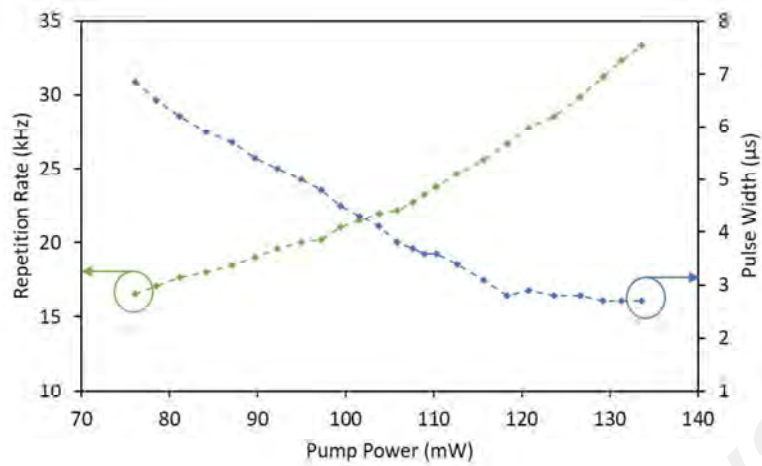
(a)
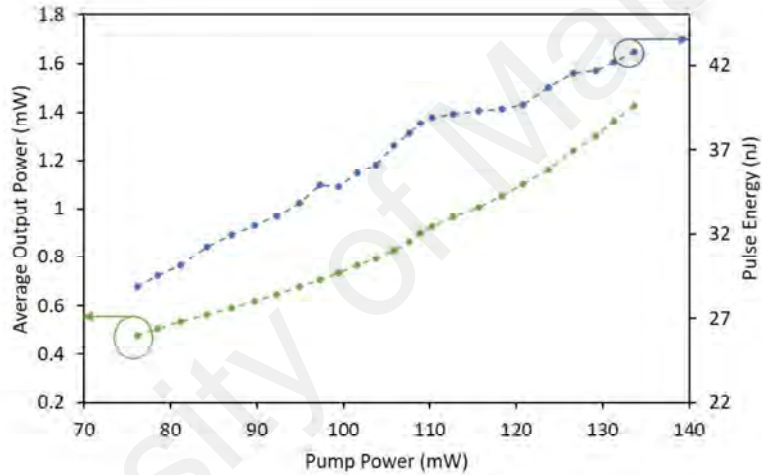
(b)

Figure 4.18: (a) Repetition rate and pulse width against the pump power and (b) average output power and pulse energy

Figure 4.18 (a) shows the trends of repetition rate and pulse width against the pump power at the central wavelength of 1502 nm. It can be seen from the figure that the repetition rate increases from 16.5 kHz at pump power 76.2 mW to 33.3 kHz at the maximum pump power of 133.6 mW. At the same time, the pulse width decreases linearly from 6.9 μs to 3.1 μs at the pump power 76.2 mW to 115.7 mW, then the pulse width starts to slow and remains constant at 2.7 μs until the maximum pump power is achieved. This is due to the full saturation of the SA for which the pump power has reached the

level where the population at ground state and excited state of the SA has become almost equal. Thus, further absorption is very minimal and results in a saturated SA (Yap, 2015).

The response of average output power and pulse energy against the pump power is seen to increase linearly, as shown in Figure 4.18 (b). The obtained maximum average output power and maximum pulse energy in this experiment are 1.4 mW and 42.8 nJ.
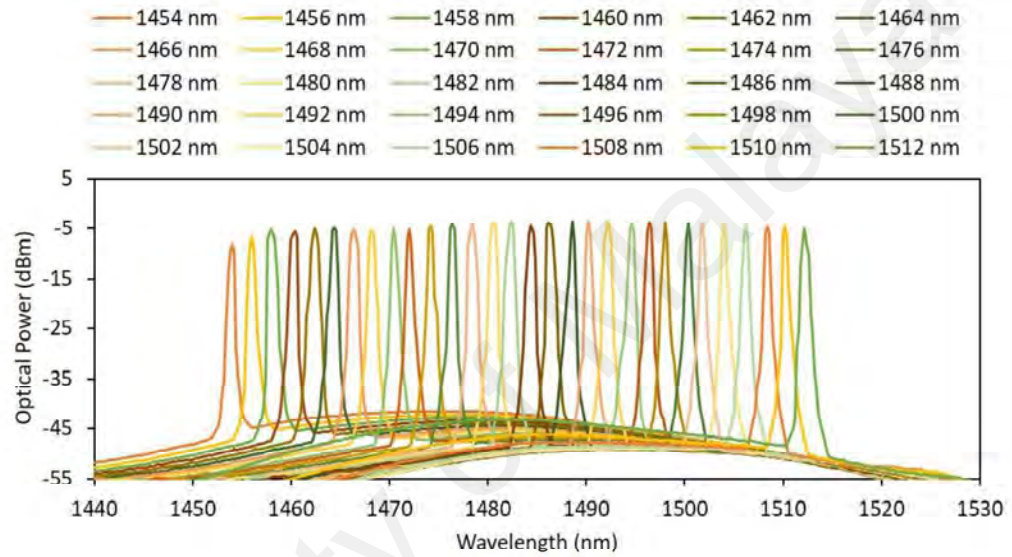
(a)
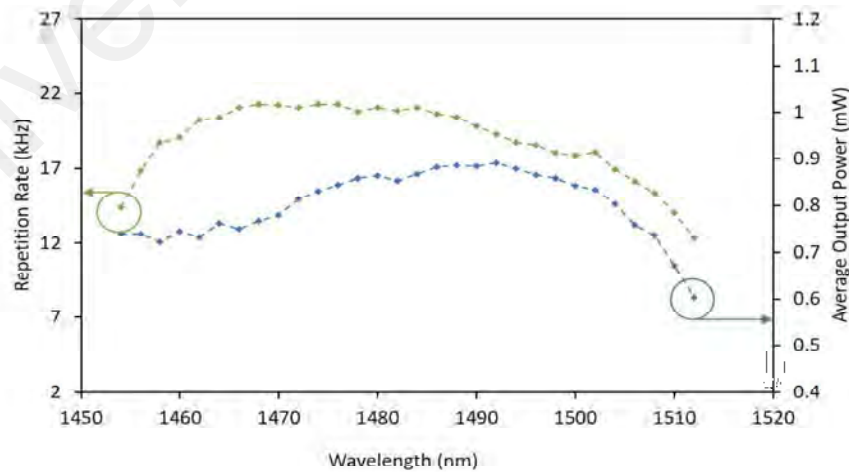
(b)

Figure 4.19: (a) Wavelength tunable Q-switching operation spectra, and (b) trends of repetition rate and average output power against the wavelength

The tunability of the Q-switching operation is given in Figure 4.19 (a). The central wavelength is tuned by the TBPF while the pump power is kept constant at 109 mW. Based on Figure 4.19, the Q-switched pulses can be tuned from 1454 nm to 1512 nm with a tuning range of 58 nm, which covers an S band region. It is also noted that there are no Q-switched pulses are obtained beyond this wavelength region, since the tunability depends highly on the TBPF's loss and the bandwidth of the gain medium (Y. Huang et al., 2014). The repetition rate and average output power against the central wavelength are shown in Figure 4.19 (b). The maximum pulse energy obtained during the tunability is 51.4 nJ. Initially, the central wavelength of the Q-switching operation is located at 1502 nm, but the central wavelength of output pulses shifted to 1498 nm as the TBPF inserted into the cavity. This is believed due to the insertion loss of TBPF within the laser system. It is observed that the central wavelength can be shifted to shorter or longer wavelengths throughout the tunability, which results in varied repetition rates and average output power. This is because of the cavity loss variation, insertion loss of TBPF, and also the gain difference of the gain medium at a different wavelength.

In this study, four types of materials that act as SAs have successfully generated passively Q-switched pulses in a TFF laser system. These materials are graphene, SWCNT, MoS_2, and GaSe. Table 3 provides a comparison of the parameters obtained for each experiment using a different SAs in the same TFF laser system.

Table 4.1: Passively Q-switched TFF laser by a different SAs

Type of SA	Graphene	SWCNT	MoS$_2$	GaSe
Operation wavelength (nm)	1501	1450 – 1512	1460.0 – 1506.0	1454 - 1512
Tuning range	-	62.0	46.0	58.0
Max pulse energy	20.9 nJ	122.8 nJ	63.2	51.4 nJ
Repetition rate (kHz)	21.5 – 36.3	12.0 – 36.4	19.9 – 35.1	16.5 – 33.3
Min pulse width (µs)	3.2	3.6	3.8	2.7

From Table 4.1, it can be seen that all of the proposed experiment generates a Q-switched pulses in S band region. The shorter central wavelength achieved in this study is located at 1450.0 nm using SWCNT as SA in the proposed TFF system. Other than that, SWCNT SA able to generate the highest repetition rate and maximum pulses energy compared to other experiments. However, the experiment using GaSe SA in the TFF laser system generates the shortest minimum pulse width at 2.7 µs. Different results obtained for different SA could be attributed to the properties of the SAs for each material as well as the fabrication of the SAs itself. In conclusion, all of the obtained Q-switched pulses show typical characteristics of Q-switched output pulses.

In comparison with other previous works utilizing the depressed-cladding EDF (DC-EDF) as a gain medium (H. Ahmad et al., 2017a), the report Q-switching operation covers only a small region of S band from 1484 nm to 1492 nm with a tuning range of ~ 8 nm and low pulse energy of about ~ 1.2 nJ. There is also a previous work conducted by Chen

et al. (Chen et al., 2014), which was able to generate high energy pulses using Bi_2Te_3 as SA. However, they only covered a small region of S band from 1510 nm to 1530 nm. There were other previous work reports on generating Q-switched pulses in the S band region, but they only involved a short region before the C-band region (Cao et al., 2011; Chen et al., 2014; Zhou et al., 2012). The generation of Q-switched TFF laser provided a significant potential in the applications of S+/S band region.

4.3 Dual-Wavelength Q-Switched Thulium-Fluoride Fiber Laser For S+/S Band Using MoS_2 SA

A dual-wavelength pulsed laser is seen to be useful in many applications such as in the field of environmental sensing, telecommunications, laser processing, and medicine. SA is used in this experiment due to its simplest approach in generating Q-switched pulses (Martinez et al., 2013). MoS_2, one of the TMDs had gained significant attention due to its stable behavior and seen to be a potential SAs to generate pulsed laser (Ahmed et al., 2016; M. Zhang et al., 2015). The generated dual-wavelength, Q-switching operation was generated from the combination of MoS_2 based SA with PCF in the laser system.

4.3.1 Experimental Setup of Dual-Wavelength Q-Switched TFF Laser Using MoS_2 SA And PCF

The experimental set-up of the dual-wavelength, Q-switched TFF based fiber laser is shown in Figure 4.20, reproduced from my earlier work (H. Ahmad et al., 2017c). A 1400 nm FOL1405RTD LD connected to the ISO is used to pump the TFF. Then, the end port of ISO is linked to the 1400 nm port of 1400/1500 WDM, where the universal port is connected to the 14.5 m long TFF. The end of the TFF fiber is linked to another ISO to ensure the unidirectional signal propagation. Next, the ISO is connected to a 90:10 output coupler, where the 10 % port is utilized to extract a portion of the signal for analyzing purposes. Another 90 % is propagating back into the cavity and now connects to a 0.5 cm

PCF, with an insertion loss and core diameter at 8 dB and 4.37 µm at the wavelength of 1550 nm. The diameter of the microscopic hole is around 5.1 µm that surrounding the solid core of the PCF. The output port of PCF is then linked to SA, and it is then connected to 1500 nm port of the WDM. Finally, the cavity is complete with a total cavity length of around 25.0 m.
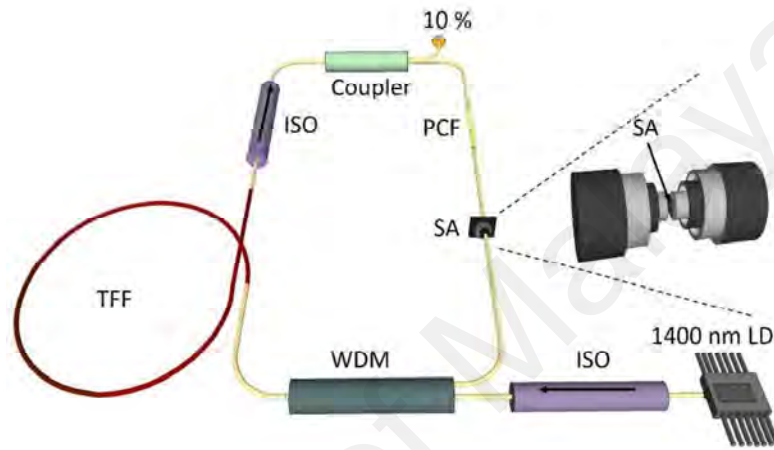
Figure 4.20: Experimental setup of dual-wavelength, Q-switched pulses based on MoS$_2$ SA[13]

Figure 4.21 (a) and (b) show the Microscopic image from the side view of the PCF and SMF-28 splicing point and cross-section of PCF, respectively (Safaei et al., 2017). Based on Figure 4.21 (a), the diameter of PCF and SMF-28 is nearly the same; thus, the diameter of the PCF is around 10.4 µm. The cross-sectional area of the PCF is around 85.0 µm^2. The number of air-holes are 36, as shown in Figure 4.21 (b)

---

[13] (Reproduced with permission from Ahmad, H., **Reduan, S.**, & Safaei, R., 2017c)
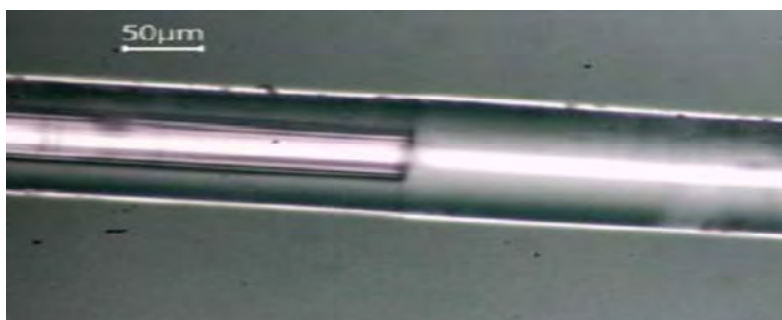
(a)
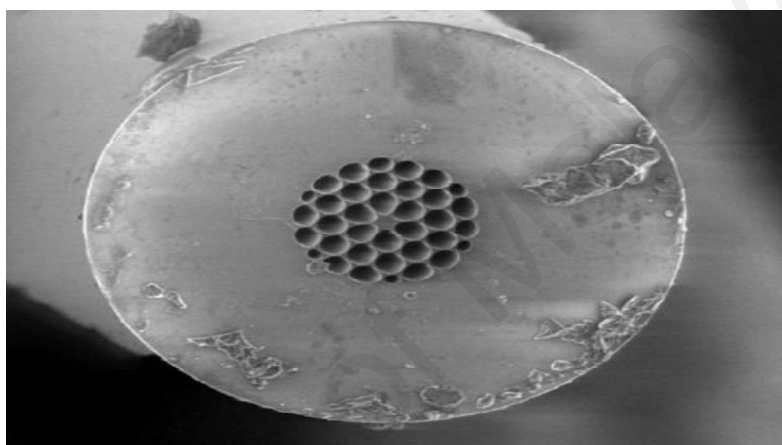
(b)

Figure 4.21: (a) Microscopic image from the side view of the PCF and SMF-28 splicing point. (b) The cross section of PCF[14]

The optical and pulse characteristics of the output signal is analyzed. Anritsu MS9740A OSA is used to analyze the optical output, whereas a Yokogawa DLM2054 OSC with 1.2 GHz photodetector is used to analyze the generated pulse trains. The SNR of the output pulses is measured using Anritsu MS2683 RFSA, whereas the average output power of the pulsed laser is measured using Thorlabs SC144C OPM.

---

[14] (Reproduced with permission from Safaei, R., Amiri, I. S., Rezayi, M. & Ahmad, H., 2017)

4.3.2 SA Characterization

In this experiment, the SA is prepared using a mechanical exfoliation technique with the process flow the same as explained in Section 4.2.4.1. The MoS_2 crystal flake is obtained from Graphene Supermarket. The Raman spectrum of the MoS_2 SA is given in Figure 4.22 using Renishaw Raman Spectrometer with an excitation wavelength of 532 nm. Two Raman peaks observed in the spectrum located at 381.9 cm^{-1} and 407.4 cm^{-1}. Based on this observation, it is confirmed that the MoS_2 sample is a pure composition, as demonstrated by comparable works (Heping Li et al., 2015; H. Zhang et al., 2014). Other than that, the number of MoS_2 layers can be estimated by measuring the peak frequency between two obtained Raman peaks, as mentioned by Li et al. (Hong Li et al., 2012). In this regard, the estimated thickness of the MoS_2 layers in this work is around 3-4 layers (Heping Li et al., 2015).
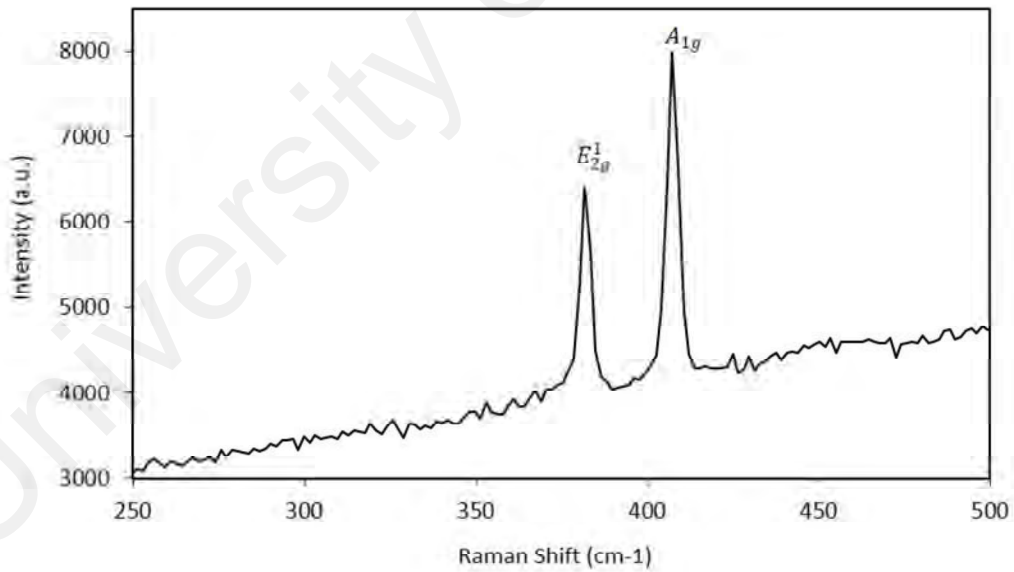
Figure 4.22: Raman spectrum of MoS$_2$
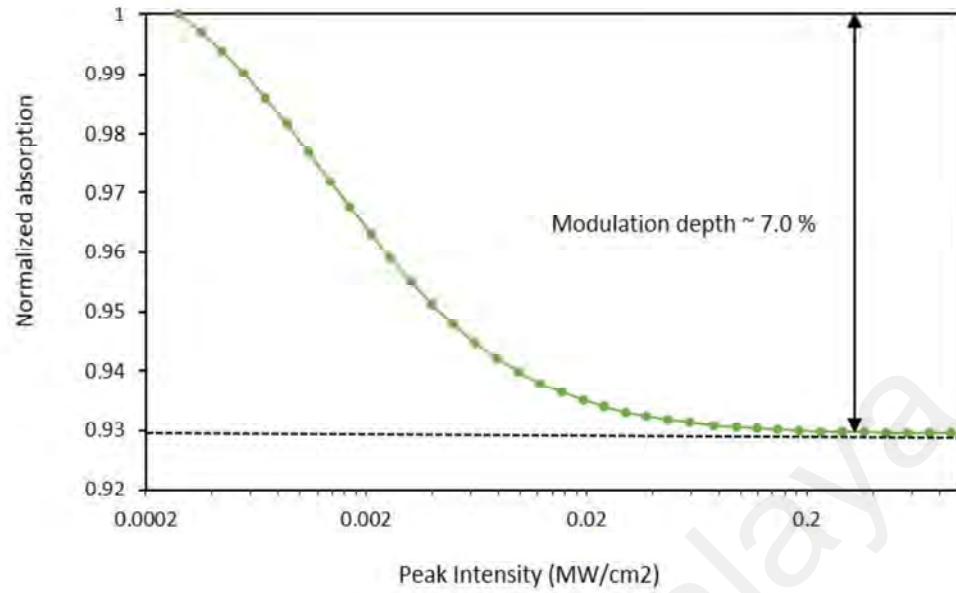
Figure 4.23: Nonlinear measurement of MoS$_2$ SA

The nonlinear absorption characteristics of MoS$_2$ SA are measured using a twin detector technique. This technique used a mode-locked laser as a laser seed with a central wavelength of 1560 nm. The obtained data is fitted into the saturation model, and the nonlinear absorption trends of the MoS$_2$ SA are obtained, as shown in Figure 4.23. The modulation depth and saturation intensity obtained in this measurement are 7.0 % and 0.002 MW/cm^2, respectively.

A 0.5 cm long PCF is used to generate a dual-wavelength output, which exhibits a core diameter of around 4.37 μm and an insertion loss of 8 dB at a wavelength of 1550 nm. Other than that, a microscopic air hole with a diameter of about 1.5 μm surrounding the solid core of PCF, with the separation of the two subsequence holes of approximately 5.5 μm. The PCF is integrated into the cavity in between the output coupler and SA assembly.

4.3.3 Results and Discussion

The MoS_2 SA plays a role in generating the Q-switched pulses while the PCF is used to generate the dual-wavelength lasing in this experiment. The CW lasing threshold starts at 101.6 mW, while the Q-switched lasing threshold is at 111.3 mW. The characteristics of the dual-wavelength, Q-switched output laser is given in Figure 4.24.
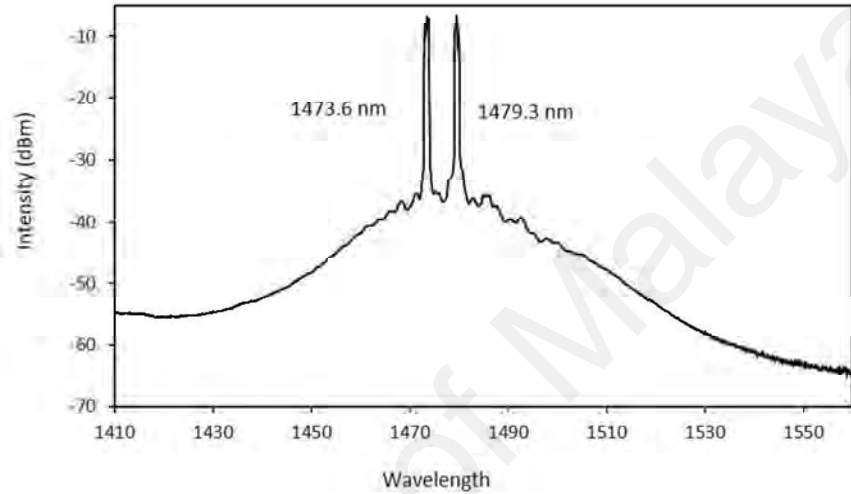
(a)
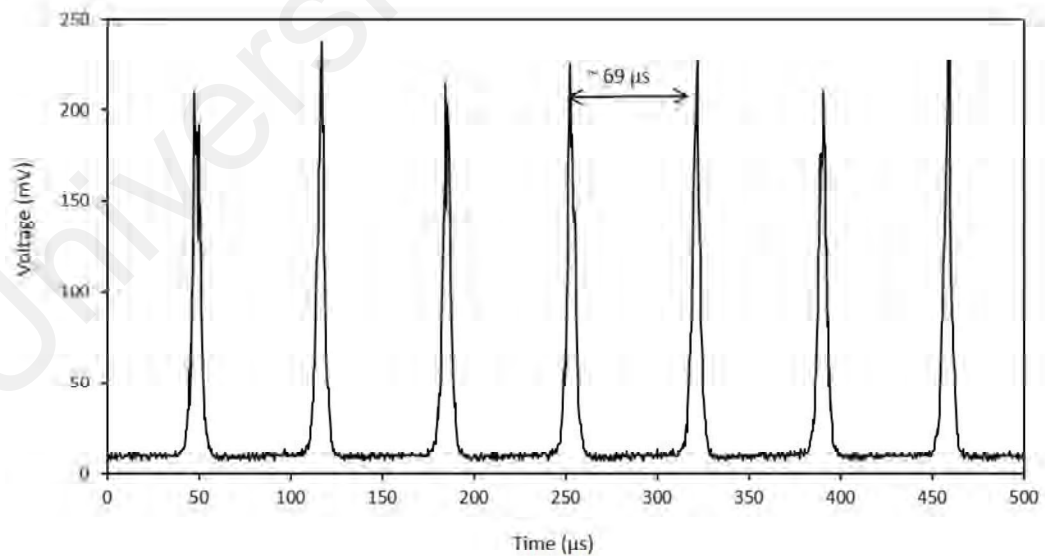
(b)
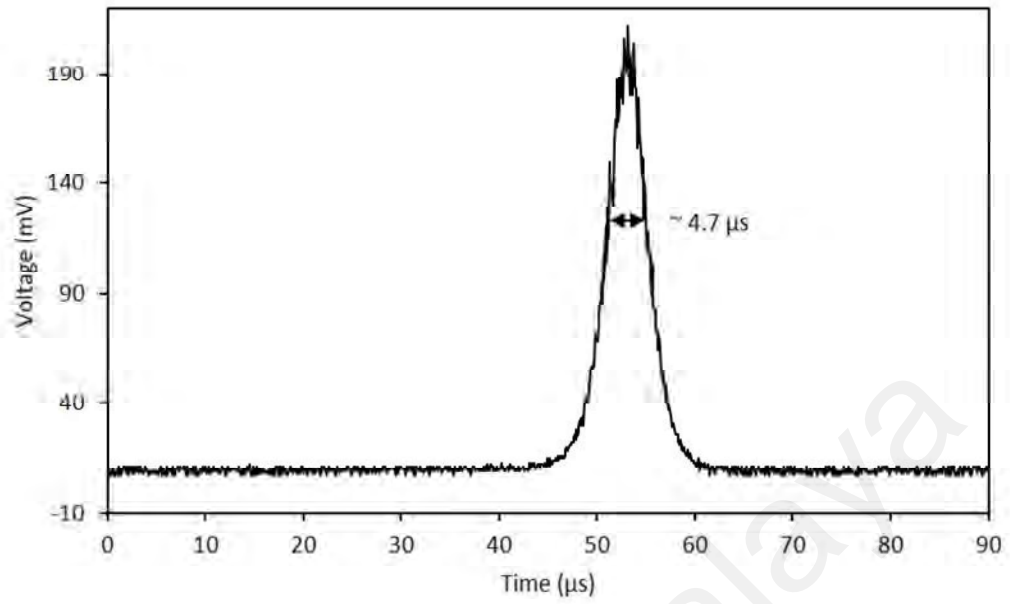
(c)
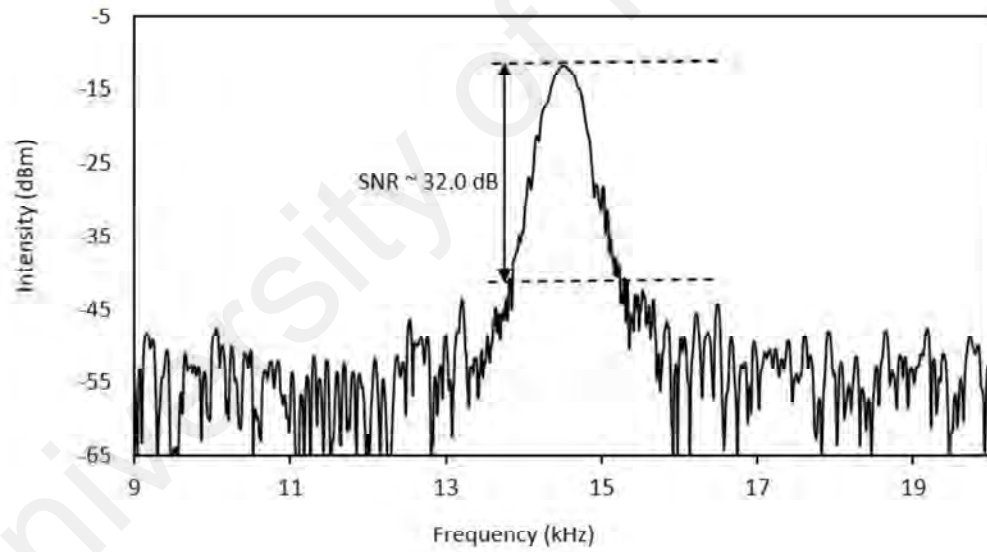
(d)

Figure 4.24: (a) optical spectrum of the dual-wavelength Q-switched output at a pump power of 121.7 mW as well as the (b) pulse train, (c) single pulse profile and (d) RF spectrum of fundamental frequency ($f_0 = 14.5$ kHz) of the dual-wavelength output at the same pump power

The optical spectrum of the output pulses is shown in Figure 4.24 (a), taken at the pump power of 121.7 mW with the wavelengths, located at 1473.6 nm, and 1479.3 nm give a spacing of around 5.7 nm. Both of the wavelengths are located in the S+/S band region, which is the crucial extending of the S band. The two lasing wavelengths have 3-dB bandwidths of around 0.1 nm and 0.3 nm, respectively. The pulse trains of the output pulses have a repetition rate of 14.5 kHz, which correspond to a period of 69.0 μs as given in Figure 4.24 (b). The pulse profile of a single pulse shown in Figure 4.24 (c) with an FWHM of around 4.7 μs and the SNR value of the output pulses of about 32. dB, as illustrated in Figure 4.24 (d).
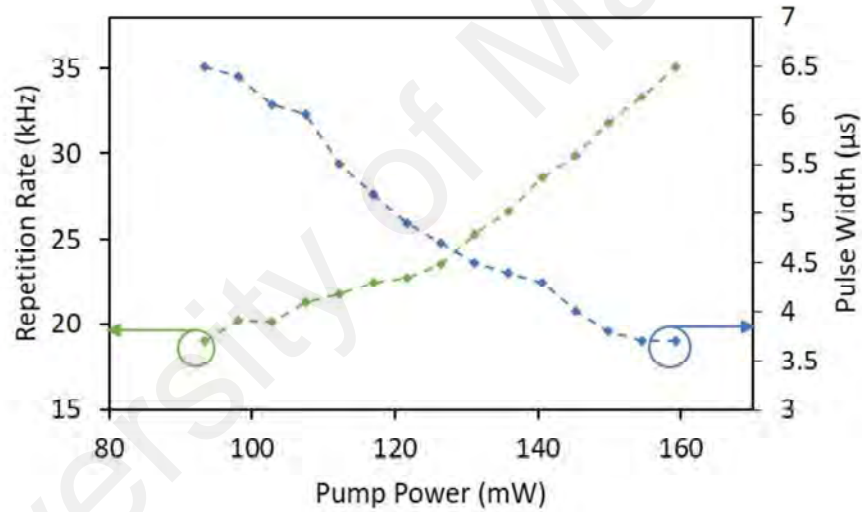
(a)
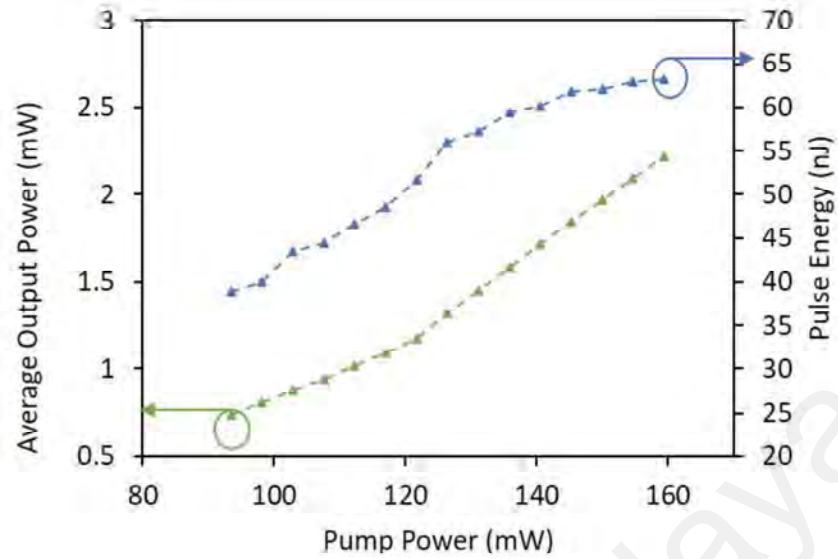
(b)

Figure 4.25: (a) Repetition rate and pulse width, and (b) average output power and pulse energy against different pump powers

The characteristics of the output pulses against the rising pump power are shown in Figure 4.25. The repetition rate and pulse width against the rising pump power are given in Figure 4.25 (a). It is observed that the repetition rate increases linearly from 9.4 kHz to 15.9 kHz, while the pulse width decreases exponentially from 7.3 μs and 4.1 μs over the pump power from 111.3 mW to 126.4 mW. The average output power and pulse energy also increase as the pump power increases, as shown in Figure 4.25 (b). The maximum average output power and maximum pulse energy obtained in this experiment are 1.3 mW and 83.7 nJ, respectively.
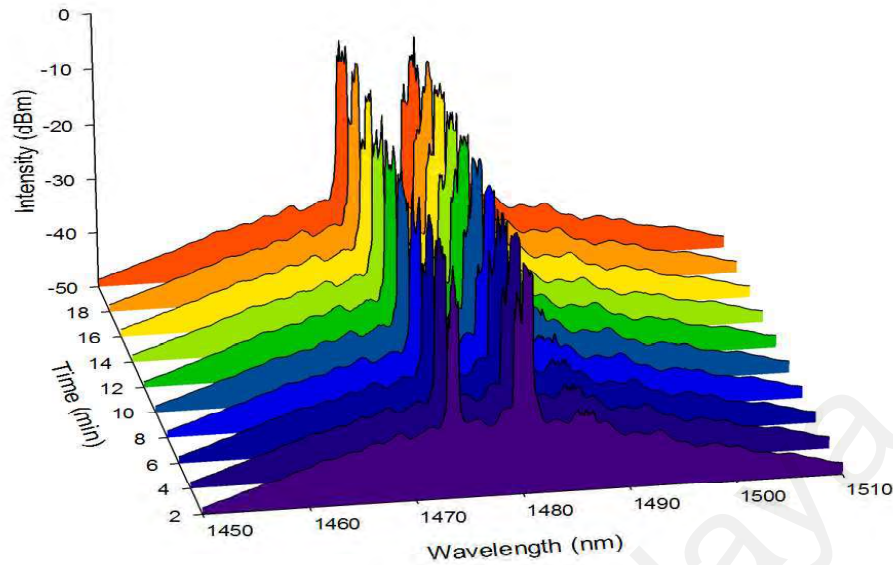
Figure 4.26: Output spectrum at a fixed wavelength of 1473.6 nm and 1479.3 nm at 2-minute intervals over a period of 20 minutes[15]

The stability of the generated output pulsed is investigated by observing the output laser for a total period of 20 minutes in a 2 minutes interval, with the pump power being kept maintained at 121.7 mW. The stability performance is given in Figure 4.26, and it shows that the generated output is in a stable state with the minimal fluctuation of peak power for both lasing outputs. Other than that, the lasing spectrum shows no shift in the wavelength range, representing that the cavity system is highly stable.

---

[15] (Reproduced with permission from Ahmad, H., **Reduan, S.**, & Safaei, R., 2017c)
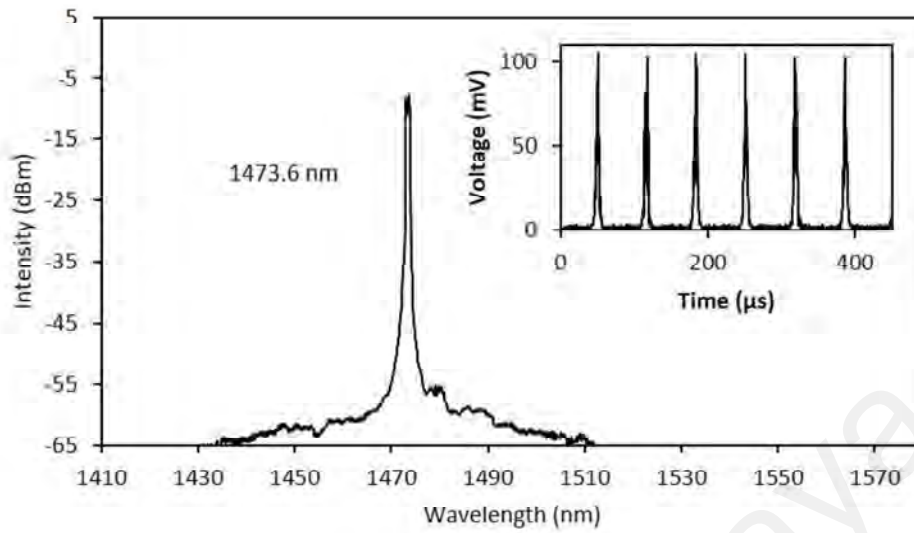
(a)
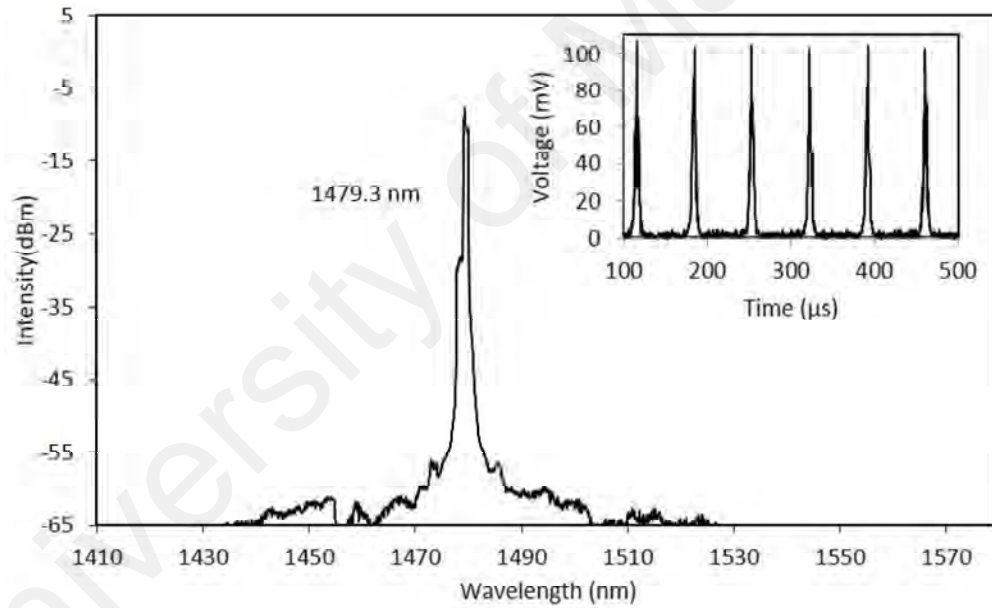
(b)

Figure 4.27: Spectrum and pulse train of the individual lasing wavelengths at (a) 1473.6 nm and (b) 1479.3 nm under a pump power of 121.7 mW

Each individual Q-switched output pulses is analyzed using a TBPF after the 10 % port of the output coupler to allow a single wavelength to filter out for analyzing purposes. Resulting single-pulse spectra is given in Figure 4.27, with a spectrum of the laser and pulse trains for a lasing wavelength at 1473.6 nm given in Figure 4.27 (a) and a lasing wavelength at 1479.3 nm given in Figure 4.27 (b). These measurements are taken at the

same pump power of 121.7 mW. It can be seen that each individual lasing wavelength has an average output power of around 0.28 mW. The total average output power for individual lasing wavelength is lower than the average output power of the dual-wavelength, Q-switched pulses due to the loss by the TBPF after the 10 % port of output coupler. However, the obtained pulse trains for each wavelength has a similar repetition rate at 14.5 kHz. The obtained laser is seen to be beneficial for the applications requiring a dual-wavelength pulsed laser at the S band region, even at the shorter wavelength of the S band.

4.4 Passively Mode-Locked Thulium-Fluoride Fiber Laser Using In$_2$Se$_3$ SA

A passively mode locked TFF laser using an In$_2$Se$_3$ SA is demonstrated in this study. A bulk In$_2$Se$_3$ crystal is purchased from 2D semiconductors. The crystal has a bandgap of 1.41 eV, equivalent to 800 nm, which is out of the region of S+/S band. However, it can still be used as the SA due to the edge-defect state (Roxlo et al., 1987; Trushin et al., 2016; M. Zhang et al., 2015) and the quantum-size effect (Y. Wang et al., 1991). As reported by previous work (Balakrishnan et al., 2018; Julien et al., 1990), In$_2$Se$_3$ is a direct bandgap semiconductor that is a suitable candidate for use in photonics applications and optoelectronic devices.

4.4.1 Experimental Setup of Passively Mode-Locked TFF Laser Using In$_2$Se$_3$

A fiber ring cavity is constructed in this experiment, as shown in Figure 4.28. The cavity consisted of a 10 m of TFF and pumped by a 1400 nm LD. The pumping source is connected to a gain medium via a 1400 nm port of 1400/1500 nm WDM. Then, the SA is inserted into the cavity after TFF and connected to a polarization-insensitive isolator (PI-ISO) to ensure the unidirectional propagation of light. An output coupler with a ratio of 90:10 is used where 90 % of the signal is connected back to the WDM, thus

closing the cavity, while the 10 % port is linked to 50:50 output coupler to enable simultaneous measurement of the generated pulse's parameters.
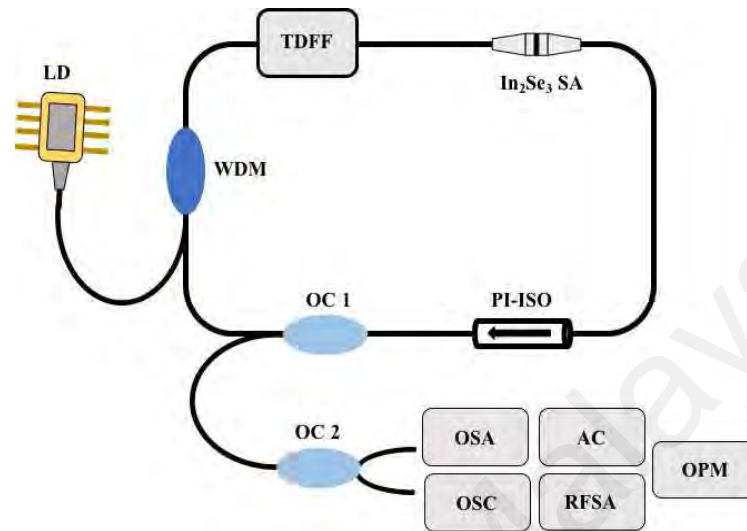
Figure 4.28: Schematic Diagram of Passively Mode-locked TFF laser using In$_2$Se$_3$ SA[16]

An OSA with a resolution of 0.02 nm is used to characterize the generated optical spectrum while the pulse train being monitored by a Yokogawa DLM2000 OSC and Thorlabs DET01CFC photodetector. A two-photon absorption Alnair HAC-200 autocorrelator is used to measure the pulse width of the generated pulse. The output power is measured using an OPM, while the frequency parameters of the pulses are analyzed using an Anritsu MS2683 RFSA.

The entire cavity of this experiment consists of 10 m of TFF and about 20 m of single-mode fiber (SMF-28), giving a total cavity length of about 30 m. The dispersion values for the TFF and SMF-28 are -20 ps/nm/km (H. B. Ahmad et al., 2017) and 14 ps/nm/km respectively at the wavelength of 1500 nm. The total dispersion of this cavity is about

---

[16] (Reproduced with permission from Ahmad, H., Reduan, S. A., Ooi, S. I., & Ismail, M. A., 2018)

0.08 ps/nm at 1500 nm. The propagation of the output pulses will be balanced by the interaction between the group velocity dispersion (GVD) and self-phased modulation (SPM) to generate soliton mode-locking (Tamura et al., 1994).

4.4.2   SA Characterization

The In_2Se_3 SA is prepared by mechanical exfoliation, as explained in Section 4.2.4.1. The In_2Se_3 crystal flakes are purchased from 2D Semiconductors, and the exfoliated In_2Se_3 SA has an insertion loss of around 5.4 dB.
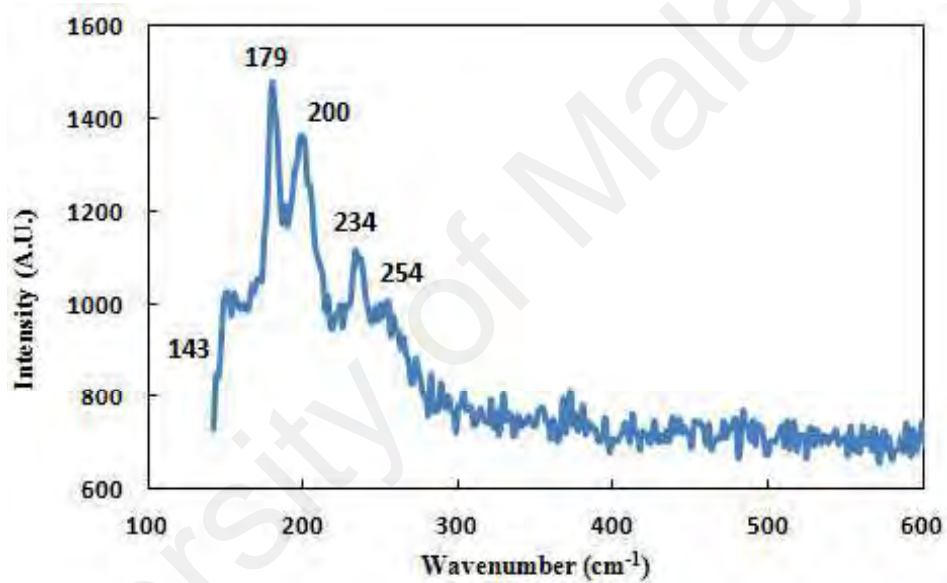
Figure 4.29: Raman Spectrum of In_2Se_3 SA[17]

The composition of the In_2Se_3 SA is verified under a Raman Spectroscopy using a Renishaw Raman System with a 532 nm excitation wavelength. The obtained spectrum shows five Raman peaks located at 143 cm^{-1}, 179 cm^{-1}, 200 cm^{-1}, 234 cm^{-1}, and 254 cm^{-1} as given in Figure 4.29. These peaks are comparable to those reported in previous work by Ho et al. (Ho, 2014) and thus confirms the presence of In_2Se_3 in the exfoliated layers.

---

[17] (Reproduced with permission from Ahmad, H., Reduan, S. A., Ooi, S. I., & Ismail, M. A., 2018)

The thickness of the exfoliated layers is estimated to be around 6 μm based on the Raman spectrum, as discussed by Ho et al. (Ho, 2014).
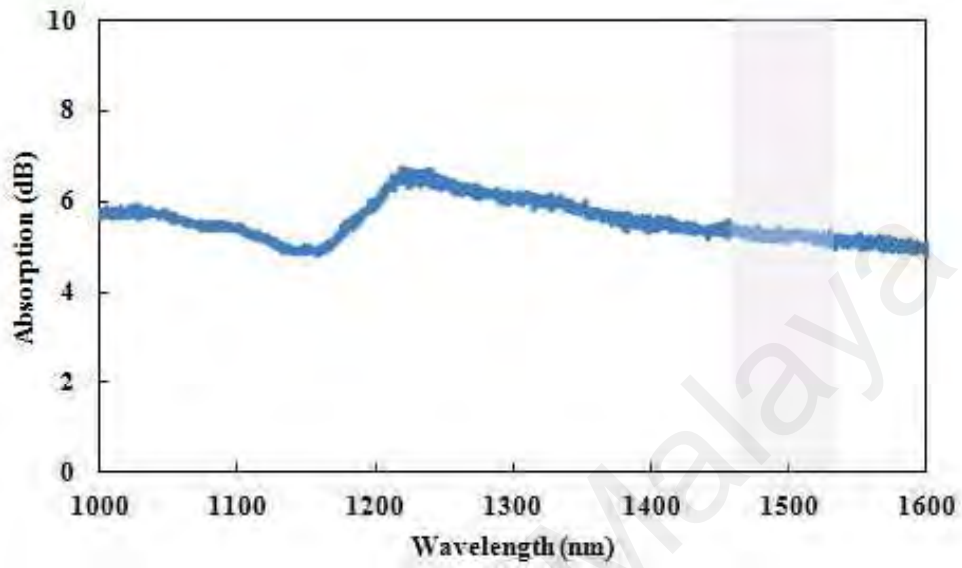
(a)
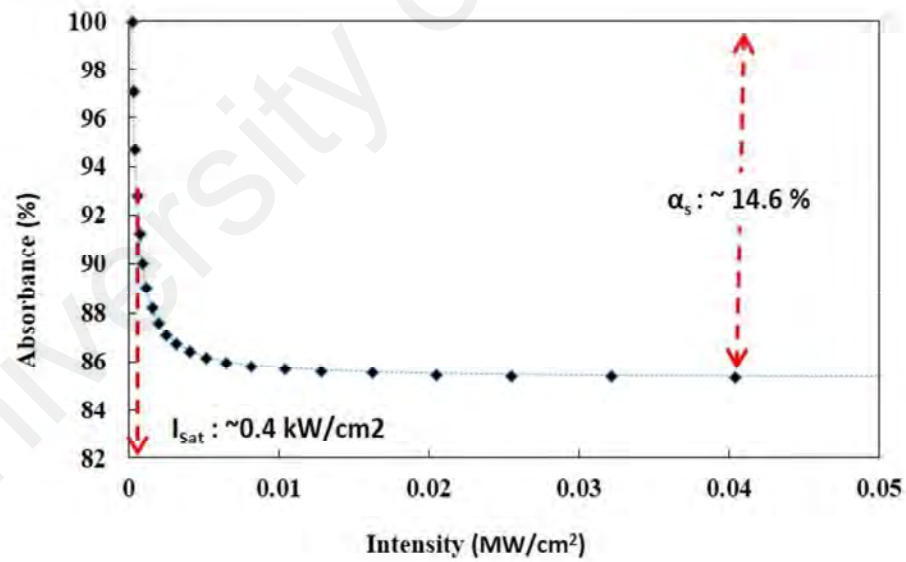
(b)

Figure 4.30: (a) Linear and (b) Nonlinear absorption spectrum of In$_2$Se$_3$ SA[18]

The linear and nonlinear absorption spectra of the In_2Se_3 SA are studied to determine the suitability of In_2Se_3 as an SA. Figure 4. 30 (a) shows the linear absorption spectrum of the SA from the wavelength range of 1000 nm to 1600 nm using white light as a source. The shaded region in the spectrum shows the absorption in the S band range. It shows that the absorption of around 5.4 dB is considerably high in the S band region, which makes it suitable to be used as an SA in the S band region.

The nonlinear absorption spectrum of In_2Se_3 SA is shown in Figure 4.30 (b). The twin detector technique is used for this measurement with a commercial ELMO femtosecond erbium laser from Menlo Systems. The mode-locked laser as a laser seed exhibits a central wavelength at 1560 nm. The obtained measurement is fitted into a saturation model, and it results in a modulation depth of around 14.6 % and a saturation intensity of 0.4 kW/cm^2.

4.4.3 Results and Discussion

In this experiment, mode-locking begins at the pump power of 221.0 mW with the integration of SA into the cavity. The output pulses have a repetition rate of 6.93 MHz, which agrees with the total length of the cavity. It can be concluded that the generated mode-locked pulses are in a fundamental state whereby only one pulse train resonates in the cavity. Figure. 4.31 (a) illustrated the pulse trains of the generated mode-locked pulses. The pulse profile of the pulse trains is observed using a two-photon absorption auto-correlator with the FWHM of 8.98 ps, as given in Figure. 4.31 (b). The final pulse width is about 5.79 ps after deconvolution using a sech^2 pulse shape.
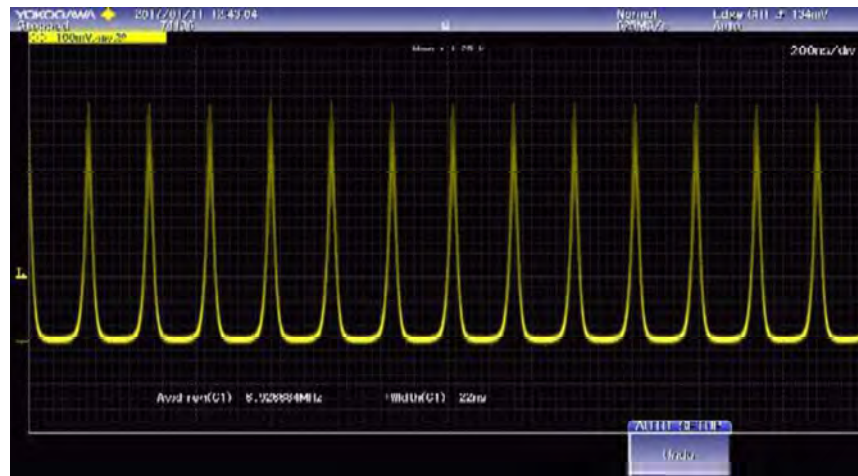
(a)
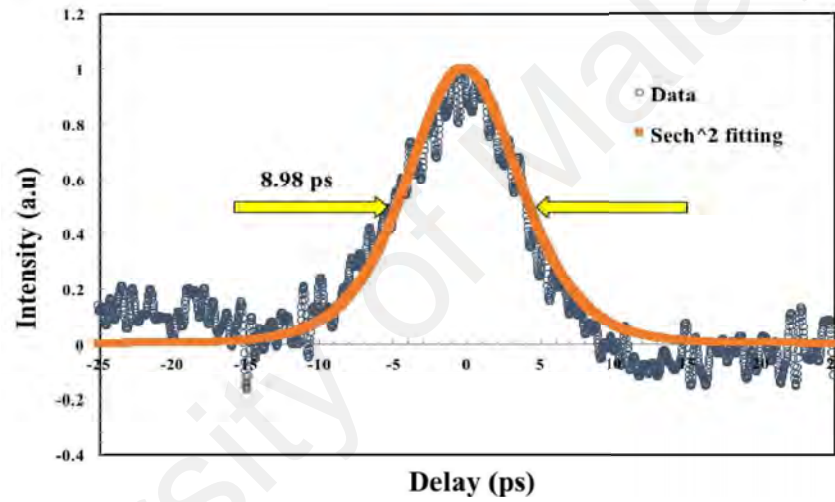
(b)

Figure 4.31: (a) Pulse train observed via OSC and (b) Pulsewidth measurement using two photon absorption AC[19]

---

[19] (Reproduced with permission from Ahmad, H., **Reduan, S. A.**, Ooi, S. I., & Ismail, M. A., 2018)
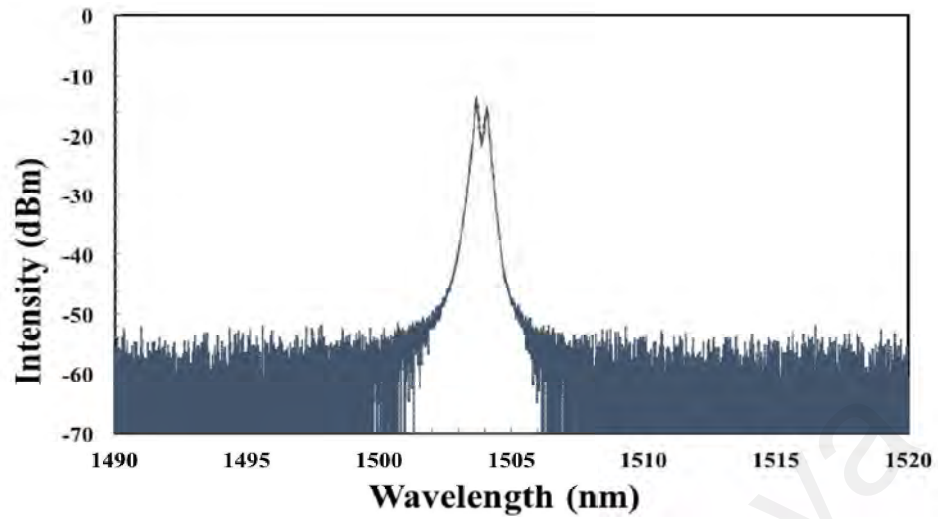
Figure 4.32: Optical spectrum of the laser when observed using OSA[11]

The optical spectrum of the generated mode-locked pulses is given in Figure 4.32, with the central wavelength of 1503.8 nm. The splitting and slight broadening of the laser's peak is due to the SPM effect (Q. Z. Wang et al., 1994). As described in previous work by Wang et al. (S. Wang et al., 2016), the SPM effect occurs in the mode-locking process, which can cause the spectrum to become broader and results in the occurring of multiple peaks. The spectrum has a 3-dB spectral width of around 0.468 nm. The quality of the output pulse can be determined by multiplying the pulse width and the 3-dB spectral width which results in a time bandwidth product (TBP) value of around 0.36. The calculated TBP suggests that the output pulses are slightly chirped. The pulse could be slightly chirped during the propagation in a transparent medium due to the effects of chromatic dispersion and nonlinearities
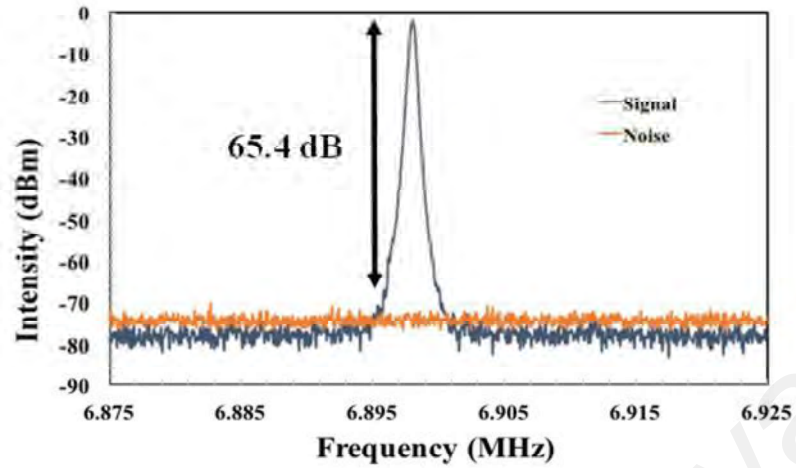
(a)
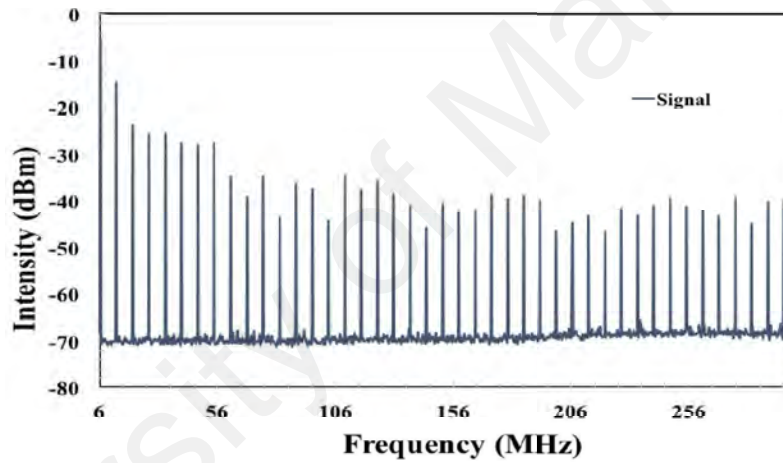
(b)

Figure 4.33: (a) The SNR of the signal when measured using RFSA. (b) The frequency components of the mode-locked pulse when the frequency span is extended until 300 MHz[20]

The RF spectrum of the generated mode-locked pulses is given in Figure 4.33 (a). The

obtained SNR value of the fundamental frequency is around 65.4 dB, as shown in Figure.

4.33 (a) using the narrowest available resolution of 300 Hz. This value indicates the

mode-locked pulses are in a stable regime (Von der Linde, 1986). As we extend the

frequency span, as seen in Figure 4.33 (b), the modes of frequency oscillate inside the cavity system. The frequency amplitude fluctuates, which could be due to the typical wideband RF spectrum for passively mode-locking operation, as discussed by Sun et al. (Zhipei Sun et al., 2010a) and Chen et al. (Y. Chen et al., 2015). These resulted in an envelope over the spectrum. The obtained average output power in this experiment is 1.242 mW, with a corresponding maximum peak power of 27.2 mW and maximum pulse energy of 0.179 nJ.

Table 4.2 shows the comparison of the performance of mode-locked pulses with different SAs in the S band region.

Table 4.2: comparison on the performance of mode-locked pulses with a different SAs in the S band region

Type of SA	In_2Se_3	Alcohol	PtAg/N-G
Modulation Depth (%)	14.6	10	22.2
Central Wavelength (nm)	1503.8	1503	1506
Repetition Rate	6.93 MHz	2.55 MHz	1.06.85 MHz
Pulse Width	5.79 ps	13.2 ns	7.43 ps
Pulse Energy (nJ)	0.179	-	0.31
Ref	This work	(Hsu et al., 2017)	(H. B. Ahmad et al., 2017)

It can be seen in Table 4.2 that In_2Se_3 Sa used in this work exhibits a higher modulation depth compared to the alcohol SA (Hsu et al., 2017) but lower than the modulation depth of PtAg/N-G SA (H. B. Ahmad et al., 2017). Nevertheless, the obtained repetition rate from this work is higher than the repetition rate of other works. Even though previous work using PtAg/N-G reported a higher pulse energy, they obtained a broader pulse width

compared to this work. In this regard, this work generates a mode-locked pulsed laser that has a potential to be utilized for the applications in the S band region.

4.5   Conclusion

In this chapter, Q-switched TFF lasers are demonstrated using different types of materials, including graphene, SWCNT, MoS_2, and GaSe. The SWCNT SA is successfully used to generate a Q-switched TFF laser with a pulse with a shorter wavelength at 1450 nm, higher maximum pulse energy of 122.8 nJ, and a higher maximum repetition rate of 36.4 kHz. The shorter pulse width achieved in this study is 2.7 μs induced by GaSe SA in a TFF laser system.

The system uses a MoS_2 to generate Q-switched pulses, while PCF to induce the dual-wavelength lasing. The dual-wavelength output pulse has a central wavelength located at 1473.6 nm and 1479.3 nm. The output pulse exhibits a pulse width of 4.1 μs, with a repetition rate of 15.9 kHz, and maximum pulse energy of 83.7 nJ. The SNR of the generated pulse is around 32.0 dB.

Dual-wavelength Q-switched pulses are also obtained in this TFF system with a dual-lasing located at 1473.6 nm and 1479.3 nm. The generated output pulses had a repetition rate and a pulse width of 15.9 kHz and 4.1 μs, respectively. The SNR of the corresponding pulses is around 32.0 dB.

Other than that, a mode-locked TFF lasing is passively generated using In_2Se_3 as SA. Simple mechanical exfoliation is used to fabricate the SA. The obtained mode-locked pulse has a repetition rate and pulse widths of 6.89 MHz and 5.79 ps, respectively.

CHAPTER 5: CONCLUSION AND FUTURE WORK

5.1   Introduction

This thesis discusses the development of fiber laser operated in the S+/S band region using the TFF as the gain medium. Chapter 1 discussed the background of the work and fiber lasers, followed by an overview of S+/S band fiber lasers as well as its history that led to the development of S+/S band fiber laser. Chapter 2 provides an understanding of thulium-fluoride glass and fibers, and its performance in the S+/S band region as fiber lasers and amplifiers. Chapter 3 is examined at the application of the TFF as an amplifier for the S+/S band, while Chapters 4 focuses on the generation of Q-switched and dual-wavelength outputs as well as mode-locked outputs respectively from the TFF. Finally, this chapter summarizes the findings of this study and discusses possible future works using the TFF. Figure 5.1 visualizes the various outputs obtained from the TFF laser in this work:
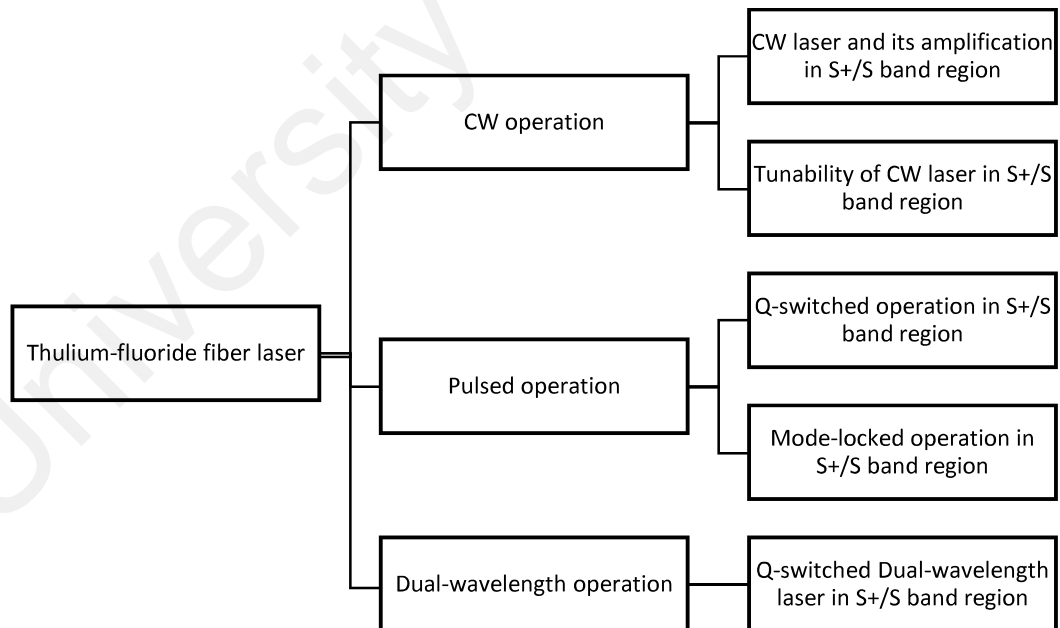
Figure 5.1: The achievement of S+/S band thulium fluoride fiber lasers

The following sections will summarize the various findings of this work, in-line with the objectives as states in Chapter 1 of this work.

5.1.1   To Design and Characterize a CW Laser Cavity using a TFF as the Linear Gain Medium and Pumped by a 1400 nm Source for S Band Lasing

The generation of the CW from the TFF laser, as well as its amplification was examined in this study. The TFF was pumped by a 1400 nm LD and emitted a single-wavelength CW output at approximately 1500 nm. The TFF's amplification capabilities were determined by calculating the gain profile, G, which was observed to be around 5.97 dB at 1500 nm. A TLS is used as an input signal for the set-up of the amplifier. The objective of this investigation is to observe the ratio of the amplified CW signal when using the TFF as a gain medium. The tunability of the CW laser was also determined to be able to cover a wavelength region from 1450 nm to 1512 nm using a TBPF. The investigation of the CW laser included a wide S band region, as well as the short extension that is the S+ band, which had a potentially new window that can be used to cater to applications such as telecommunications and sensing.

5.1.2   To Design and Characterize a Passively Q-Switched Laser Cavity using a TFF as the Linear Gain Medium for Operation in the S+/S Band Region

Following this, a passively Q-switched TFF laser was designed and demonstrated for operation in the S+/S band region. The ring cavity laser consisted of an LD operating at 1400 nm, a 1400/1500 nm fused WDM, the TFF, an ISO and a 90/10 coupler along with an SA incorporated into the cavity to generate to induce the desired Q-switched pulses passively. Four types of materials were used as SAs, namely SWCNTs, Graphene, MoS_2, and GaSe. The observed output results for each SAs showed typical stable Q-switched pulses characteristics. The Q-switched pulses based on SWCNTs had a tunability ranging from 1450 nm to 1492 nm. The corresponding maximum repetition rate and minimum

pulse width were 36.4 kHz and 3.6 µs, respectively. Whereas, the Q-switching operation based on graphene as the SA results of the output pulses had a central wavelength of 1501 nm with a maximum repetition rate of 36.3 kHz and a minimum pulse width of 3.2 µs. The corresponding output pulses had a maximum average output power of 0.76 mW and maximum pulse energy of 20.9 nJ. The passively Q-switched pulsed laser using MoS_2 generated pulses with a repetition rate and pulse width of 19.9 kHz to 35.1 kHz and 3.8 µs and 6.5 µs, respectively. The maximum average output power and maximum pulse energy of the output pulsed were 2.2 mW and 63.2 nJ. The generated Q-switched pulses can be tuned from 1460 nm to 1506 nm, which covered an S+/S band region.

Finally, the GaSe based SA was capable of achieving a Q switched pulsed in the S+/S band region. The maximum repetition rate and minimum pulse width achieved were 33.3 kHz and 2.7 µs, at a central wavelength of 1502 nm. The output pulses exhibited maximum pulse energy of 51.4 nJ. All the Q-switched pulsed fiber laser-generated in this study showed a stable pulse with the SNR of more than 40 dB, proving that the output pulses were in a stable regime.

The observed output pulses in this study indicated the behavior of Q-switched TFF laser in the S band region, especially the shorter wavelength of S band using a passive technique. However, the performance of the laser output needed to be improved by optimizing the cavity design, such as the coupling ratio and cavity length, as well as the quality of the SAs. However, the development of Q-switched TFF laser in the S+/the S band region enabled the recognition in the applications of optical spectroscopy, coarse wavelength division multiplexing and fiber to the premise (FTTP) system.

5.1.3 To Design and Characterize a Passively Q-switched Dual-Wavelength Laser Cavity using a TFF as the Linear Gain Medium for Operation in the S+/S band region

Extending from the design of the Q-switched pulse laser, a dual-wavelength output was then obtained from the TFF in the S band region. PCFs were used as an additional fiber with the properties of the photonic crystal to generate dual-wavelength laser output. The usage of the PCF into the laser cavity was to produce the Mach-Zehnder interferometry effect on the laser operation that could generate a dual-wavelength laser output. The operation involved the mechanism of Mach-Zehnder filter that was affected by the differences in terms of length and the phase differences between two sources, which were generally based on the interference between two coherent monochromatic sources.

MoS$_2$ was used as an SA to generate the pulsed laser in the fiber laser cavity. The combination of PCF and MoS$_2$ in the TFF laser cavity system resulted in a dual-wavelength Q switched pulsed laser in an S+/S band region. The dual-wavelength output laser was located at the wavelength of 1473.6 nm and 1479.3 nm, with maximum repetition rate and minimum pulse width of 15.9 kHz and 4.1 µs, respectively. The dual-wavelength pulsed laser output had a maximum average output power of 1.3 mW and maximum pulse energy of 83.7 nJ. The generation of the dual-wavelength Q-switched fiber laser will contribute to the availability of the application in photonics such as in environmental sensing, biomedical diagnostics, and laser processing, especially in a shorter wavelength of the S band region.

5.1.4 To Design and Characterize a Passively Mode-Locked Laser Cavity using a TFF as the Linear Gain Medium for Operation in the S+/S Band Region

Subsequently, a passively mode-locked TFF laser at S band region was demonstrated in this study. An In_2Se_3 based SA was used to generate the pulsed output laser by integrating the SA into the complete cavity. The generated passively mode-locked pulses had a center wavelength of 1503.8 nm with a 3-dB spectral width of around 0.468 nm. The output pulses had the pulse duration and repetition rate of 5.79 ps and 6.93 MHz, respectively. The observed maximum average output power was around 1.24 mW with a corresponding pulse energy of 0.18 nJ. The SNR of the output pulses was around 65.4 dB, which indicated a good stability of the pulsed laser. The complete laser cavity has a total GVD of 0.08 ps/nm at 1500 nm, indicated that the generation of soliton mode-locking pulses was observed in the study. The mode-locked system has a TBP of 0.36 which suggested that the output pulses slightly chirped.

The passively mode locked TFF laser was successfully demonstrated in this study at the central wavelength of 1503.8 nm. The generation of the mode-locked fiber laser, based on cost-effective SA, had become a great interest to provide an alternative transmission window for communication, especially in the S+/S band region. Other than that, the generated mode-locked pulses had a high potential for the use of photonics applications in the S band region.

5.2 Future Works

Based on the above achievements, this study provides the behavior of TFF lasers in the S+/S band region. However, there are several phenomena that not yet been proved by utilizing the TFF to generates an output laser. This is because of the limitation of time and instruments. These limitations provide research opportunities to be addressed in the future.

The development of mode-locked fiber laser with a gigahertz repetition rate in an S band region has become attractive because of their application in the field of medicine, sensing, and telecommunications. As discussed in Chapter 4, the mode-locked that is generated passively using In_2Se_3 has output pulses with a repetition rate of 6.93 MHz, which is limited by the cavity length of the fiber system which is mainly contributed by the longer length of the TFF as a gain medium. Thus, the performance of the mode-locking operation in a TFF laser cavity can be enhanced by optimizing the cavity design by shortening the length of the gain medium. Other than that, the generation of mode-locked by active technique could be an option to generate a pulsed laser with a more significant repetition rate, especially in the S band region that should be investigated in future work.

The generation of a stimulated Brillouin scattering (SBS) based multi-wavelength TFF laser is also possible by exploiting the SBS effect of the fiber cavity. It is reported that the threshold power of SBS is much lower in SMF-28 than in the TFF, which is seen to be advantageous for the applications of telecommunication. However, there are several difficulties in generating the SBS effect in the TFF, as the TFF has lower phonon energy. Therefore, the SBS effect on the TFF cavity system should be investigated as part of future research efforts.

The performance of the output laser includes the laser tunability, CW output power, and laser efficiency, are related to the cavity design of the laser system such as the cavity length and the coupling ratio. Therefore, improvising the cavity design of the TFF laser cavity system could lead to better laser performance, which will contribute to the applications of photonics in various fields such as medicine, telecommunications, sensing, and spectroscopy.

REFERENCES

Agrawal, G. (2001). *Applications of nonlinear fiber optics*: Academic press.

Ahmad, H., Ismail, M., Sathiyan, S., Reduan, S., Ruslan, N., Lee, C., Zulkifli, M., Thambiratnam, K., Ismail, M., & Harun, S. (2017a). S-band Q-switched fiber laser using MoSe$_2$ saturable absorber. *Optics Communications, 382*, 93-98.

Ahmad, H., Ismail, M. A., Suthaskumar, M., Tiu, Z. C., Harun, S. W., Zulkifli, M. Z., Samikannu, S., & Sivaraj, S. (2016). S-band Q-switched fiber laser using molybdenum disulfide (MoS$_2$) saturable absorber. *Laser Physics Letters, 13*(3), 035103.

Ahmad, H., Lee, C., Ismail, M., Ali, Z., Reduan, S., Ruslan, N., Ismail, M., & Harun, S. (2016a). Zinc oxide (ZnO) nanoparticles as saturable absorber in passively Q-switched fiber laser. *Optics Communications, 381*, 72-76.

Ahmad, H., Reduan, S., Hassan, N., Ooi, S., & Tiu, Z. (2017b). S-band Q-switched thulium fluoride fiber laser using graphene saturable absorber. *Laser Physics, 27*(7), 075103.

Ahmad, H., Reduan, S., & Safaei, R. (2017c). Dual-wavelength Q-switched thulium-fluoride fiber laser for S+/S band using molybdenum disulfide (MoS$_2$) as a saturable absorber. *Laser Physics, 27*(6), 065103.

Ahmad, H., Reduan, S. A., Ali, Z. A., Ismail, M., Ruslan, N., Lee, C., Puteh, R., & Harun, S. (2016b). C-Band Q-Switched Fiber Laser Using Titanium Dioxide (TiO$_2$) As Saturable Absorber. *IEEE Photonics Journal, 8*(1), 1-7.

Ahmad, H., Reduan, S. A., Ooi, S. I., & Ismail, M. A. (2018). Mechanically exfoliated In$_2$Se as a saturable absorber for mode-locking a thulium-doped fluoride fiber laser operating in S-band. *Applied optics, 57*(24), 6937-6942. doi: 10.1364/AO.57.006937

Ahmad, H., Soltanian, M., Pua, C., Alimadad, M., & Harun, S. W. (2014). Photonic crystal fiber based dual-wavelength Q-switched fiber laser using graphene oxide as a saturable absorber. *Applied optics, 53*(16), 3581-3586.

Ahmad, H., Soltanian, M. R. K., Narimani, L., Amiri, I. S., Khodaei, A., & Harun, S. W. (2015). Tunable S-Band Q-Switched Fiber Laser Using Bi$_2$Se$_3$ as the Saturable Absorber. *Photonics Journal, IEEE, 7*(3), 1-8. doi: 10.1109/JPHOT.2015.2433020

Ahmad, H. B., Tajdidzadeh, M., Rezayi, M., & Ahmed, I. S. A. (2017). Passive mode-locking at S-band by single-mode thulium-doped fluoride fiber using a thin film PtAg/NG saturable absorber. *Journal of Nanophotonics, 11*(2), 026008.

Ahmed, M., Latiff, A., Arof, H., Ahmad, H., & Harun, S. (2016). Femtosecond mode-locked erbium-doped fiber laser based on MoS$_2$–PVA saturable absorber. *Optics & Laser Technology, 82*, 145-149.

Aozasa, S., Sakamoto, T., Kanamori, T., Hoshino, K., Kobayashi, K., & Shimizu, M. (2000a). Tm-doped fiber amplifiers for 1470-nm-band WDM signals. *IEEE Photonics Technology Letters, 12*(10), 1331-1333.

Aozasa, S., Sakamoto, T., Kanamori, T., Hoshino, K., & Shimizu, M. (2000b). Gain-shifted thulium-doped fibre amplifiers employing novel high concentration doping technique. *Electronics Letters, 36*(5), 418-419.

Arbore, M. A. (2005a). *Application of fundamental-mode cutoff for novel amplifiers and lasers.* Paper presented at the Optical Fiber Communication Conference.

Arbore, M. A. (2005b). Communication system using S-band Er-doped fiber amplifiers with depressed cladding: Google Patents.

Arbore, M. A., & Keaton, G. L. (2005). Fiber amplifiers with depressed cladding and their uses in Er-doped fiber amplifiers for the S-band: Google Patents.

Balakrishnan, N., Steer, E. D., Smith, E. F., Kudrynskyi, Z. R., Kovalyuk, Z. D., Eaves, L., Patanè, A., & Beton, P. H. (2018). Epitaxial growth of γ-InSe and α, β, and γ-In_2Se_3 on ε-GaSe. *2D Materials, 5*(3), 035026.

Bao, Q., Zhang, H., Wang, Y., Ni, Z., Yan, Y., Shen, Z. X., Loh, K. P., & Tang, D. Y. (2009). Atomic-Layer Graphene as a Saturable Absorber for Ultrafast Pulsed Lasers. *Advanced Functional Materials, 19*(19), 3077-3083. doi: 10.1002/adfm.200901007

Becker, P. M., Olsson, A. A., & Simpson, J. R. (1999). *Erbium-doped fiber amplifiers: fundamentals and technology*: Elsevier.

Bonaccorso, F., & Sun, Z. (2014). Solution processing of graphene, topological insulators and other 2d crystals for ultrafast photonics. *Optical Materials Express, 4*(1), 63-78. doi: 10.1364/OME.4.000063

Bünzli, J.-C. G., & Piguet, C. (2005). Taking advantage of luminescent lanthanide ions. *Chemical Society Reviews, 34*(12), 1048-1077.

Buxens, A., Poulsen, H. N., Clausen, A., & Jeppesen, P. (2000). Gain flattened L-band EDFA based on upgraded C-band EDFA using forward ASE pumping in an EDF section. *Electronics Letters, 36*(9), 1.

Cao, W., Wang, H., Luo, A., Luo, Z., & Xu, W. (2011). Graphene-based, 50 nm wide-band tunable passively Q-switched fiber laser. *Laser Physics Letters, 9*(1), 54.

Caspary, R., Unrau, U. B., & Kowalsky, W. (2003). *Recent progress on S-band fiber amplifiers.* Paper presented at the Transparent Optical Networks, 2003. Proceedings of 2003 5th International Conference on.

Caves, C. M. (1982). Quantum limits on noise in linear amplifiers. *Physical Review D, 26*(8), 1817.

Chen, B., Zhang, X., Wu, K., Wang, H., Wang, J., & Chen, J. (2015). Q-switched fiber laser based on transition metal dichalcogenides MoS_2, $MoSe_2$, WS_2, and WSe_2. *Optics express, 23*(20), 26723-26737.

Chen, Y., Jiang, G., Chen, S., Guo, Z., Yu, X., Zhao, C., Zhang, H., Bao, Q., Wen, S., & Tang, D. (2015). Mechanically exfoliated black phosphorus as a new saturable absorber for both Q-switching and mode-locking laser operation. *Optics express, 23*(10), 12823-12833.

Chen, Y., Zhao, C., Chen, S., Du, J., Tang, P., Jiang, G., Zhang, H., Wen, S., & Tang, D. (2013). Large energy, wavelength widely tunable, topological insulator Q-switched erbium-doped fiber laser. *IEEE Journal of Selected Topics in Quantum Electronics, 20*(5), 315-322.

Chen, Y., Zhao, C., Chen, S., Du, J., Tang, P., Jiang, G., Zhang, H., Wen, S., & Tang, D. (2014). Large energy, wavelength widely tunable, topological insulator Q-switched erbium-doped fiber laser. *IEEE Journal of Selected Topics in Quantum Electronics, 20*(5), 315-322.

Chiu, J.-C., Lan, Y.-F., Chang, C.-M., Chen, X.-Z., Yeh, C.-Y., Lee, C.-K., Lin, G.-R., Lin, J.-J., & Cheng, W.-H. (2010). Concentration effect of carbon nanotube based saturable absorber on stabilizing and shortening mode-locked pulse. *Optics express, 18*(4), 3592-3600.

Derickson, D. (1998). *Fiber optic test and measurement.* Paper presented at the Fiber optic test and measurement/edited by Dennis Derickson. Upper Saddle River, NJ: Prentice Hall, c1998.

Digonnet, M. J. (1989). Fiber laser sources and amplifiers: Bellingham, WA (USA); Society of Photo-Optical Instrumentation Engineers.

Digonnet, M. J. (2001). *Rare-earth-doped fiber lasers and amplifiers, revised and expanded*: CRC press.

Djordjevic, I., Ryan, W., & Vasic, B. (2010). Fundamentals of Optical Communication *Coding for Optical Channels* (pp. 25-73): Springer.

Du, J., Wang, Q., Jiang, G., Xu, C., Zhao, C., Xiang, Y., Chen, Y., Wen, S., & Zhang, H. (2014). Ytterbium-doped fiber laser passively mode locked by few-layer Molybdenum Disulfide (MoS_2) saturable absorber functioned with evanescent field interaction. *Scientific reports, 4*.

El-Nahal, F. I., & Husein, A. H. M. (2013). Thulium Doped Fiber Amplifier (TDFA) for S-band WDM Systems. *Open Journal of Applied Sciences, 2*(04), 5.

Emmanuel, D., & Zervas, M. (1994). Erbium-doped fiber amplifiers: principles and applications: New York: Wiley Interscience.

Floridia, C., Carvalho, M., Lüthi, S., & Gomes, A. (2004). Modeling the distributed gain of single-(1050 or 1410 nm) and dual-wavelength-(800+ 1050 nm or 800+ 1410 nm) pumped thulium-doped fiber amplifiers. *Optics letters, 29*(17), 1983-1985.

Frerichs, C., & Unrau, U. B. (1996). Passive Q-switching and mode-locking of erbium-doped fluoride fiber lasers at 2.7 μm. *Optical Fiber Technology, 2*(4), 358-366.

Ganikhanov, F., Evans, C. L., Saar, B. G., & Xie, X. S. (2006). High-sensitivity vibrational imaging with frequency modulation coherent anti-Stokes Raman scattering (FM CARS) microscopy. *Optics letters, 31*(12), 1872-1874. doi: 10.1364/OL.31.001872

Gaufrès, E., Tang, N.-W., Lapointe, F., Cabana, J., Nadon, M.-A., Cottenye, N., Raymond, F., Szkopek, T., & Martel, R. (2014). Giant Raman scattering from J-aggregated dyes inside carbon nanotubes for multispectral imaging. *Nature Photonics, 8*(1), 72-78.

Gomes, A., Carvalho, M., Sundheimer, M., Bastos-Filho, C., Martins-Filho, J., e Silva, M. C., Von der Weid, J., & Margulis, W. (2003). Characterization of efficient dual-wavelength (1050+ 800 nm) pumping scheme for thulium-doped fiber amplifiers. *IEEE Photonics Technology Letters, 15*(2), 200-202.

Harun, S., Ismail, M., Ahmad, F., Ismail, M., Nor, R., Zulkepely, N., & Ahmad, H. (2012). A Q-switched erbium-doped fiber laser with a carbon nanotube based saturable absorber. *Chinese Physics Letters, 29*(11), 114202.

Ho, C.-H. (2014). Amorphous effect on the advancing of wide-range absorption and structural-phase transition in γ-In_2Se_3 polycrystalline layers. *Scientific reports, 4*, 4764.

Hsu, Y., Yeh, C.-H., & Chow, C.-W. (2017). Mode-locking S-band erbium fiber laser by employing alcohol-based saturable-absorber. *Optical and Quantum Electronics, 49*(11), 360.

Hu, G., Mizuguchi, T., Oe, R., Nitta, K., Zhao, X., Minamikawa, T., Li, T., Zheng, Z., & Yasui, T. (2018). Dual terahertz comb spectroscopy with a single free-running fibre laser. *Scientific reports, 8*.

Huang, S.-W., Zhou, H., Yang, J., McMillan, J., Matsko, A., Yu, M., Kwong, D.-L., Maleki, L., & Wong, C. (2015). Mode-locked ultrashort pulse generation from on-chip normal dispersion microresonators. *Physical review letters, 114*(5), 053901.

Huang, Y., Luo, Z., Li, Y., Zhong, M., Xu, B., Che, K., Xu, H., Cai, Z., Peng, J., & Weng, J. (2014). Widely-tunable, passively Q-switched erbium-doped fiber laser with few-layer MoS 2 saturable absorber. *Optics express, 22*(21), 25258-25266.

Ismail, E., Kadir, N., Latiff, A., Ahmad, H., & Harun, S. (2016). Black phosphorus crystal as a saturable absorber for both a Q-switched and mode-locked erbium-doped fiber laser. *RSC Advances, 6*(76), 72692-72697.

Ismail, M. A. (2015). *Development of Passive Q-switched and Mode-locked Fiber Lasers Using Carbon-based Saturable Absorbers.* Jabatan Kejuruteraan Elektrik, Fakulti Kejuruteraan, Universiti Malaya.

Jay, J. A. (2010). An overview of macrobending and microbending of optical fibers. *White paper of Corning*, 1-21.

Jia, C. (2017). *Near-infrared Tm3+: ZBLAN Fiber Lasers.* McGill University Libraries.

Julien, C., Chevy, A., & Siapkas, D. (1990). Optical properties of In_2Se_3 phases. *physica status solidi (a), 118*(2), 553-559.

Kasamatsu, T., Yano, Y., & Sekita, H. (1999). 1.50-μm-band gain-shifted thulium-doped fiber amplifier with 1.05-and 1.56-μm dual-wavelength pumping. *Optics letters, 24*(23), 1684-1686.

Keller, U. (2004). Ultrafast solid-state lasers. *Progress in optics, 46*, 1-115.

Kim, S.-J., Park, J., Jeong, Y., Go, H., Lee, K., Hong, S., & Seong, M.-J. (2014). Metal-particle-induced enhancement of the photoluminescence from biomolecule-functionalized carbon nanotubes. *Nanoscale research letters, 9*(1), 1.

Kozak, M., Caspary, R., & Kowalsky, W. (2004). *Thulium-doped fiber amplifier for the S-band.* Paper presented at the Proceedings of 2004 6th International Conference on Transparent Optical Networks (IEEE Cat. No. 04EX804).

Kübler, C., Huber, R., Tübel, S., & Leitenstorfer, A. (2004). Ultrabroadband detection of multi-terahertz field transients with GaSe electro-optic sensors: Approaching the near infrared. *Applied Physics Letters, 85*(16), 3360-3362.

Late, D. J., Liu, B., Matte, H., Rao, C., & Dravid, V. P. (2012). Rapid characterization of ultrathin layers of chalcogenides on SiO2/Si substrates. *Advanced Functional Materials, 22*(9), 1894-1905.

Lee, J., Jung, M., Koo, J., Chi, C., & Lee, J. H. (2015). Passively Q-Switched 1.89-μm fiber laser using a bulk-structured Bi_2Te_3 topological insulator. *IEEE Journal of Selected Topics in Quantum Electronics, 21*(1), 31-36.

Lee, J., Koo, J., Chi, C., & Lee, J. H. (2014). All-fiberized, passively Q-switched 1.06 μm laser using a bulk-structured Bi2Te3 topological insulator. *Journal of Optics, 16*(8), 085203.

Lei, S., Ge, L., Liu, Z., Najmaei, S., Shi, G., You, G., Lou, J., Vajtai, R., & Ajayan, P. M. (2013). Synthesis and photoresponse of large GaSe atomic layers. *Nano letters, 13*(6), 2777-2781.

Leigh, G. J. (1990). *Nomenclature of inorganic chemistry: recommendations 1990*: Blackwell scientific publications Oxford.

Leontie, L., Evtodiev, I., Nedeff, V., Stamate, M., & Caraman, M. (2009). Photoelectric properties of Bi_2O_3/GaSe heterojunctions. *Applied Physics Letters, 94*(7), 071903.

Li, H., Xia, H., Lan, C., Li, C., Zhang, X., Li, J., & Liu, Y. (2015). Passively Q-switched erbium-doped fiber laser based on few-layer MoS_2 saturable absorber. *IEEE Photonics Technology Letters, 27*(1), 69-72.

Li, H., Zhang, Q., Yap, C. C. R., Tay, B. K., Edwin, T. H. T., Olivier, A., & Baillargeat, D. (2012). From bulk to monolayer MoS_2: evolution of Raman scattering. *Advanced Functional Materials, 22*(7), 1385-1390.

Li, R., Fan, W., Wang, X., & Li, X. (2019). Improvement of Noise and Gain Characteristics of Low-Repetition-Rate Double-Pass Fiber Amplifiers. *IEEE Photonics Journal, 11*(3), 1-11.

Li, X., Lin, M.-W., Puretzky, A. A., Idrobo, J. C., Ma, C., Chi, M., Yoon, M., Rouleau, C. M., Kravchenko, I. I., & Geohegan, D. B. (2014). Controlled vapor phase growth of single crystalline, two-dimensional GaSe crystals with high photoresponse. *Scientific reports, 4.*

Lin, J., Hu, Y., Chen, C., Gu, C., & Xu, L. (2015). Wavelength-tunable Yb-doped passively Q-switching fiber laser based on WS_2 saturable absorber. *Optics express, 23*(22), 29059-29064.

Liu, D., Ngo, N., Ning, G., Shum, P., & Tjin, S. (2006). Tunable microwave photonic notch filter using a dual-wavelength fiber laser with phase modulation. *Optics Communications, 266*(1), 240-248.

Liu, J., Wu, S., Yang, Q.-H., & Wang, P. (2011). Stable nanosecond pulse generation from a graphene-based passively Q-switched Yb-doped fiber laser. *Optics letters, 36*(20), 4008-4010.

Liu, J., Xu, J., & Wang, P. (2012). Graphene-based passively Q-switched 2μm thulium-doped fiber laser. *Optics Communications, 285*(24), 5319-5322.

Lou, F., Zhao, R., He, J., Jia, Z., Su, X., Wang, Z., Hou, J., & Zhang, B. (2015). Nanosecond-pulsed, dual-wavelength, passively Q-switched ytterbium-doped bulk laser based on few-layer MoS_2 saturable absorber. *Photonics Research, 3*(2), A25-A29.

Lou, Q., Zhou, J., He, B., & Zhou, H. (2008). Fiber lasers and their coherent beam combination. *Optics and Photonics News, 19*(5), 46-51.

Luo, Z., Huang, Y., Weng, J., Cheng, H., Lin, Z., Xu, B., Cai, Z., & Xu, H. (2013). 1.06 μm Q-switched ytterbium-doped fiber laser using few-layer topological insulator Bi_2Se_3 as a saturable absorber. *Optics express, 21*(24), 29516-29522.

Luo, Z., Huang, Y., Zhong, M., Li, Y., Wu, J., Xu, B., Xu, H., Cai, Z., Peng, J., & Weng, J. (2014). 1-, 1.5-, and 2-μm Fiber Lasers Q-Switched by a Broadband Few-Layer MoS_2 Saturable Absorber. *Journal of Lightwave Technology, 32*(24), 4077-4084.

Maiman, T. H. (1960). Stimulated Optical Radiation in Ruby. *Nature, 187*(4736), 493-494. doi: 10.1038/187493a0

Manzoni, C., Polli, D., & Cerullo, G. (2006). Two-color pump-probe system broadly tunable over the visible and the near infrared with sub-30 fs temporal resolution. *Review of scientific instruments, 77*(2), 023103.

Martinez, A., & Sun, Z. (2013). Nanotube and graphene saturable absorbers for fibre lasers. *Nat Photon, 7*(11), 842-845. doi: 10.1038/nphoton.2013.304

Mears, R. J., Reekie, L., Jauncey, I., & Payne, D. N. (1987). Low-noise erbium-doped fibre amplifier operating at 1.54 μm. *Electronics Letters, 23*(19), 1026-1028.

Mohd Zamani, Z. (2012). *Study of S-band optical amplifiers and its applications/Mohd Zamani Zulkifli.* University of Malaya.

Muhammad, F., Zulkifli, M., & Ahmad, H. (2014). Graphene based Q-switched tunable S-band fiber laser incorporating arrayed waveguide gratings (AWG). *Journal of Nonlinear Optical Physics & Materials, 23*(01), 1450004.

Muhammad, F. D. (2014). *Graphene as Saturable Absorber for Photonics Applications.* Jabatan Fizik, Fakulti Sains, Universiti Malaya.

Ni, Y., Wu, H., Huang, C., Mao, M., Wang, Z., & Cheng, X. (2013). Growth and quality of gallium selenide (GaSe) crystals. *Journal of Crystal Growth, 381*, 10-14.

Orazio, S. (2010). Principles of lasers: Springer, New York.

Paschotta, R., Häring, R., Gini, E., Melchior, H., Keller, U., Offerhaus, H., & Richardson, D. (1999). Passively Q-switched 0.1-mJ fiber laser system at 1.53 μm. *Optics letters, 24*(6), 388-390.

Peterka, P., Faure, B., Blanc, W., Karasek, M., & Dussardier, B. (2004). Theoretical modelling of S-band thulium-doped silica fibre amplifiers. *Optical and Quantum Electronics, 36*(1-3), 201-212.

Popa, D., Sun, Z., Hasan, T., Torrisi, F., Wang, F., & Ferrari, A. (2011). Graphene Q-switched, tunable fiber laser. *Applied Physics Letters, 98*(7), 073106.

Popa, D., Sun, Z., Hasan, T., Torrisi, F., Wang, F., & Ferrari, A. C. (2011). Graphene Q-switched, tunable fiber laser. *Applied Physics Letters, 98*(7), 073106. doi: 10.1063/1.3552684

Poulain, M., Poulain, M., & Lucas, J. (1975). Verres fluores au tetrafluorure de zirconium proprietes optiques d'un verre dope au Nd^{3+}. *Materials Research Bulletin, 10*(4), 243-246.

Reduan, S. A., & Ahmad, H. (2017). Molybdenum disulfide (MoS_2)–based, tunable passively Q switched thulium-fluoride fiber (TFF) laser. *Malaysian Journal of Fundamental and Applied Sciences, 13*(4), 572-575.

Richardson, D., Nilsson, J., & Clarkson, W. (2010). High power fiber lasers: current status and future perspectives [Invited]. *JOSA B, 27*(11), B63-B92.

Roxlo, C., Chianelli, R., Deckman, H., Ruppert, A., & Wong, P. (1987). Bulk and surface optical absorption in molybdenum disulfide. *Journal of Vacuum Science & Technology A: Vacuum, Surfaces, and Films, 5*(4), 555-557.

Safaei, R., Amiri, I. S., Rezayi, M., & Ahmad, H. (2017). A stable dual-wavelength Q-switch using a compact passive device containing photonics crystal fiber embedded with carbon platinum. *Laser Physics, 28*(1), 016201.

Sakamoto, T. (2001). *S-band fiber optic amplifiers.* Paper presented at the Optical Fiber Communication Conference and Exhibit, 2001. OFC 2001.

Sharma, U., Kim, C.-S., Kang, J. U., & Fried, N. M. (2004). *Highly stable tunable dual-wavelength Q-switched fiber laser for DIAL applications.* Paper presented at the Laser Applications to Chemical and Environmental Analysis.

Siegman, A. E. (1986). Lasers university science books. *Mill Valley, CA, 37*(208), 169.

Sierra-Hernandez, J., Rojas-Laguna, R., Vargas-Rodriguez, E., Estudillo-Ayala, J., Mata-Chavez, R., Jauregui-Vazquez, D., Hernandez-Garcia, J., Andrade-Lucio, J., & Gutierrez-Gutierrez, J. (2013). A tunable multi-wavelength laser based on a Mach–Zehnder interferometer with photonic crystal fiber. *Laser Physics, 23*(5), 055105.

Simpson, D. A., Gibbs, W. K., Collins, S. F., Blanc, W., Dussardier, B., Monnom, G., Peterka, P., & Baxter, G. W. (2008). Visible and near infra-red up-conversion in Tm^{3+}/Yb^{3+} co-doped silica fibers under 980 nm excitation. *Optics express, 16*(18), 13781-13799.

Siniaeva, M. L., Siniavsky, M. N., Pashinin, V. P., Mamedov, A. A., Konov, V. I., & Kononenko, V. V. (2009). Laser ablation of dental materials using a microsecond Nd:YAG laser. *Laser Physics, 19*(5), 1056-1060. doi: 10.1134/s1054660x09050314

Snitzer, E. (1961). Optical maser action of Nd^{+3} in a barium crown glass. *Physical review letters, 7*(12), 444.

Soltanian, M. R. K., Amiri, I. S., Alavi, S. E., & Ahmad, H. (2015). Dual-wavelength erbium-doped fiber laser to generate terahertz radiation using photonic crystal fiber. *Journal of Lightwave Technology, 33*(24), 5038-5046.

Stone, J., & Burrus, C. A. (1973). Neodymium-doped silica lasers in end-pumped fiber geometry. *Applied Physics Letters, 23*(7), 388-389.

Sun, Z., Hasan, T., & Ferrari, A. (2012). Ultrafast lasers mode-locked by nanotubes and graphene. *Physica E: Low-dimensional Systems and Nanostructures, 44*(6), 1082-1091.

Sun, Z., Hasan, T., Torrisi, F., Popa, D., Privitera, G., Wang, F., Bonaccorso, F., Basko, D. M., & Ferrari, A. C. (2010). Graphene mode-locked ultrafast laser. *ACS nano, 4*(2), 803-810. doi: 10.1021/nn901703e

Sun, Z., Hasan, T., Torrisi, F., Popa, D., Privitera, G., Wang, F., Bonaccorso, F., Basko, D. M., & Ferrari, A. C. (2010a). Graphene mode-locked ultrafast laser. *ACS nano, 4*(2), 803-810.

Sun, Z., Hasan, T., Wang, F., Rozhin, A. G., White, I. H., & Ferrari, A. C. (2010b). Ultrafast stretched-pulse fiber laser mode-locked by carbon nanotubes. *Nano Research, 3*(6), 404-411.

Sun, Z., Popa, D., Hasan, T., Torrisi, F., Wang, F., Kelleher, E. J., Travers, J. C., Nicolosi, V., & Ferrari, A. C. (2010c). A stable, wideband tunable, near transform-limited, graphene-mode-locked, ultrafast laser. *Nano Research, 3*(9), 653-660.

Svelto, O. (2010). *Principles of Lasers*: Springer US.

Tamura, K., Doerr, C., Haus, H., & Ippen, E. (1994). Soliton fiber ring laser stabilization and tuning with a broad intracavity filter. *IEEE Photonics Technology Letters, 6*(6), 697-699.

Tan, S. J., Harun, S. W., Arof, H., & Ahmad, H. (2013). Switchable Q-switched and mode-locked erbium-doped fiber laser operating in the L-band region. *Chinese Optics Letters, 11*(7), 073201.

Tanabe, S., & Tamaoka, T. (2003). Gain characteristics of Tm-doped fluoride fiber amplifier in S-band by dual-wavelength pumping. *Journal of non-crystalline solids, 326*, 283-286.

Taylor, N. (2002). *LASER: The inventor, the Nobel laureate, and the thirty-year patent war*: Simon and Schuster.

Thambiratnam, K., Ahmad, H., & Paul, M. C. (2016). Dual-Wavelength Fiber Lasers for the Optical Generation of Microwave and Terahertz Radiation. *Fiber Laser*, 111.

Trushin, M., Kelleher, E. J., & Hasan, T. (2016). Theory of edge-state optical absorption in two-dimensional transition metal dichalcogenide flakes. *Physical Review B, 94*(15), 155301.

Tsai, T.-Y., & Fang, Y.-C. (2009). A saturable absorber Q-switched all-fiber ring laser. *Optics express, 17*(3), 1429-1434.

Urquhart, P. (1988). Review of rare earth doped fibre lasers and amplifiers. *IEE Proceedings J-Optoelectronics, 135*(6), 385-407.

Von der Linde, D. (1986). Characterization of the noise in continuously operating mode-locked lasers. *Applied Physics B, 39*(4), 201-217.

Wang, Q. H., Kalantar-Zadeh, K., Kis, A., Coleman, J. N., & Strano, M. S. (2012). Electronics and optoelectronics of two-dimensional transition metal dichalcogenides. *Nature nanotechnology, 7*(11), 699.

Wang, Q. Z., Liu, Q., Liu, D., Ho, P. P., & Alfano, R. (1994). High-resolution spectra of self-phase modulation in optical fibers. *JOSA B, 11*(6), 1084-1089.

Wang, S., Zhao, Z., & Kobayashi, Y. (2016). Wavelength-spacing controllable, dual-wavelength synchronously mode locked Er: fiber laser oscillator based on dual-branch nonlinear polarization rotation technique. *Optics express, 24*(25), 28228-28238.

Wang, Y., & Herron, N. (1991). Nanometer-sized semiconductor clusters: materials synthesis, quantum size effects, and photophysical properties. *The Journal of Physical Chemistry, 95*(2), 525-532.

Wartak, M. S. (2013). *Computational photonics: an introduction with MATLAB*: Cambridge University Press.

Whitaker, J. C. (2005). *The electronics handbook*: Crc Press.

Woodward, R., Hasan, T., & Kelleher, E. (2015a). *Optical nonlinearity of few-layer MoS$_2$ devices and applications in short-pulse laser technology.* Paper presented at the Opto Electronics Communications Conf.(OECC).

Woodward, R., Howe, R., Runcorn, T., Hu, G., Torrisi, F., Kelleher, E., & Hasan, T. (2015b). Wideband saturable absorption in few-layer molybdenum diselenide (MoSe$_2$) for Q-switching Yb-, Er-and Tm-doped fiber lasers. *Optics express, 23*(15), 20051-20061.

Woodward, R., Kelleher, E., Howe, R., Hu, G., Torrisi, F., Hasan, T., Popov, S., & Taylor, J. (2014). Tunable Q-switched fiber laser based on saturable edge-state absorption in few-layer molybdenum disulfide (MoS$_2$). *Optics express, 22*(25), 31113-31122.

Xiang, M., Fu, S., Tang, M., Tang, H., Shum, P., & Liu, D. (2014). Nyquist WDM superchannel using offset-16QAM and receiver-side digital spectral shaping. *Optics express, 22*(14), 17448-17457.

Xu, C., & Wise, F. (2013). Recent advances in fibre lasers for nonlinear microscopy. *Nature photonics, 7*(11), 875-882.

Yam, S.-H., & Kim, J. (2006). Ground state absorption in thulium-doped fiber amplifier: Experiment and modeling. *IEEE Journal of Selected Topics in Quantum Electronics, 12*(4), 797-803.

Yan, P., Lin, R., Ruan, S., Liu, A., Chen, H., Zheng, Y., Chen, S., Guo, C., & Hu, J. (2015). A practical topological insulator saturable absorber for mode-locked fiber laser. *Scientific reports, 5*.

Yan, Y., Wang, J., Zhang, A. P., Shen, Y., & Tam, H. (2016). *Tunable L-band Mode-Locked Bi-EDF Fiber Laser Based on Chirped Fiber Bragg Grating.* Paper presented at the Bragg Gratings, Photosensitivity, and Poling in Glass Waveguides.

Yao, Y., Chen, X., Dai, Y., & Xie, S. (2006). Dual-wavelength erbium-doped fiber laser with a simple linear cavity and its application in microwave generation. *IEEE Photonics Technology Letters, 18*(1), 187-189.

Yap, Y. K. (2015). *Chemical synthesis and characterization of graphene oxide for use as saturable absorber and broadband polarizer/Yap Yuen Kiat.* University of Malaya.

Yuan, X., Tang, L., Liu, S., Wang, P., Chen, Z., Zhang, C., Liu, Y., Wang, W., Zou, Y., & Liu, C. (2015). Arrayed van der Waals vertical heterostructures based on 2D GaSe grown by molecular beam epitaxy. *Nano letters, 15*(5), 3571-3577.

Yüksek, M., Kürüm, U., Yaglioglu, H. G., Elmali, A., & Ateş, A. (2010). Nonlinear and saturable absorption characteristics of amorphous InSe thin films. *Journal of Applied Physics, 107*(3), 033115.

Zhang, H., Lu, S., Zheng, J., Du, J., Wen, S., Tang, D., & Loh, K. (2014). Molybdenum disulfide (MoS_2) as a broadband saturable absorber for ultra-fast photonics. *Optics express, 22*(6), 7249-7260.

Zhang, M., Howe, R. C. T., Woodward, R. I., Kelleher, E. J. R., Torrisi, F., Hu, G., Popov, S. V., Taylor, J. R., & Hasan, T. (2015). Solution processed MoS_2-PVA composite for sub-bandgap mode-locking of a wideband tunable ultrafast Er:fiber laser. *Nano Research, 8*(5), 1522-1534. doi: 10.1007/s12274-014-0637-2

Zhao, J., Wang, Y., Yan, P., Ruan, S., Zhang, G., Li, H., & Tsang, Y. (2013). An L-band graphene-oxide mode-locked fiber laser delivering bright and dark pulses. *Laser Physics, 23*(7), 075105.

Zhou, D.-P., Wei, L., Dong, B., & Liu, W.-K. (2010). Tunable passively-switched erbium-doped fiber laser with carbon nanotubes as a saturable absorber. *IEEE Photonics Technology Letters, 22*(1), 9-11.

Zhou, D.-P., Wei, L., & Liu, W.-K. (2012). Tunable graphene Q-switched erbium-doped fiber laser with suppressed self-mode locking effect. *Applied optics, 51*(14), 2554-2558.

Zhu, F., Hundertmark, H., Kolomenskii, A. A., Strohaber, J., Holzwarth, R., & Schuessler, H. A. (2013). High-power mid-infrared frequency comb source based on a femtosecond Er: fiber oscillator. *Optics letters, 38*(13), 2360-2362.

Zulkifli, M., Jemangin, M., Harun, S., & Ahmad, H. (2011). Gain-flattened S-band depressed cladding erbium doped fiber amplifier with a flat bandwidth of 12 nm using a Tunable Mach-Zehnder Filter. *Laser Physics, 21*(9), 1633-1637.

Zulkifli, M. Z., Jemangin, M., Harun, S. W., & Ahmad, H. (2011). Gain-flattened S-band depressed cladding erbium doped fiber amplifier with a flat bandwidth of 12 nm using a Tunable Mach-Zehnder Filter. *Laser Physics, 21*(9), 1633.